Existing Performance and Effect of Retrofit of High-Rise Steel Buildings Subjected to Long-Period Ground Motions

March 2010

Yulin CHUNG

TABLE OF CONTENTS

CHAPTER 1

Introduction

1.1 Background

Large ocean-ridge earthquakes, with a magnitude over eight have been occurring along the subduction zones that run off the coast of the southwest part of Japan. The Philippine Sea plate subducts beneath the overriding Eurasian Plate in the northwest direction at a rate of approximately 4.5 cm/yr (Mochizuki et al. 2003) and causes the large earthquake to occur with return periods of one hundred to one hundred and fifty years. The 1854 Ansei Tokai Earthquake, which occurred along the subduction zone about 150 years ago, was the last of such an ocean-ridge earthquake. Japan will most probably experience another by the middle of this century (Kamae et al. 2004; Kawabe et al. 2008; Nakagawa et al. 2008). Subduction zone earthquakes are known to generate long-period ground motions on land, especially in the basin areas where large cities such as Tokyo, Nagaya and Osaka are located. Their predominant periods range from several to ten seconds, and the durations of primary motion extend over several minutes. Long-period ground motions tend to resonate high-rise buildings whose fundamental natural periods are a few seconds. Suita et al. (2007) conducted a serious of numerical analyses on a 75 and 150 m height high-rise buildings which designed by referring to the average of existing buildings, long-period ground motions could demand significantly larger energy dissipation than the design waves commonly used in Japanese seismic design, especially to beam-to-column connections, with anticipated cumulative deformations amassed to several to ten times larger than those expected for the design waves. The maximum inter-story drift angle reached 1.8% under the long-period ground motion loading. Cumulative deformations would increase significantly in those buildings, and severe structural damage may occur. On the other hand, damage to nonstructural components due to large velocities and inter-story deformation may also lead to great functional losses or make people be injured or killed by damaged or falling nonstructural components. Because high-rise buildings perform very important roles in the Japanese economy, severe damage to them will cause extreme difficulties throughout Japan.

The 1994 Northridge earthquake and the 1995 Hyogoken-Nanbu earthquake tested the seismic performance of steel moment frames, and severe damage was observed in their welded unreinforced flanges and bolted web connections (WUF-B) (FEMA 350; Bertero et al. 1994; Nakashima et al.

2000; Nakashima et al. 1998). A number of Japanese high-rise buildings built in the 1970s had also adopted the welded unreinforced flanges, although connection details differed rather significantly. Long-period ground motions are likely to demand much larger energy dissipation in such connections than that expected in seismic design.

Considering these observations, the seismic performance of existing high-rise buildings should be evaluated with urgency. Note that no earthquake that is larger than seven in magnitude has taken place in the Kanto basin after the 1923 great Kanto earthquake. Because these buildings have not experienced long-period ground motions, no actual data are available on possible seismic damage.

Retrofit is the most appealing alternative to enhance the capacity of beam-to-column connections to satisfy the raised demand by long-period ground motions. After the Northridge earthquake, connections like weld unreinforced flange, weld web (WUF-W), reduced beam section (RBS), welded bottom haunch (WBH) among others have been recommended for the Ordinary Moment Frame (OMF) and Special Moment Frame (SMF), and all have been qualified as the ductile connections that can satisfy the maximum deformation of 4% drift angle for two cycle without resistance decrease (FEMA 350, AISC 2005). For the retrofit of existing connections, however, these recommended connections have difficulties in application because of the presence of RC floor slab. It is also notable that most of the tests based on which the recommendations were stipulated were for bare beams rather than for beams with RC floor slab. According to some past tests (Okada et al. 2001, Kim et al. 2004), the slab could cause two time larger strain concentration at the bottom and reduce the cumulative deformation capacity by half compared with those experienced by the cases for bare beam. The effects of slab cannot be ignored in the seismic capacity evaluation of connections. In Japan, many tests had been conducted after the Hyogoken-Nanbu earthquake for the evaluation and enhancement of ductility capacity of beam-to-column connections. New types of connection details like a new shape of weld access hole and construction guidelines for the seismic retrofit of existing steel buildings (AIJ. 1996) were proposed. In these guidelines, however, retrofit mainly focus on the connections in the middle and low-rise buildings. Few data have been available for retrofit of the large size connections used in the high-rise buildings. In addition, most of the connection retrofit tests did not consider the effects of RC slabs, either. The actual data about the seismic performance of retrofitted connections are deemed still very limited.

1.2 Objective

To evaluate the existing performance such as the cumulative deformation capacity of beam-to-column connections, functional loss and risk of interior space in high-rise buildings subjected to long-period ground motions, a full-scale shaking table test can help provide actual data. However, there is no existing shaking table facility that is capable of accommodating the real size of high-rise buildings. Thus, a substructure test method is proposed as shown in Figure 1.1. A test specimen that represents a steel high-rise building will be shaken on a very large shaking table,

dubbed as the E-Defense shaking table (Ogawa et al. 2001, Nakashima et al. 2008). The test specimen consists of a four-story frame structure that features full-scale steel members and reinforced concrete slabs, and substitute layers that are placed on top of the frame and represents the upper stories. Two types of connections, both popularly used for Japanese high-rise buildings constructed in late 1960s to 1970s, will be adopted in the frame: the field weld connection, which is a type of WUF-B, and the shop weld connection, in which the beam web is welded rather than bolted, and the entire connection is fabricated in the shop (Nakashima et al. 2000). Ground motions, including one motion used in Japanese seismic design and long-period ground motions is applied sequentially with increasing magnitudes until the fractures of multiple connections to evaluate their capacity and the demands of long-period ground motions. Nonstructural components such as the dry wall partitions or ALC (Autoclaved Lightweight Concrete) partitions are also installed to examine their seismic performance under the long-period ground motions.

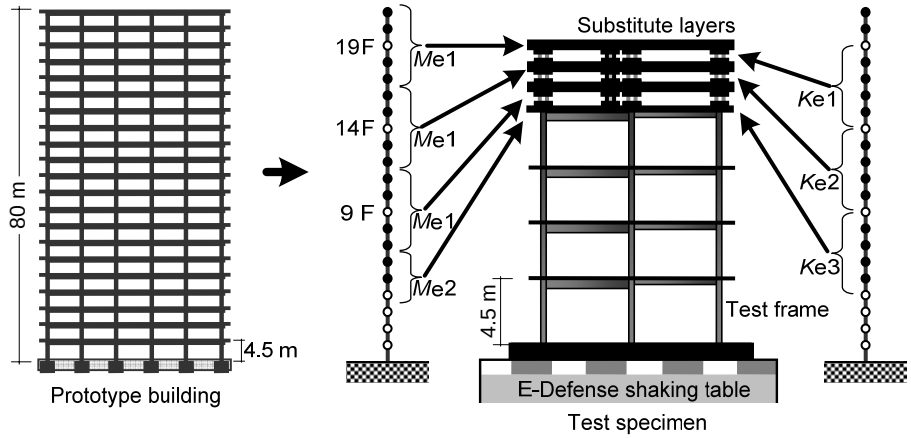

Figure 1.1 Proposed substructure test method

Examination into the seismic capacity of retrofitted high-rise buildings is the second phase of the study after the evaluations of existing performance. First, a series of quasi-static member tests is conducted on the field weld connection, which is adopted in the full-scale E-Defense test, using various retrofit methods. These retrofit methods have been decided in reference to some previous tests on retrofitted connections and considering the construction feasibility and the effect of RC slab. Multiple plastic cycles, which is be determined in reference to the response obtained from the E-Defense shaking table test, is applied until connection fractures for the purpose of evaluating the retrofit performance with respect to the long-period ground motion. In the third phase, the qualified retrofit connections is applied on a full-scale test specimen that is designed to be identical with the original E-Defense test specimen: a four-story, two-span by one-bay frame structure and topped with a concrete mass and rubber bearings system. A series of shaking table tests is conducted again to acquire the real data on retrofit performance by comparison with the test results obtained from the unretrofitted E-Defense test. The specimen is tested up to the fractures of multiple connections by the repeated applications of the specified input wave, thus providing quantitative retrofit performance.

To summarize, two main objectives are embedded in this study. The first is to acquire the real

data on the existing performance of steel high-rise buildings subjected to long-period ground motions. The maximum deformation, damage progress and deterioration of the steel frame, cumulative deformation demands of the long-period ground motions, and cumulative plastic deformation capacity of beam-to-column connections that consider the effects of RC floor slabs are examined by a series of full-scale shaking table tests. Second is to evaluate the seismic performance of a retrofitted high-rise building in which various types of reinforcement are applied to the field weld connections. A series of tests are conducted to investigate and provide quantitative information for engineers to facilitate the seismic resistance evaluation or retrofit design of existing high-rise buildings.

1.3 Organization

This dissertation consists of seven chapters. Chapter 1 presents the background of this study, and Chapter 7 is the summary and conclusions. Chapter 2 through 6 constitute the main part of the dissertation: (1) development of a shaking table test method to assess the seismic resistance capacity of a high-rise steel frame; (2) global behavior and damage distribution in steel frame; (3) seismic capacity of beam-to-column connection of the high-rise building; (4) member tests on the performance of retrofitted field weld connection; and (5) seismic capacity of a retrofitted steel high-rise building.

In Chapter 2, a substructure test method is proposed, and a test specimen representing a twenty-one story steel high-rise building is shaken on the E-Defense shaking table. First, the concept and design procedure of the test specimen are presented. The second part demonstrates the equivalence between the test specimen and the prototype building by means of the natural periods and corresponding mode shapes obtained from preliminary vibration tests.

In Chapter 3, performance of the test specimen is examined by checking the maximum deformation and story shear force distributions. The long-period ground motions were inputted sequentially until connection fractures to evaluate the performance, capacity, damage progress and deterioration of the test specimen. Functionality of interior space is also evaluated from the damage observation of the nonstructural components subjected to various levels of seismic loadings.

Chapter 4 is a continuation of Chapter 2 and Chapter 3 but focuses on the response of beam-to-column connections. The cumulative plastic rotation and ductility capacity of these connections are quantified in reference to the test results. Connection fractures are reasoned by means of fracture surface investigation. The effect of RC floor slab on the connection behavior is also investigated by comparing the results obtained from the tests with those of the bare beam tests obtained in the past.

In Chapter 5, quasi-static tests on the field weld connection where three types of retrofit methods are used are conducted. Design policies, construction methods, and strength equations of the retrofitted connections are described. The adopted retrofit performance is evaluated by comparing the cumulative plastic rotation ratios and cumulative ductility ratios of all connections.

The maximum strength is compared to the estimated strength to evaluate the effectiveness of the design equations. Strain values at the toe of weld access holes are compared to evaluate the strain concentration and retrofit performance of all connections.

In Chapter 6, the retrofit methods prequalified in Chapter 5 are applied in a full-scale shaking table test specimen that is designed to be identical with the unretrofitted E-Defense test specimen shown in Chapter 2. The design and construction of the retrofitted connections is presented to supply supplemental information on the retrofit design of the existing connections. The response characteristics of the connections are evaluated from the damage observation and corresponding hysteretic behavior. The fracture characteristics are examined in terms of the strain concentrations that appear in beam flanges. The retrofit performance of connections is evaluated by comparing their cumulative plastic rotation capacities with those obtained for the unretrofitted field weld connections in the unretrofitted E-Defense test. The quantified retrofitted performance is also summarized.

REFERENCES

[1.1] American institute of Steel Construction, Inc.: Seismic Provisions for Structural Steel Buildings, March 2005.

[1.2] Bertero, V.V., Anderson, J.C., Krawinkler, H. (1994): Performance of steel building structures during the Northridge earthquake, *Rep. UCB/EERC-94/09*, EERC, Univ. of California, Berkely.

[1.3] Federal Emergency Management Angency: FEMA350, Recommended Seismic Design Criteria for New Steel Moment-Frame buildings, July 2000.

[1.4] Japan Society of Civil Engineering. Architectural Institute of Japan. (2006). Report of seismic performance improvement of civil, architectural structures subjected to long-period ground motions generated by subduction zone. (in Japanese).

[1.5] Kamae, K., Kawabe, H., Irikura, K. (2004). Strong ground motion prediction for huge subduction earthquakes using a characterized source model and several simulation techniques. *Proc. 13th World Conf. Earthq. Eng.*, Vancouver, BC, Canada, 655-666.

[1.6] Kawabe, H., Kaname, K., Irikura, K. (2008). Damage prediction of long-period structures during subduction earthquakes-Part 1: Long-period ground motion prediction in the Osaka basin for future Nankai Earthquakes. *Proc. 14th World Conf. Earthq. Eng.*, Beijing, China.

[1.7] Kim, Y.J., Oh, S.H., Moon, T.S. (2004). Seismic behavior and retrofit of steel moment connections considering slab effects. *Eng. Struct.*, 26(13), 1993-2005.

[1.8] Machizuki, K., Obana, L., Seismic Activities along the Nankai Trough. Bull. Earthq. Res. Inst. Univ. Tokyo, Vol. 78 (2003) pp. 185-195.

[1.9] Nakagawa, Y., Kaname, K., Kawabe, H., Irikura, K. (2008). Damage prediction of long-period structures during subduction earthquakes-Part 2: Long-period ground motion prediction in the Osaka basin for future Nankai Earthquakes. *Proc. 14th World Conf. Earthq. Eng.*

[1.10] Nakashima, M., Inoue, K., and Tada, M. (1998). Classification of damage to steel buildings

observed in the 1995 Hyogoken-Nanbu earthquake. *Eng. Struct.*, 20(4-6), 271-281.

[1.11] Nakashima, M., Roeder, C. W., and Maruoka, Y. (2000). Steel moment frames for earthquakes in United Stated and Japan. *J. Struct. Eng.*, 126(8), 861-868.

[1.12] Nakashima M. (2008). Roles of Large Structural Testing for The advance of Earthquake Engineering. *Proc. 14th World Conf. Earthq. Eng*., Beijing, China.

[1.13] Ogawa, N., Ohtani, K., Katayama, T., Shibata, H. (2001). Construction of a three-dimensional, large-scale shaking table and development of core technology. *Phil. Trans. R. Soc. Lond.*, 359, 1725-1751.

[1.14] Seismic provisions for structural steel buildings. (1992). American Institute of Steel Construction (AISC), Chicago, Ill.

[1.15] Suita. K., Kitamura, Y., Goto, T., Iwata, T., Kamae, K. (2007) Seismic Response of High-Rise Buildings Constructed in 1970s Subjected to Long-Period Ground Motions. *Journal of structural and construction engineering, Architectural Institute of Japan.* 611, 055-061. (in Japanese with English abstract).

[1.16] The Japan Building Disaster Prevention Association. Architectural Institute of Japan. (1996) Construction Manual for Seismic Retrofit of Existing Steel Buildings.

LIST OF PUBLICATIONS

Journals Papers (full paper reviewed by multiple reviewers and published in recognized journals):

[1] **Yulin Chung**, Takuya Nagae, Toko Hitaka, Masayoshi Nakashima, Seismic Resistance Capacity of High-Rise Buildings Subjected to Long-Period Ground Motions: E-Defense Shaking Table Test, ***Journal of Structural Engineering ASCE*****.** (Accepted)

[2] Takuya Nagae, **Yulin Chung**, Yu Shimada, Kunio Fukuyama, Kouichi Kajiwara, Takahito Inoue, Masayoshi Nakashima, Taiki Saito, Haruyuki Kitamura, Nobuo Fukuwa, Toko Hitaka, Development of frame test system to assess seismic performance of high-rise buildings: E-Defense Shaking Table Test, **J. Struct. Constr. Eng., AIJ**, Vol. 74, No. 640, 1163-1171, Jun., 2009 (in Japanese).

[3] Tomohiro Matsumiya, **Yulin Chung**, Takuya Nagae, Test on retrofit effects of field welded beam-to-column connections with RC floor slab in high-rise building, **J. Struct. Constr. Eng., AIJ**. (under review).

Conference Papers (abstracts reviewed by multiple reviewers and presented in international conference):

[1] **Yulin Chung**, Takuya Nagae, Kunio Fukuyama, Kouichi Kajiwara, Takahito Inoue, Toko Hitaka, and Masayoshi Nakashima, Seismic Resistance Capacity of High-Rise Buildings subjected to Long-Period Ground Motions - E-Defense Shaking Table Test: The 14th World Conference on Earthquake Engineering, Beijing, China, Oct., 2008.

[2] **Yulin Chung**, Takuya Nagae, Kunio Fukuyama, Kouichi Kajiwara, Takahito Inoue, Toko Hitaka, and Masayoshi Nakashima, Full-Scale Test of Composite Frame subjected to Long-Period Ground Motions –E-Defense Shaking Table Test: The 11th East Asia-Pacific Conference on Structural Engineering & Construction, Taipei, Taiwan, Nov., 2008.

[3] **Yulin Chung**, Tomohiro Matsumiya, Takuya Nagae, Kunio Fukuyama, Toko Hitaka, and Masayoshi Nakashima, Test on Retrofit Effects of Steel Beam-to-Column Connections with RC Floor Slabs: 7th CUEE and 5th ICEE Joint Conference Tokyo, Japan, *March 3-5, 2010*.

Technical papers presented at domestic conferences:

[1] **Yulin Chung**, Takuya Nagae, Kunio Fukuyama, Kouichi Kajiwara, Takahito Inoue, Toko Hitaka, and Masayoshi Nakashima, Development of Substructures Test System for Earthquake Responses of High-Rise Steel Buildings Using E-Defense Shaking Table. Proceedings of Technical Papers of Kinki Branch, Jun., 2008 (in Japanese).

[2] Takahito Inoue, Takuya Nagae, Kouichi Kajiwara, Kunio Fukuyama, Masayoshi Nakashima, Taiki Saito, Haruyuki Kitamura, Nobuo Fukuwa, Toko Hitaka, E-Defense Shaking Table Test for Evaluation of Seismic Performance of High-Rise Building, Part 1: Overview of 'Reasearch Project on Damage Reduction Measure for Long-period Ground Motion'. Summaries of technical papers of Annual Meeting Architectural Institute of Japan. C-1, 823-824, Sep., 2008 (in Japanese).

[3] Kunio Fukuyama, **Yulin Chung**, Yu Shimada, Takuya Nagae, Kouichi Kajiwara, Takahito Inoue, Masayoshi Nakashima, Taiki Saito, Haruyuki Kitamura, Nobuo Fukuwa, Toko Hitaka, E-Defense Shaking Table Test for Evaluation of Seismic Performance of High-Rise Building, Part 2: Proposal and Design of the Test System. Summaries of technical papers of Annual Meeting Architectural Institute of Japan. C-1, 825-826, Sep., 2008 (in Japanese).

[4] Takuya Nagae, **Yulin Chung**, Kouichi Kajiwara, Kunio Fukuyama, Takahito Inoue, Masayoshi Nakashima, Taiki Saito, Haruyuki Kitamura, Nobuo Fukuwa, Toko Hitaka, E-Defense Shaking Table Test for Evaluation of Seismic Performance of High-Rise Building, Part 3: Outline of the Steel Frame and Test Schedule. Summaries of technical papers of Annual Meeting Architectural Institute of Japan. C-1, 827-828, Sep., 2008 (in Japanese).

[5] Kouichi Kajiwara, **Yulin Chung**, Ryuta Enokida, Xiaodong Ji, Takuya Nagae, Kunio Fukuyama, Takahito Inoue, Masayoshi Nakashima, Toko Hitaka, E-Defense Shaking Table Test for Evaluation of Seismic Performance of High-Rise Building, Part 4: System Identification and Seismic Response in Elastic Range. Summaries of technical papers of Annual Meeting Architectural Institute of Japan. C-1, 829-930, Sep., 2008 (in Japanese).

[6] Toko Hitaka, **Yulin Chung**, Takuya Nagae, Kouichi Kajiwara, Kunio Fukuyama, Takahito Inoue, Masayoshi Nakashima, E-Defense Shaking Table Test for Evaluation of Seismic Performance of High-Rise Building, Part 5: Dynamic Response and Hysteresis of Steel Moment

Frame. Summaries of technical papers of Annual Meeting Architectural Institute of Japan. C-1, 831-932, Sep., 2008 (in Japanese).

[7] **Yulin Chung**, Takuya Nagae, Kouichi Kajiwara, Kunio Fukuyama, Takahito Inoue, Masayoshi Nakashima, Haruyuki Kitamura, Toko Hitaka, E-Defense Shaking Table Test for Evaluation of Seismic Performance of High-Rise Building, Part 6: Patterns of Failure and Deformation Capacities in the Steel Frame. Summaries of technical papers of Annual Meeting Architectural Institute of Japan. C-1, 833-934, Sep., 2008 (in Japanese).

[8] Matsutaro Seki, Takuya Nagae, **Yulin Chung**, Kunio Fukuyama, Kouichi Kajiwara, Takahito Inoue, Masayoshi Nakashima, Taiki Saito, E-Defense Shaking Table Test for Evaluation of Seismic Performance of High-Rise Building, Part 7: Damage Behaviors of Interior Dry Wall Partitions. Summaries of technical papers of Annual Meeting Architectural Institute of Japan. C-1, 835-936, Sep., 2008 (in Japanese).

[9] **Yulin Chung**, Tadamasa Daibou, Tomohiro Matsumiya, Takuya Nagae, Kunio Fukuyama, Toko Hitaka, Masayoshi Nakashima, Test on Strengthening Effects of Steel Beam-to-Column Connections with RC Floor Slabs Part 1. Outline and unretrofitted specimen. Proceedings of Technical Papers of Kinki Branch, Jun., 2009 (in Japanese).

[10] Tadamasa Daibou, **Yulin Chung**, Tomohiro Matsumiya, Takuya Nagae, Kunio Fukuyama, Toko Hitaka, Masayoshi Nakashima, Test on Strengthening Effects of Steel Beam-to-Column Connections with RC Floor Slabs Part 2. Results of retrofitted specimens. Proceedings of Technical Papers of Kinki Branch, Jun., 2009 (in Japanese).

[11] Tomohiro Matsumiya, **Yulin Chung**, Tadamasa Daibou, Takuya Nagae, Kunio Fukuyama, Toko Hitaka, Masayoshi Nakashima, Test on Strengthening Effects of Steel Beam-to-Column Connections with RC Floor Slabs Part 3. Effects of composite action. Proceedings of Technical Papers of Kinki Branch, Jun., 2009 (in Japanese).

[12] **Yulin Chung**, Tadamasa Daibou, Tomohiro Matsumiya, Takuya Nagae, Kunio Fukuyama, Toko Hitaka, Masayoshi Nakashima, Test on Strengthening Effects of Steel Beam-to-Column Connections with RC Floor Slabs Part 1: Outline. Summaries of technical papers of Annual Meeting Architectural Institute of Japan. C-1, 835-936, Sep., 2009 (in Japanese).

[13] Tadamasa Daibou, **Yulin Chung**, Tomohiro Matsumiya, Takuya Nagae, Kunio Fukuyama, Toko Hitaka, Masayoshi Nakashima, Test on Strengthening Effects of Steel Beam-to-Column Connections with RC Floor Slabs Part 2: Unretrofitted specimens of this test and E-Defense test. Summaries of technical papers of Annual Meeting Architectural Institute of Japan. C-1, 835-936, Sep., 2009 (in Japanese).

[14] Masayoshi Nakashima, **Yulin Chung**, Tadamasa Daibou, Tomohiro Matsumiya, Takuya Nagae, Kunio Fukuyama, Toko Hitaka, Test on Strengthening Effects of Steel Beam-to-Column Connections with RC Floor Slabs Part 3: Results of retrofitted specimens. Summaries of

technical papers of Annual Meeting Architectural Institute of Japan. C-1, 835-936, Sep., 2009 (in Japanese).

[15] Tomohiro Matsumiya, **Yulin Chung**, Tadamasa Daibou, Takuya Nagae, Kunio Fukuyama, Toko Hitaka, Masayoshi Nakashima, Test on Strengthening Effects of Steel Beam-to-Column Connections with RC Floor Slabs Part 4: Effects of composite action. Summaries of technical papers of Annual Meeting Architectural Institute of Japan. C-1, 835-936, Sep., 2009 (in Japanese).

CHAPTER 2

Development of Shaking Table Test Method to Assess Seismic Resistance Capacity of Steel Frame in High-Rise Building

2.1 Introduction

2.1.1 Organization

This chapter reports a series of shaking table tests on a high-rise building. A substructure test method was employed, and a test specimen representing a twenty-one story steel high-rise building was shaken on the E-Defense shaking table. The test specimen consisted of a four-story test frame featuring full-scale steel members and reinforced concrete slabs. Substitute layers were placed on top of the frame to represent upper stories.

The first of the section below presents the concept and design procedure of the test specimen. The second demonstrates the equivalence between the test specimen and the prototype building by means of the natural periods and corresponding mode shapes obtained from preliminary vibration tests.

2.1.2 High-rise buildings in Japan

High-rise buildings play very important roles in the economy of our society and appearances of these buildings reflect the technology levels, and society's wealth at the time. Since the Japanese building code was modified in 1963, the first high-rise building whose height was over 60 m was built in 1964 (Fukushima et al. 1999; Fukushima et al. 2000; BRI. 2005; Taiki et al. 2005). Until 2000, over 1000 high-rise buildings were built in large cities throughout Japan. Structural systems and member details of high-rise buildings have been changed with time. The moment frame system was commonly used in most high-rise buildings built from 1960s to early 1970s before seismic resistance members like braces and dampers became popular. For structure members in the steel moment frame system, columns especially at the corners sustain large axial force when subjected to lateral forces. Considering the large axial force at corner columns and the benefit of isotropic characteristics, large size built-up box sections were commonly adopted instead of wide flange sections. For beams, honeycomb beams, which were processed from the rolled section of a wide

flange beam were adopted in some cases to increase the stiffness and/or provide space for interior piping. Furthermore, beams with a thinner web plate were also adopted in some cases to save cost (FD design, for example, the width-thickness ratio larger than 41 in the N490 steel material).

Figure 2.1 shows the base shear coefficient (C_B) versus the first mode period ($_1T$) relationship of those buildings (Fukushima et al. 2000). The base shear coefficient (C_B) of high-rise buildings are mostly located between one to two times the standard value stipulated in the design code (for standard shear force coefficient C_0=0.2, period of soil T_c=0.6 and zone factor Z=1.0). The standard shear force coefficient ($_1T \cdot C_B$) of steel high-rise buildings mostly fall in about 0.3. In seismic design, standard waves and a long-period wave was mostly adopted. The standard waves of the El Centro wave and Taft wave were used for over 90% of the design of existing high-rise buildings. The long-period wave of Hachinohe whose dominate period is 2.5 sec and duration is about 120 sec was adopted for over 60% of the buildings. Genuine long-period, long duration ground motions generated by subduction zone earthquakes were not considered in the past seismic design.

Fukushima et al. conducted a series of surveys on existing high-rise buildings built from 1960s to 1990s (Fukushima et al. 1999; Fukushima et al. 2000). Over one thousand buildings were collected in this statistics. About 90% of the buildings are used either is office or apartment. The geometric values of the two types of buildings were shown in Figure 2.2. In early time buildings (before 1980s), the average height was 85 m, the standard floor area was about 1000 m^2, and the standard story height of office buildings and apartments were 3.7 and 2.9 m, respectively.

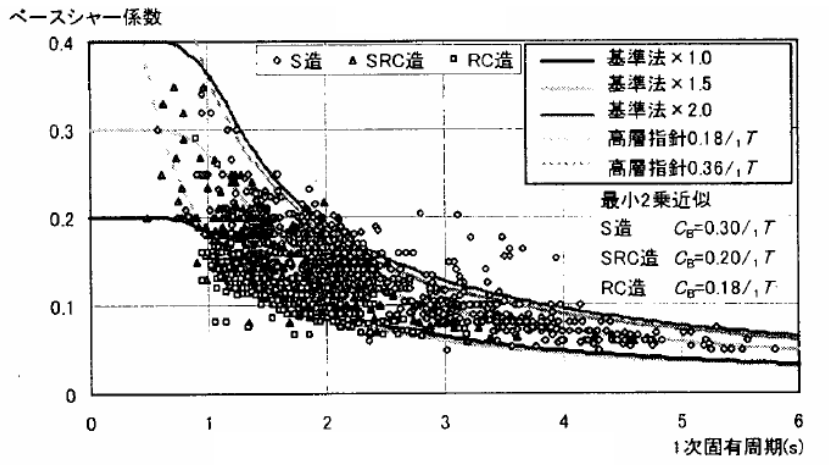

Figure 2.1 Base shear coefficient and first mode period (Fukushima et al. 2000)

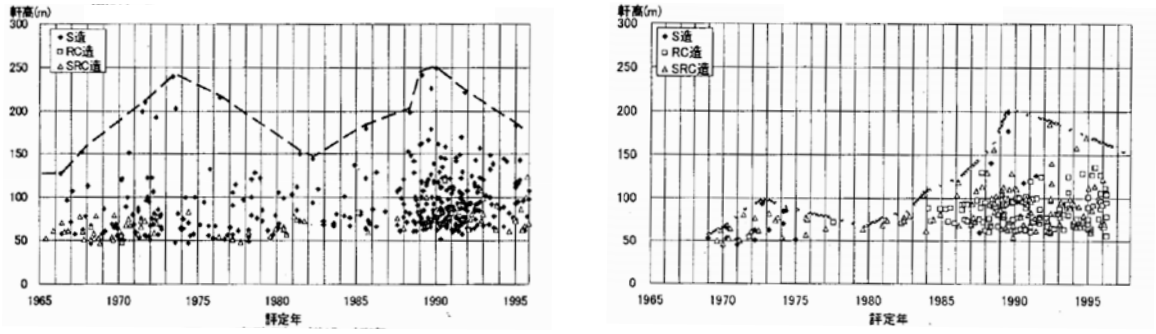

(a) (b)

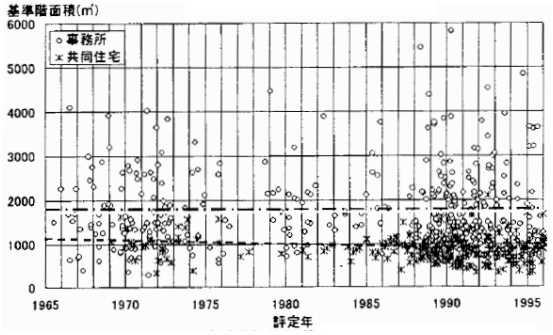

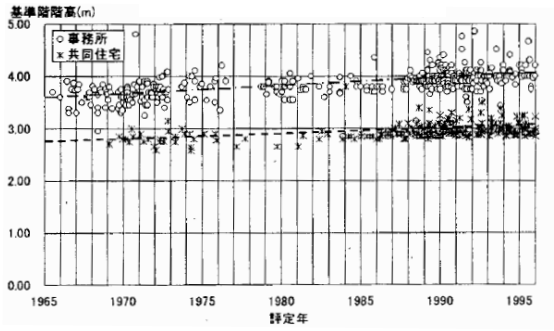

(c) (d)

Figure 2.2 Statistic material of existing high-rise buildings: (a) Story height of office buildings; (b) Story height of apartment buildings; (c) Standard floor area of office and apartment buildings; (e) Story height of office and apartment buildings (Fukushima et al. 2000)

2.2 E-Defense shaking table and test specimen

2.2.1 Capacity of E-Defense shaking table

In the 1995 Hyogoken-Nanbu earthquake, more than 6000 people were killed as a result of collapses of buildings (Report on the Hanshin-Awaji Earthquake Disaster, 1997). This earthquake highlighted the needs of large-scale structural tests to represent the real seismic behaviors of buildings and other structural systems. In the reflection of the needs, a three-dimensional, full-scale, earthquake-testing facility as one of the core research facilities for earthquake disaster prevention was built by the National Research Institute of Earth Science and Disaster Prevention (NIED) and the Science and Technology Agency of the Japanese Government (STA) and completed in 1998. Table 2.1 shows the major specifications of the E-Defense shaking table. The table is 20 m by 15 m in plan dimension and can produce a velocity of 2.0 m/s and a displacement of ± 1.0 m in two horizontal directions simultaneously. It can accommodate a specimen up to a weight of 1,200 metric tons and a height of 22 m. As far as table capacity is concerned, this shaking table is the largest in the world (Ogawa et al. 2001; Nakashima et al. 2006; Nakashima et al. 2008).

According to the statistics on the total height, story height and floor area of Japanese high-rise buildings built in the past thirty years in Japan (Fukushima et al. 1999; Fukushima et al. 2000; BRI. 2005), a twenty-one story 80m height building was adopted as the prototype and designed with reference to past design materials. This building has five-span, 24 m long in the longitudinal direction and three-bay width 30 m long in the transverse direction. The first story is 4.5m in height, and 3.8m in height for the remaining stories. The standard floor area is 952 m^2. Figure 2.3 shows the prototype and the dimensions of the E-Defense shaking table. The height of the prototype is about four times what E-Defense can accommodate. Here, the concept adopted for the test was to establish a partial frame structure having full-scale steel members and being able to reproduce the possible seismic responses of the prototype. A physical model that represents the

prototype was developed, and to design a test specimen that complies with the concept, a modified model, in which the degrees of freedom of the physical model are condensed, was developed. Finally, the test specimen was designed in view of the properties of the modified model.

Table 2.1 Major specification of the E-Defense shaking table

Payload	12 MN (1,200 tonf)	
Plan	20×15 m	
Shaking direction	Horizontal	Vertical
Max. acceleration	9 m/s^2	1.5 m/s^2
Max. Velocity	2 m/s	0.7 m/s
Max. displacement	1 m	0.5 m

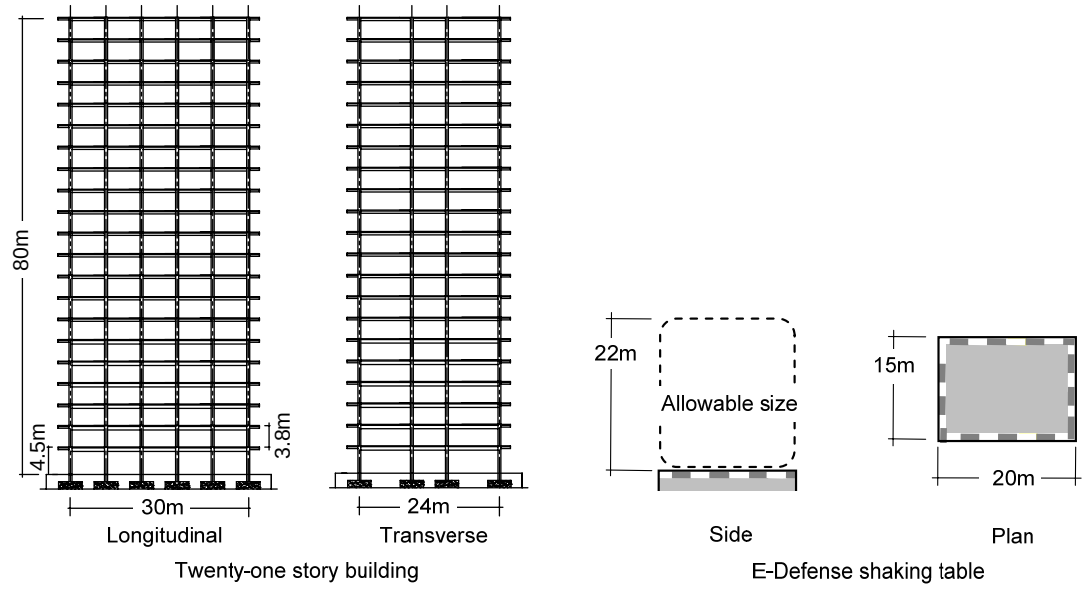

Figure 2.3 A generic high-rise building and E-Defense shaking table

2.2.2 Prototype model

For the past thirty years, the story strength and stiffness distribution has remained essentially unchanged in the design of high rise buildings in Japan. The design adopts the following major criteria. One: to keep the building elastic and limit the maximum inter-story drift angle to not greater than 0.5% for the level 1 seismic force. Two: keep the deformations of the building within minor plasticity and limit the maximum inter-story drift angle to not greater than 1.0% for the level 2 seismic force. The level 1 and 2 seismic forces are stipulated in the Japanese seismic design code (Nakashima et al. 1998), and the level 1 seismic force corresponds to a ground motion with a PGA of 0.15 to 0.2 m/s^2 and a PGV of 0.25 m/s, and the level 2 seismic force corresponds to a PGA of 0.3 to 0.4 m/s^2 and PGV of 0.5 m/s.

The physical model that represented the prototype was determined by past design materials

subjected to those criteria. The model was a stick model with twenty-one story masses and story stiffnesses, as shown in Figure 2.4. According to the assumed building height of 80 m, the first mode period T_1 of the prototype model was set up at 2.4 s. The stiffness distribution in the vertical direction was determined by the Japanese building standards. Note that the stiffness distribution is similar to that stipulated in IBC codes (Nakashima et al. 2000). The story force versus deformation relationship was defined to be tri-linear. In reference to the building height of 80 m, a design base shear ratio C_b of 0.12 was chosen for the elastic limit. The base shears corresponding to the two threshold points of the tri-linear relationship were determined to be 1.4 and 2.0 times the base shear values. The second and third stiffnesses were 0.6 and 0.1 times the story initial stiffness, respectively. These values were chosen in reference to the statistics in past design practice.

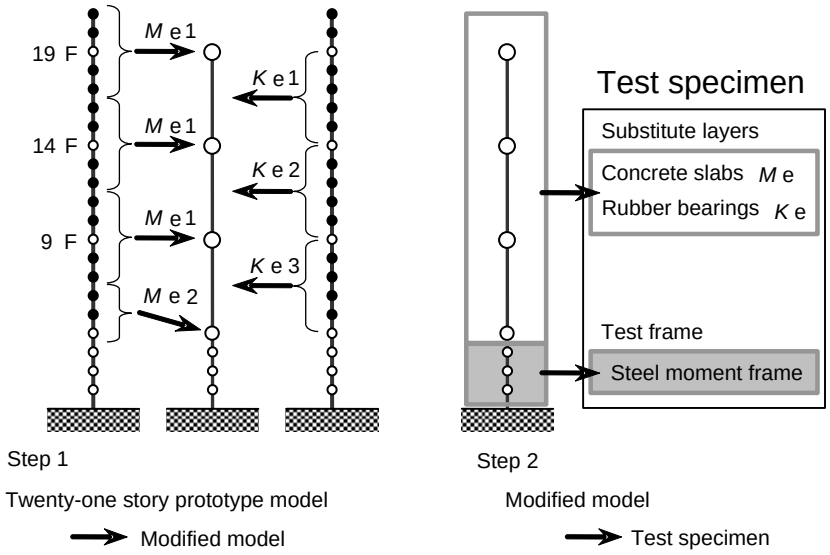

Figure 2.4 Development from prototype to test specimen

2.2.3 Procedure to modify the prototype model

A series of time-history analyses were conducted for the model. According to the responses obtained, the maximum inter-story drifts occurred in lower stories subjected to long-period ground motions. For this reason, the lower part of the prototype was selected as the physically tested structure (named hereafter as the test frame), and the remaining upper part was replaced by layers, each consisting of a thick concrete slab and rubber bearings.

Figure 2.4 shows the procedure for constructing the modified model within a few degrees of freedom of the original model with twenty-one degrees of freedom. The number of stories of the test frame was chosen to be four in reference to the preliminary analyses. According to the associated eigenvalue analysis, the first three modes covered over 90% of the mode participation, based on which the substituted part was to comprise three layers (Table 2.2). The responses of the three masses in the substitute layers were assumed to represent the responses of the ninth, fourteenth, and nineteenth floors of the original model. Procedures to determine the properties of

the substitute layers were as follows: 1) the masses of every five stories masses were summed and assigned to an equivalent lumped mass M_e; 2) the horizontal stiffnesses of every five stories horizontal stiffnesses were combined in series so that the equivalent stiffness K_e of each substitute layer would represent the deformations of the corresponding five stories; and 3) the substitute layer's yielding strength Q_e was estimated by the average of the corresponding story yield strengths. The image of the test specimen is shown in Figure 2.5. The bottom four stories of the modified model is represented by a full-scale four-story test frame, and the substitute layers are represented by rubber bearings, dampers and concrete slabs.

In the eigenvalue analysis, the first mode period of the modified model was 2.37 s. Figure 2.6 compares the original model and modified model subjected to two ground motions whose details will be described at a later section. One is the N-S component of the 1940 El Centro wave whose PGV was scaled at 0.5 m/s. The other was a long-period ground motion with a predominant period at around three seconds, named the San wave. The distributions of the prototype and modified model are very close to each other. It is notable that the maximum deformations occur at lower stories for the San wave. These results formed the basis of design for the test specimen.

Table 2.2 Mode participation coefficient

Modified model			Prototype model	
Period (sec)		Mode participation coefficient (%)	Period (sec)	Mode participation coefficient (%)
T_1	2.37	77	2.37	78
T_2	0.92	10	0.91	11
T_3	0.59	5	0.56	4
T_4	0.43	5	0.40	2
T_5	0.18	2	0.32	2
Total		99		97

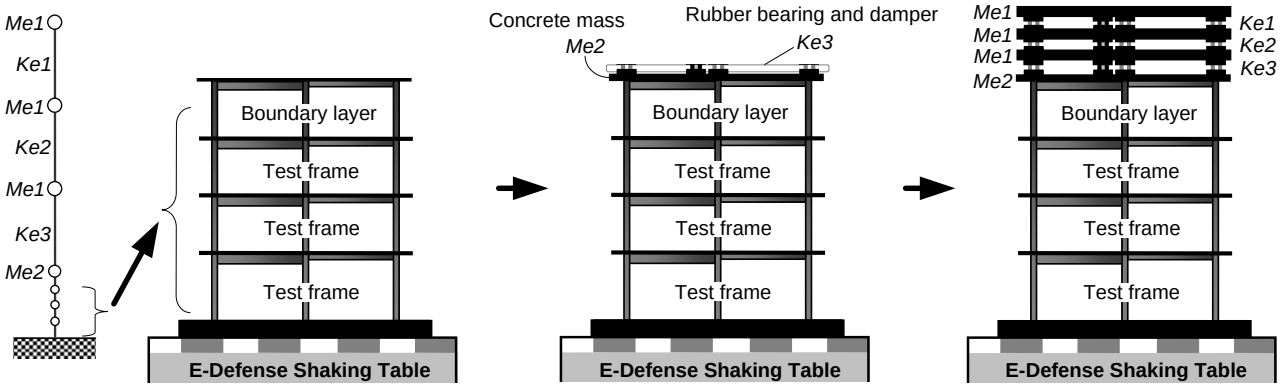

Figure 2.5 Physical image of the test specimen

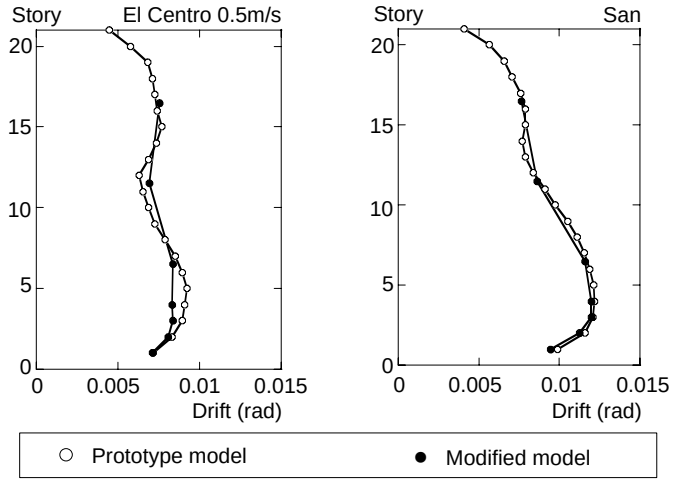

(a) (b)

Figure 2.6 Inter-story drift responses of prototype model and modified model:
(a) El Centro-NS 0.5m/s; (b) San-EW

2.3 Design of the test specimen

Figures 2.7 and 2.8 show the designed test specimen. The lower part is the test frame. The upper part consists of three substitute layers made of thick concrete slabs and rubber bearings. The test specimen is totally 21.8 m in the total height and 1120 matric ton in weight.

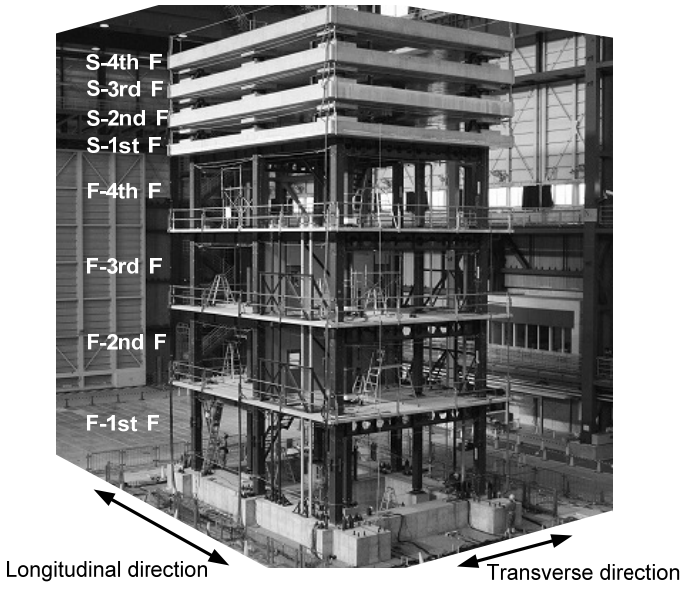

Figure 2.7 Global view of test specimen

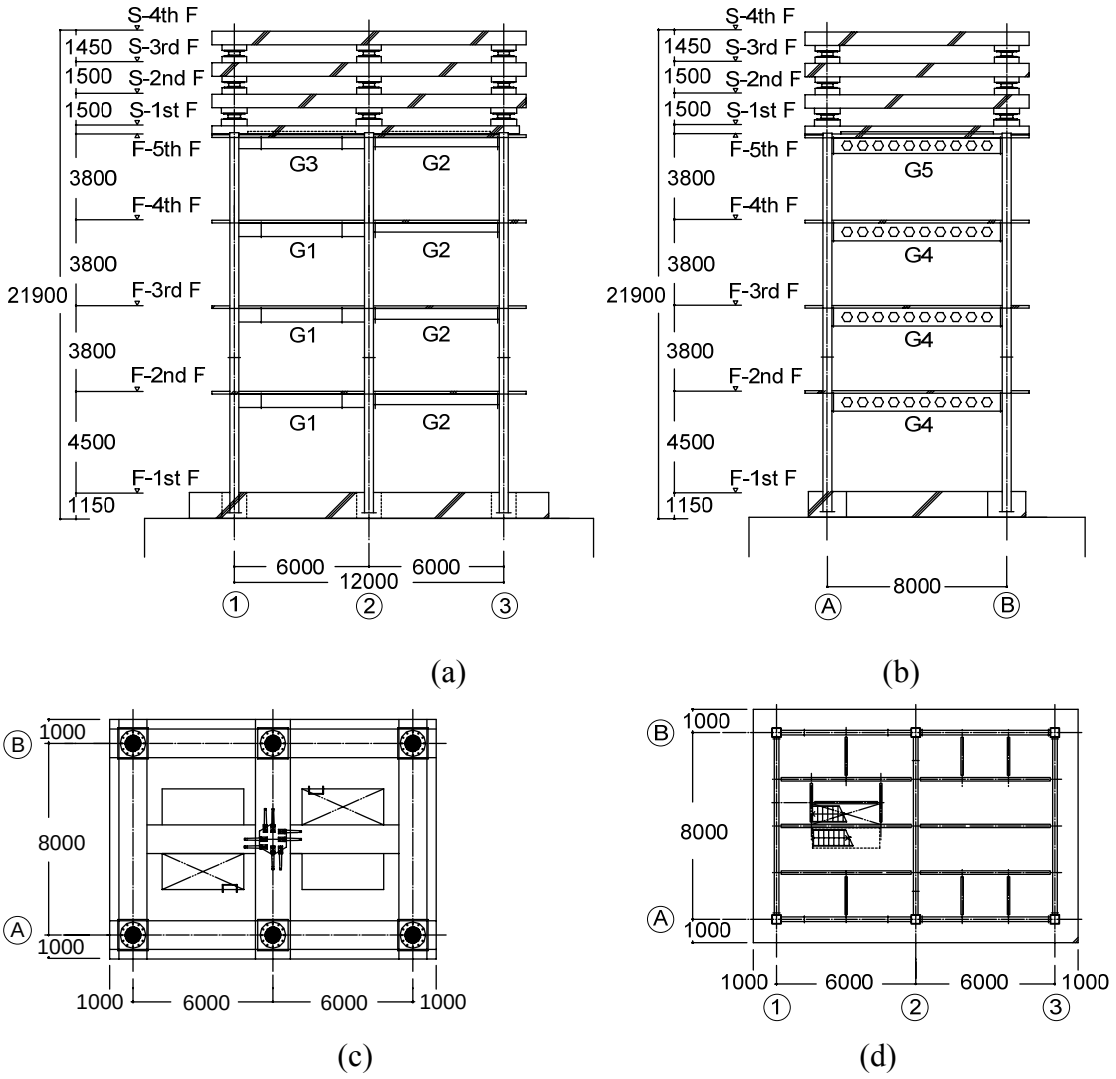

Figure 2.8 Plan and elevation of test specimen:
(a) Elevation-A; (b) Elevation-1; (c) S-1st Fl Plan; (d) F-2nd Fl Plan

2.3.1 Test frame

As shown Figure 2.8, the frame has two spans in the longitudinal direction and one in the transverse. The member sizes were determined using the allowable stress design method, with a base shear ratio C_b of 0.12.

Two types of connection were adopted in the test frame: the field weld connection and shop weld connection. In high-rise buildings built in 1960s and early 1970s, shop weld connections were often used due to the concerns about the weld quality and weld shrinkage. In such shop weld connections, the beam is cut into halves in the mid span, and the flanges and web of the half beam are all-welded to the column in shop. Then, the shop welded assemblage that consists of a column and half beams is transported to the construction site. Finally, the shop welded half beams are bolted to each other at the mid span. With gradual development of nondestructive testing, construction management, and accumulated experiences of welding, the field weld connection with welded flanges and bolted web gained popularly in early 1970s. Thus, these two types of connection were

mixed in high-rise buildings constructed in early 1970s. With the advantages of better constructability and lower cost, the field weld connections were adopted more preferably, but due to better quality control, the shop-welded connections were still used when the beam span was relatively short. Considering those situations at that time, both types of connection were adopted in the test. Figure 2.9 shows these two types of connection details. In the longitudinal direction, a built-up wide flange section of H 600×200×9×19 was arranged with the shop weld connection. In the transverse direction, a honeycomb section of H 800×199×10×15, which was processed from a rolled section of H 596×199×10×15, was arranged with the field weld connection detail. The details of beams and beam-to-column connections were chosen based on historical design practice. Two types of web design were adopted in the field weld connections (Figure 2.9(b)). One was a then typical design in which the web bolts were assumed to sustain only the beam shear force. The other was a design in which the web bolts took both the shear force and partial bending moment of the beam. The two connections turned out to have nine and thirteen bolts in the web. The nine bolts connection was arranged for the second and forth story beams and the thirteen bolts design was arranged for the third story beams, respectively. In each of the second to forth stories, eight connections were chosen for detailed recording, which resulted in a total of twenty four connections for investigation of detailed hysteretic behavior.

The columns had a box section of 400×400×25 with inner-diaphragms at connections. The columns were stronger than beams in terms of the column-to-beam strength ratio of 1.5 considering the effect of axial forces exerted in the columns. Under gravity load, the axial forces sustained by the first-story columns were about 0.2 in terms of the axial force ratio. The ratio was close to those of the interior columns of actual high-rise buildings. Reinforced concrete slabs with a thickness of 120 mm were cast at every floor. The first-story column bases were embedded in strong RC beam foundations to a depth of 0.9 m so that they could reasonably be considered fixed.

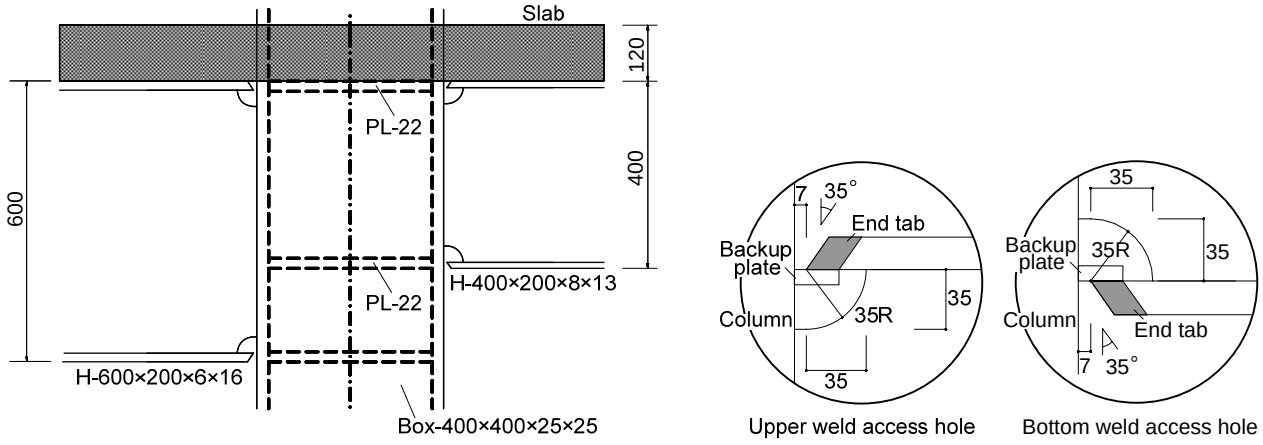

(a)

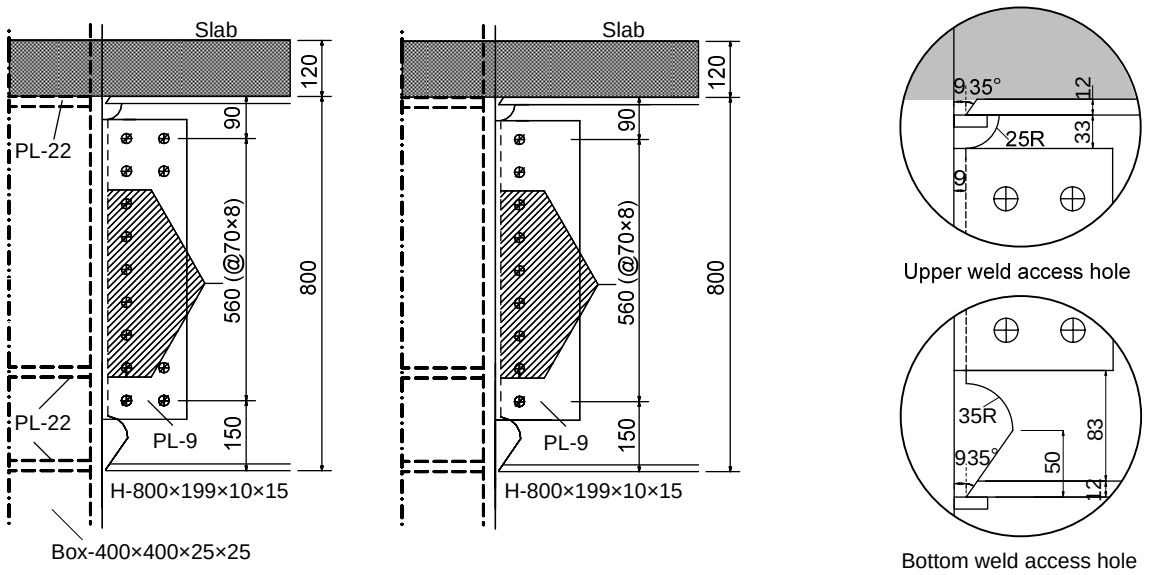

(b)

Figure 2.9 Beam-to-column connection details: (a) Shop-weld connection; (b) Field-weld connection (unit: mm)

Specifications of the structural components and measured material properties are listed in Table 2.3. The story weights, specifications of the rubber bearings and dampers are shown in Table 2.4 to 2.6. Charpy V-notch (CVN) impact tests were conducted for the margin members and deposited metals of welds (Table 2.7). The measured CVN values of the shop weld and field weld deposits were 105 J and 88 J at 0 ^{o}C, respectively. The CVN value at 20 ^{o}C, the temperature of the laboratory at the time of tests, was 155 J. These values all satisfied the demands of the criteria that the CVN value at 0 ^{o}C should be not smaller than 70J (BCJ 2003)

Table 2.3 Specimen specifications and material properties

			σ_y (MPa)	σ_u (MPa)
Column (SM 490A)		□ 400×400×25	343	515
Beam (SM 490A)	G1	H 600×200×9×19	357	532
	G2	H 400×200×8×13	426	576
	G3	H 500×200×9×16	366	532
	G4	H 800×199×10×15	377	526
	G5	H 650×199×9×14	344	514
Concrete				30

Table 2.4 Story weight

Story	Weight (t)	Story	Weight (t)
RFL	180	4F	53
7F	195	3F	53
6F	195	2F	56
5F	166	1F	221

Table 2.5 Specification of rubber bearings

Story	Diameter of rubber bearing (mm)	G (N/mm^2)	Rubber thickness (mm)
7	500	0.39	124
6	600	0.44	117
5	600	0.59	135

Table 2.6 Specification of dampers and rubber bearing system

Story	Diameter of rubber bearing (mm)	G (N/mm^2)	Rubber thickness (mm)	U type damper
7	800	0.59	90	NSUD50×6
6	900	0.59	90	NSUD50×8
5	1100	0.59	90	NSUD50×8

Table 2.7 Charpy V-notch impact tests results

		CVN values	
		0 °C (J)	20 °C (J)
(1) Base medal-Flange			
Built-up H Beam	H600	93	109
Rolled H Beam	H800	104	135
(2) Weld medal-Flange			
Built-up H Beam	H600	105	159
Rolled H Beam	H800	88	190

2.3.2 Substitute layers

Rubber bearings and steel dampers were placed at each substitute layer. The steel dampers were used to mimic possible nonlinearity and energy dissipation of the upper part with the substitute layers. Six rubber bearings were arranged at the column positions. The damper was placed at the centroid of each layer. In the design, the rubber bearing and damper were modeled to be linear and bi-linear, respectively. The stiffnesses and strengths of the devices were carefully adjusted. As shown in Figure 2.10, the total stiffness of six rubber bearings of each layer corresponds to the second stiffness of each layer and was designed to be 0.6 times of the story initial stiffness. The

story stiffness was set at 3.7 to 7.5 MN/m, according to the stiffness distribution. The damper was made of U-shaped steel rods with a rubber bearing placed underneath to adjust its initial stiffness. For this damper unit, the combination of damper stiffness (K_d), yield strength (Q_{dy}), and rubber bearing stiffness (K_{rs}) were determined so that it could best match the initial stiffness and first yield point in the design tri-linear relationship. The first yield points of 348 to 608 kN, estimated based on the strength distribution, were assigned as a result of this consideration. According to this procedure, the second yield point of the tri-linear relationship could not be modeled in the substitute layers. Note, however, that the upper part of the prototype model did not go into the third branch even in the largest response considered. Figure 2.11 shows the results of pushover analysis of the specimen and the corresponding designed tri-linear relationship. The relationships of pushover analysis match satisfactorily the design relationships.

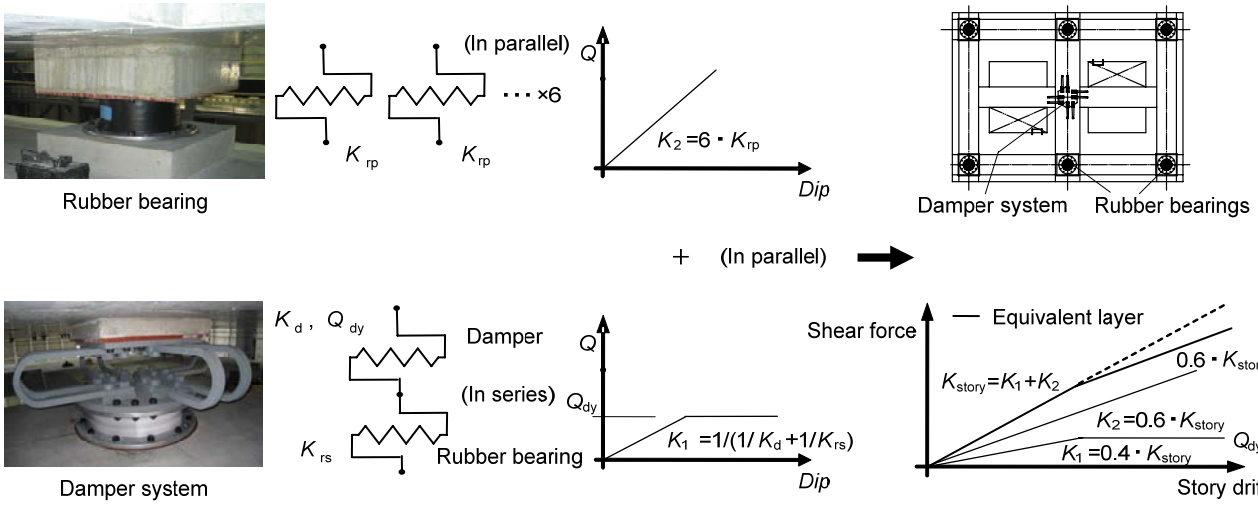

Figure 2.10 Model and design of substitute layers

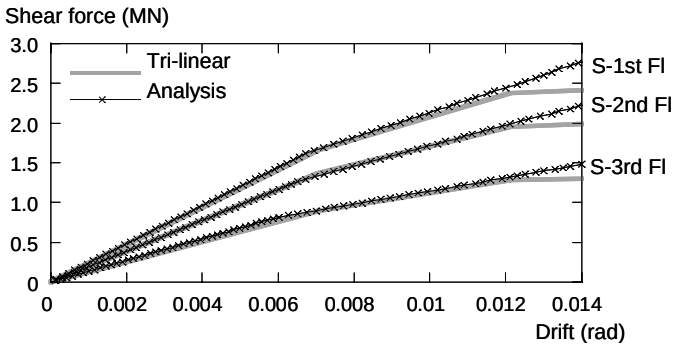

Figure 2.11 Pushover analysis for substitute layers

The fourth story in the test frame was assigned as the boundary layer between the frame and the substituted upper part. Figure 2.12 shows the boundary details. To decrease the stiffness of the boundary layer, only short columns above the frame were connected with the concrete slab of the substitute layer, and a styrofoam layer was inserted between the beams and the concrete slab.

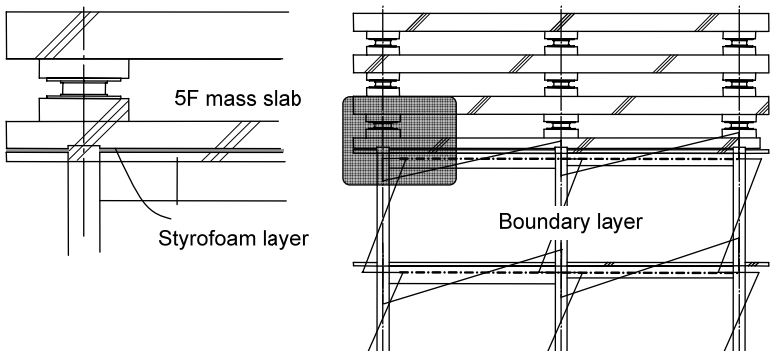

Figure 2.12 Boundary detail between the frame and substitute layers

2.3.3 Construction

A few construction stages are shown in Figure 2.13. Construction of the specimen and welds of the connections followed as closely as possible the actual situation in the construction field. The box section column with inner-diaphragms was shop welded with the bracket beam in the shop. In the construction field, this column was bolted with the first story column which was embedded in the RC foundation beam in the first. Then the bracket beams were bolted with the central part of the beams in the longitudinal directions of the test specimen. Beams in the transverse direction of test specimen were connected with the column using the field weld detail of welded unreinforced flanges and bolted web. Welders had to work on unstable scaffolds in a high altitude, about 15m height in the E-Defense specimen. Due to presence of the beam web, weld at the bottom flange had to be interrupted at the web. The welder had to move to the other side of beam to weld the next pass after he finishes every pass in front of him. All welders were certified, and all groove welds were ultrasonically tested and qualified by an independent welding-inspection firm and all satisfied the demands of UT test criteria (AIJ 2008). Nonstructural components included the dry wall partitions and ALC (Autoclaved Lightweight Concrete) partitions were installed at the second and third story. The construction of the test frame was completed outside. Then the test frame was moved in the test building, and the foundation beams were connected with the shaking table. Finally the concrete slabes, rubber bearings, and dampers were installed in the order of the sixth, seventh, and roof floors.

(b)

(c)

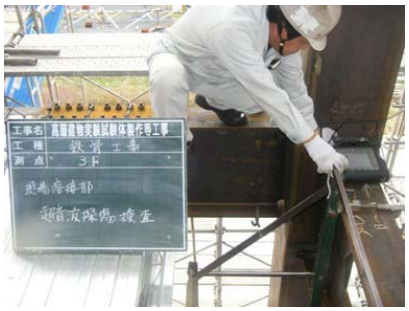

(d)

(a)

(e)

(f)

(g)

Figure 2.13 Construction process: (a) Test frame; (b) Shop welding; (c) Field welding; (d) Ultrasonic test; (e) RC floor slab placing; (f) Drywall partitions; (g) Install of the substitute layers

2.4 Measurement

A total of 678 channels of data were collected in the test, including sixty-seven accelerometers, 121 displacement transducers, and 396 strain gauges. The accelerometers were placed on the shaking table and each floor slab to record accelerations in three directions. The displacement transducers were arranged to measure the inter-story displacements, rotations of beam ends, and shear displacements of connection panel zones. As shown in Figure 2.14, the strain gauges were glued to the surface of structural steel members. Strain gauges were glued at two sections in the middle part of beams. Using the calculated the section moments, the bending moments of the beam ends were estimated. Strain gauges were also glued to the beam ends to monitor the level of inelastic strains. To estimate the shear force and bending moments of columns, strain gauges were glued on wo sections of each floor. Four gauges were glued on each face of the section. Video cameras were used to take the global views and details of the behavior of connections, dampers, and rubber bearings.

For the measuring system, 24 bit A/D converters were used, and the data were recorded at an interval of 0.005 s.

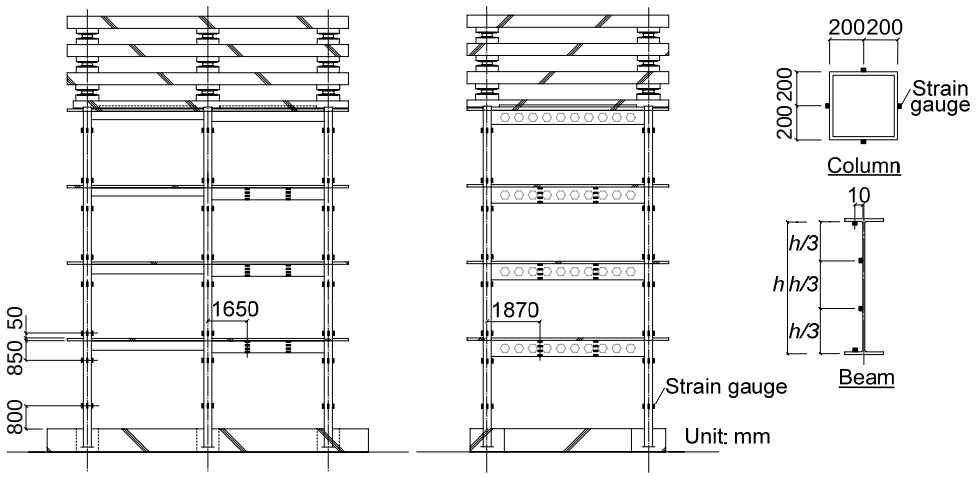

Figure 2.14 Measurement plan

2.5 Loading program

Bi-directional shaking table tests were conducted at three levels with increasing magnitudes of input waves. Figure 2.15 shows the time histories of the input waves. For long-period ground motions, two synthesized waves were adopted. The Hog wave (PGA=1.45 m/s^2, PGV= 0.40 m/s) was predicted at a Kawasaki site, which is next to Tokyo, and rupture of the Tokai trough was assumed. The San wave (PGA=1.86 m/s^2, PGV= 0.51 m/s) was predicted at a Nagoya site, and simultaneous ruptures of the Tokai and Tounankai troughs were assumed. These two waves had predominant periods of about three seconds and durations of 200 and 320 s. In addition to the long-period ground motions, two near-fault ground motions were adopted. The El Centro wave was commonly used in the seismic design in Japanese design code. The Tok wave is a synthesized wave of Tokyo site. Figure 2.16 shows the pseudo relative velocity response spectra of the input waves. At the period of 2.4 s, the Hog wave is about 1.2 times larger in amplitude than the level 2 El Centro wave (scaled to 0.5 m/s in PGV), and the San wave is about two times larger than the level 2 El Centro wave. Hence, the Hog wave can be categorized as a level 2 seismic force, and the San wave can be classified as a level 3 seismic force. First, the level 1 El Centro (scaled to 0.25 m/s in PGV) wave was applied. Then, the level 2 El Centro wave and Hog wave (level 2) and the San wave (level 3) were applied sequentially.

Figure 2.17 shows the velocity spectrum of the input waves and the response from the RC beam foundations of the test specimen. The shaking table shows notable representation on these waves.

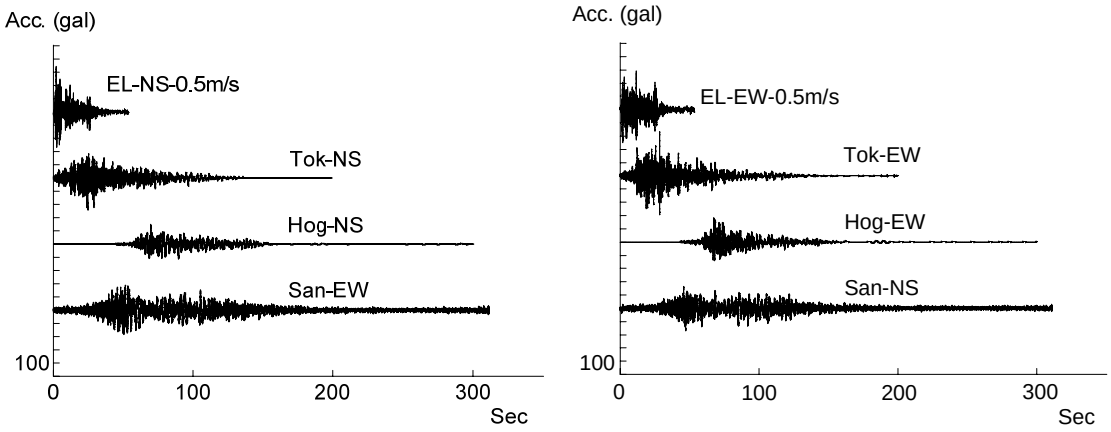

(a) (b)

Figure 2.15 Time histories of input waves: (a) Longitudinal direction; (b) Transverse direction

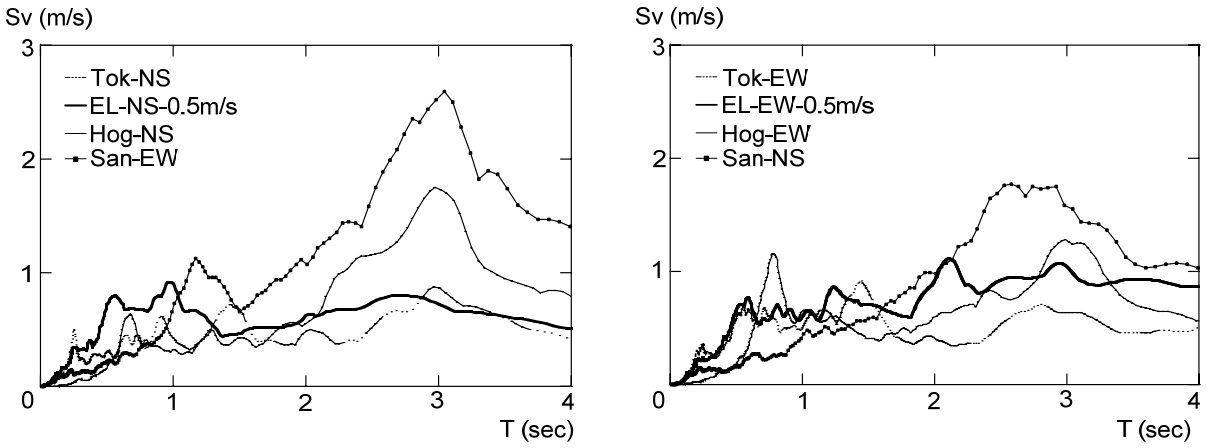

(a) (b)

Figure 2.16 Pseudo velocity response spectra of input waves: (a) Longitudinal direction; (b) Transverse direction

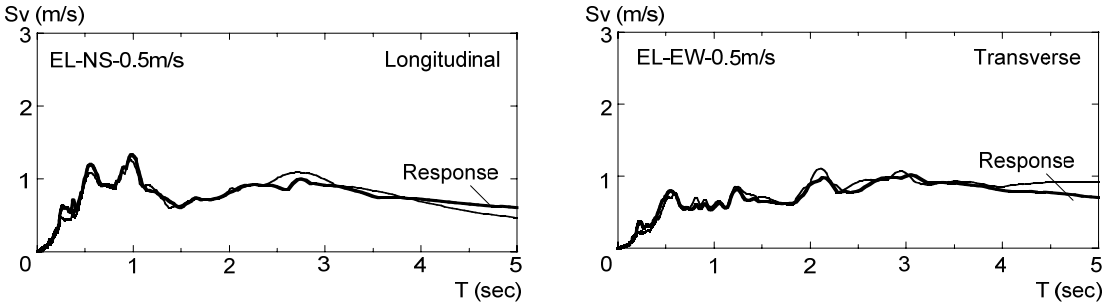

(a)

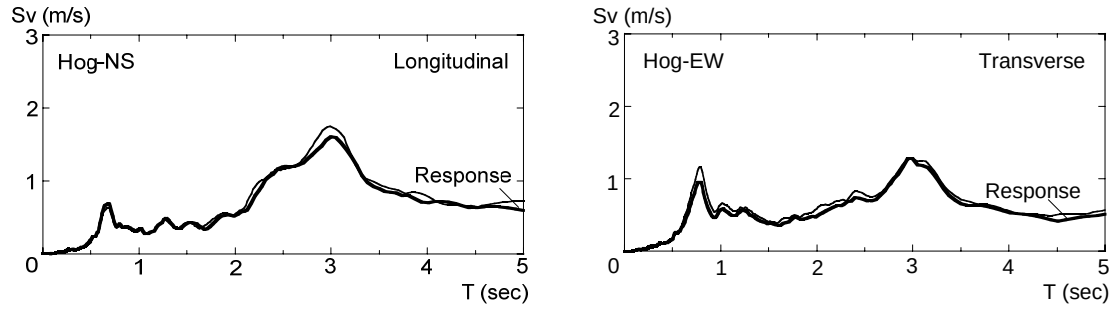

(b)

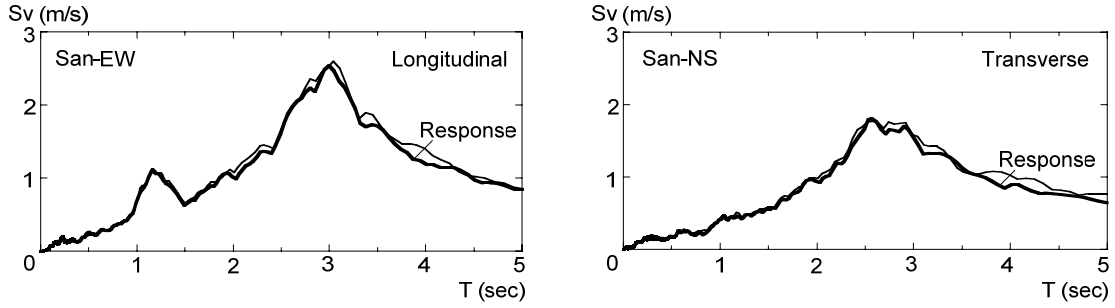

(c)

Figure 2.17 Pseudo velocity response spectra of input waves and response of foundation beams : (a) Response of El Centro wave; (b) Response of Hog wave; (c) Response of San wave

2.6 Vibration characteristic

White-noise inputs were applied prior to each main test. The input was with RMS of 0.6 m/s^2, 250 s in duration, and 0.2 to 20 Hz in frequency bandwidth, and gave a maximum inter-story drift angle of 0.4 to 0.5% in the test frame, and a maximum shear strain of 70% in the rubber bearings.

Table 2.8 shows the frequencies and damping ratios of the first three modes of the test specimen obtained from the test. The first-mode periods were 2.13 s and 2.24 s in the longitudinal and transverse directions, and they were shorter by 11% and 7%, respectively, than the period of 2.4 s assumed for the prototype. In the actual construction, the total weight of the test specimen was about 10% lighter than the design value, which was a primary source of discrepancy. The damping ratios of the first to third modes ranged from 2.6 to 4.7%. Figure 2.18 shows the transfer function of the numerical prototype model, and the test specimen subjected to white noise excitation. The initial story stiffness of prototype model was tuned to fit the first mode period of the test specimen. The first mode damping ratio of the specimen was adopted in the prototype model. The first three mode periods and magnitude of these two curves show notable similarity. Using a transfer function curve fitting method (Birgitte et al. 1992), the first three mode shapes of the specimen were estimated, as shown in Figure 2.19. The first, second and third substitute layers are plotted at the equivalent heights of the prototype, that is, at the ninth, fourteenth, and nineteenth floors. Comparison between the two mode shapes is very reasonable for all three modes.

Table 2.8 Summary of test results from white noise vibrations

(a) Longitudinal direction

Mode	1st	2nd	3rd
Frequency (Hz)	0.47	1.25	1.90
Period (s)	2.13	0.80	0.53
Damping (%)	2.6	3.4	4.7

(b) Transverse direction

Mode	1st	2nd	3rd
Frequency (Hz)	0.45	1.23	1.95
Period (s)	2.24	0.82	0.51
Damping (%)	2.7	2.7	3.4

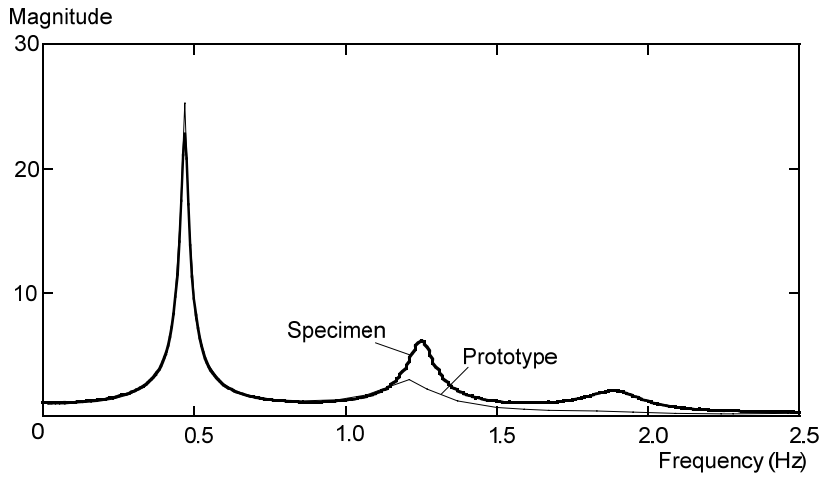

Figure 2.18 Transfer function of test specimen and prototype model

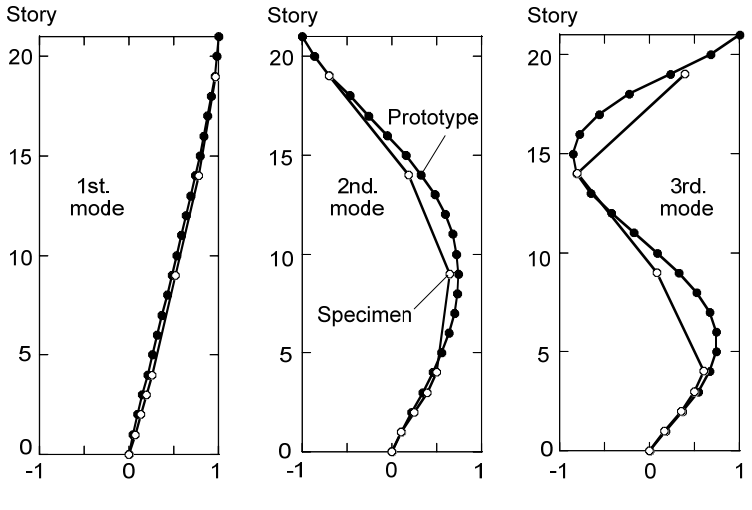

(a) (b) (c)

Figure 2.19 Mode shapes: (a) 1st mode; (b) 2nd mode; (c) 3rd mode

2.7 Conclusions

To evaluate the existing performance of high-rise buildings subjected to long-period ground motions, a series of large scale shaking table tests were conducted using the E-Defense shaking table. The main observations are summarized below:

1. To represent the realistic response of an 80 m height high-rise building, a substructure test method was proposed. The test specimen was developed that consisted of a four-story test frame in the lower part and the substitute layers on top of the frame. The substitute layers made of concrete slabs and rubber bearings were used to represent the vibration characteristics of the prototype.
2. From preliminary vibration tests, the equivalence between the test specimen and the prototype was verified to match reasonably for the first three mode natural periods and corresponding mode shapes.

REFERENCES

[2.1] Architectural Institute of Japan. (2006). Standard for the Ultrasonic Inspection of Weld Defects in Steel structures. (in Japanese)

[2.2] Birgitte, B.J., Jesper, B.J., Soren, D.M., Joegen, T.S. (1992). Curve-Fitting Method for Transfer Function Determination. *Institute of Electrical and Electronics Engineers.,* 71-74.

[2.3] Building Research Institute. (2005). The research report about the influence and seismic retrofit technology to the building subjected to long-period ground motion. Tokyo, Japan. (in Japanese).

[2.4] Editorial Committee for the Report on the Hanshin-Awaji Earthquake Disaster (1997), Report on the Hanshin-Awaji Earthquake Disaster, building Series Volume 3, Structural Damage to Steel Buildings (in Japanese).

[2.5] Fukushima,, T., Ichimura, S., Teramoto, T. (1999). The basic feature history of high rise buildings. *Architectural Institute of Japan.*, 1999, 307-308. (in Japanese).

[2.6] Fukushima, T., Ichimura, S., Teramoto, T. (2000). The design feature history of high rise buildings. *Architectural Institute of Japan.*, 1999, 307-308. (in Japanese).

[2.7] Nakagawa, Y., Kaname, K., Kawabe, H., Irikura, K. (2008). Damage prediction of long-period structures during subduction earthquakes-Part 2: Long-period ground motion prediction in the Osaka basin for future Nankai Earthquakes. *Proc. 14th World Conf. Earthq. Eng*.

[2.8] Nakashima, M., Inoue, K., and Tada, M. (1998). Classification of damage to steel buildings observed in the 1995 Hyogoken-Nanbu earthquake. *Eng. Struct.*, 20(4-6), 271-281.

[2.9] Nakashima, M., Roeder, C. W., and Maruoka, Y. (2000). Steel moment frames for earthquakes in United Stated and Japan. *J. Struct. Eng*., 126(8), 861-868.

[2.10] Nakashima M. (2006). Test on collapse behavior of structural system. *Science & Technology in Japan*, 96, 14-19.

[2.11] Nakashima, M., Matsumiya, T., Suita, K., Liu, D.W. (2006). Test on full-scale three-storey steel moment frame and assessment of ability of numerical simulation to trace cyclic inelastic behavior. *Earthquake Engng. Struct. Dyn.*, 35, 3-19.

[2.12] Nakashima, M. (2008). Roles of Large Structural Testing for the Advancement of Earthquake Engineering. *Proc. 14th World Conf. Earthq. Eng*.

[2.13] Ogawa, N., Ohtani, K., Katayama, T., Shibata, H. (2001). Construction of a three-dimensional, large-scale shaking table and development of core technology. *Phil. Trans. R. Soc. Lond.*, 359, 1725-1751.

[2.14] Taiki, S., Kouich, M., Sekimi, K., Toshio, O. (2008). Study on the seismic safety of high-rise buildings under earthquake ground motions with long period component : Part 1 Structural characteristics of existing high-rise buildings. *Architectural Institute of Japan.*, 2005, 0113-0114. (in Japanese)

[2.15] The Building Center of Japan. (2003). Guidelines for preventing brittle fracture at welded beam-to-column connections in Steel Structures. (in Japanese)

CHAPTER 3

Global Behaviors and Damage Distribution in Steel Frame

3.1 Introduction

The global behaviors and the response of the beam-to-column connections of the test specimen which was presented in Chapter 2 will be described in this chapter and Chapter 4. In this chapter, the reasonability of the test specimen will be confirmed by checking the maximum deformation and story shear force distributions. Second, the long-period ground motions were input sequentially until the fractures to evaluate the performance, capacity, damage progress and deterioration of the test specimen. Finally, the functionality of interior space will be evaluated from the damage observation of the nonstructural components subjected to different levels of seismic loadings.

3.2 Maximum inter-story drifts and global behaviors

Figure 3.1 summarizes the maximum inter-story drift responses of the test specimen under various levels of loading. The responses of the substitute layers are plotted at the corresponding floors. For the level 1 El Centro wave, the maximum inter-story drifts in the second and third stories were slightly smaller than the design limit of 0.5%. For the level 2 El Centro wave, the maximum inter-story drift was slightly smaller than the design limit of 1%. In these scaled El Centro waves, the maximum inter-story drifts were relatively uniform along the height. For the Hog wave, however, the maximum inter-story drifts tended to grow in the lower part. The maximum inter-story drifts in the second and third story were slightly larger than 1%. The maximum strain values measured at the bottom flange reached 0.5% in the level 2 response, but neither cracking nor local buckling was observed.

For the level 3 San wave, the inter-story drifts of the test frame became notably larger after yielding, while the inter-story drifts of the substitute layers remained relatively small. The maximum inter-story drifts in the second and third stories exceeded a drift angle of 1.7% in both the longitudinal and transverse directions. The maximum strain value exceeded 2.4% in the beam ends. Fractures of beam ends occurred at four field weld connections arranged in the transverse direction, while no obvious damage was observed in the shop weld connections placed in the longitudinal direction. The

San wave was inputted in the longitudinal direction sequentially until fractures occurred in the beam-to-column connections. The deformation became larger under the second and the third San wave loadings. Four shop weld connections fractured during the third San wave loading (San-3), and the maximum drift angle grew to 2.2% after the fractures. Figure 3.2 shows the instants of recorded fractures in the time history of the second-story drift angle. Figure 3.3 summarizes the locations of all fractures including the four field weld connections and four shop weld connections (two in the 600mm depth beams and two in the 400mm depth beams). Compared with the corresponding numerical analysis shown in Figure 2.6, the lower part shows about 1.5 times larger inter-story drifts due to those fractures.

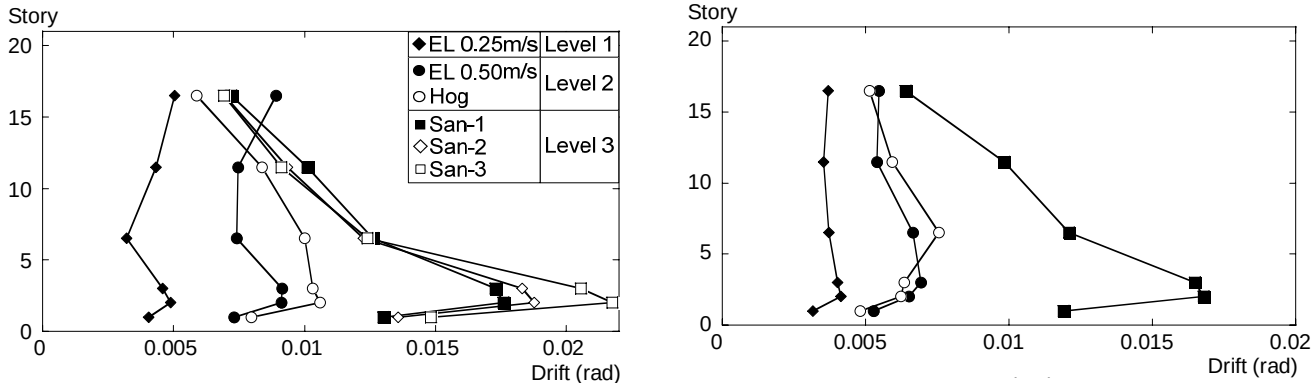

Figure 3.1 Max. inter-story drift angles: (a) Longitudinal direction; (b) Transverse direction

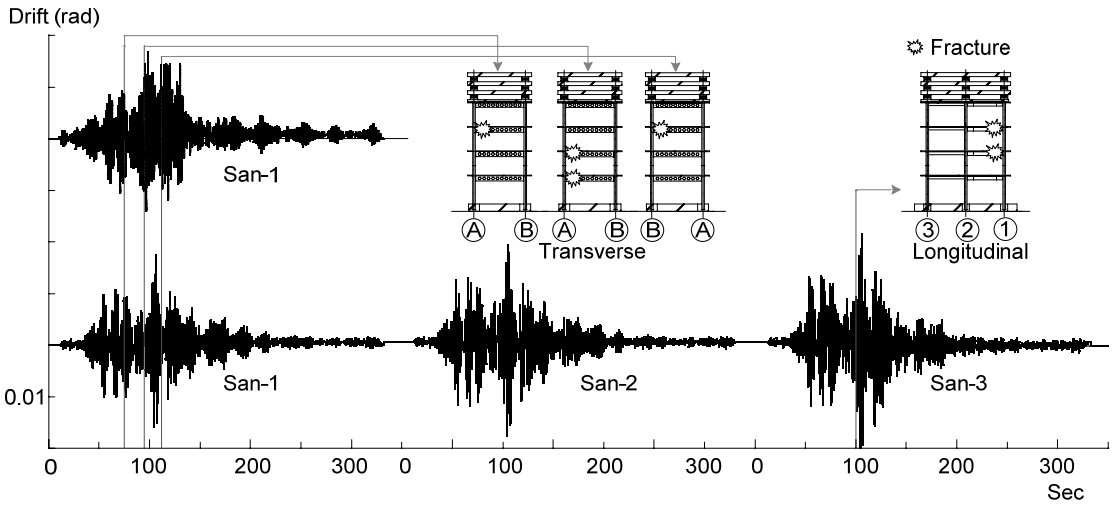

Figure 3.2 Inter-story drift time history (F-3rd Fl) in the transverse direction during the San wave

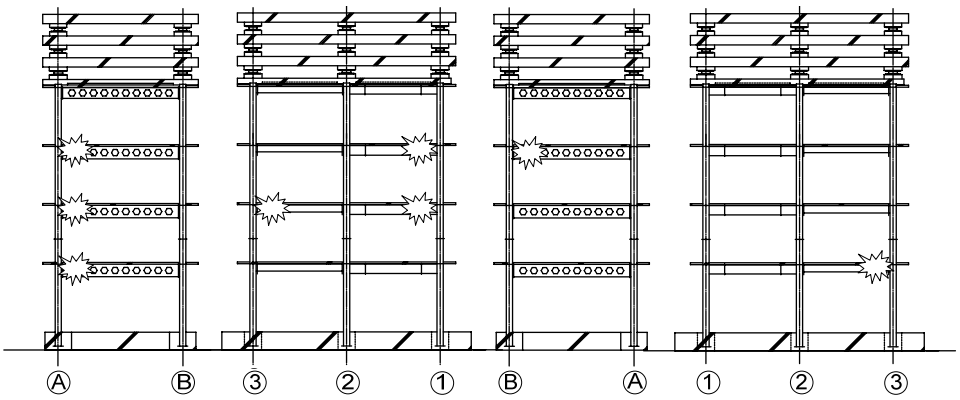

Figure 3.3 Fracture locations

3.3 Seismic response of the test specimen

Figure 3.4 shows the distribution of maximum story shear forces over the height of the test specimen. The shear forces were obtained as the measured acceleration times the story mass and plotted for the corresponding floors. The distributions of the long-period ground motion (the San wave) are similar to the distribution specified in the Japanese building standards (Nakashima et al. 2000). Some effects of higher modes appear for the design El Centro wave, but the first mode dominates overall.

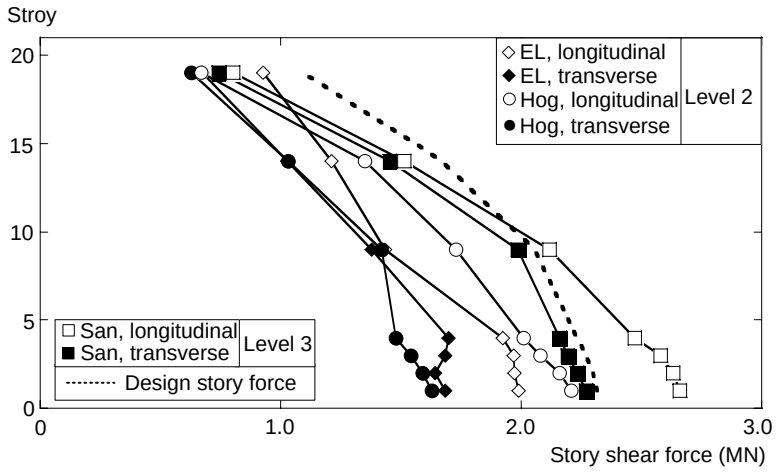

Figure 3.4 Maximum story shear force distribution

3.3.1 Story force and deformation relationship

Figure 3.5 shows the story force and drift angle relationships of the first, second, third, and fifth stories under the level 2 El Centro wave. The shear force coefficient was obtained as the measured acceleration times the story mass and normalized by the floor weights of the upper stories. Yielding of the dampers made the substitute layers possible to exhibit inelastic behavior as similar to the test frame. In reference to the tri-linear relationship adopted based on the statistics in past design practice,

the stiffness and yield strength of the test specimen are notably similar. This indicates that the specimen reasonably followed the Japanese design codes and represented the averaged characteristics of existing high-rise buildings.

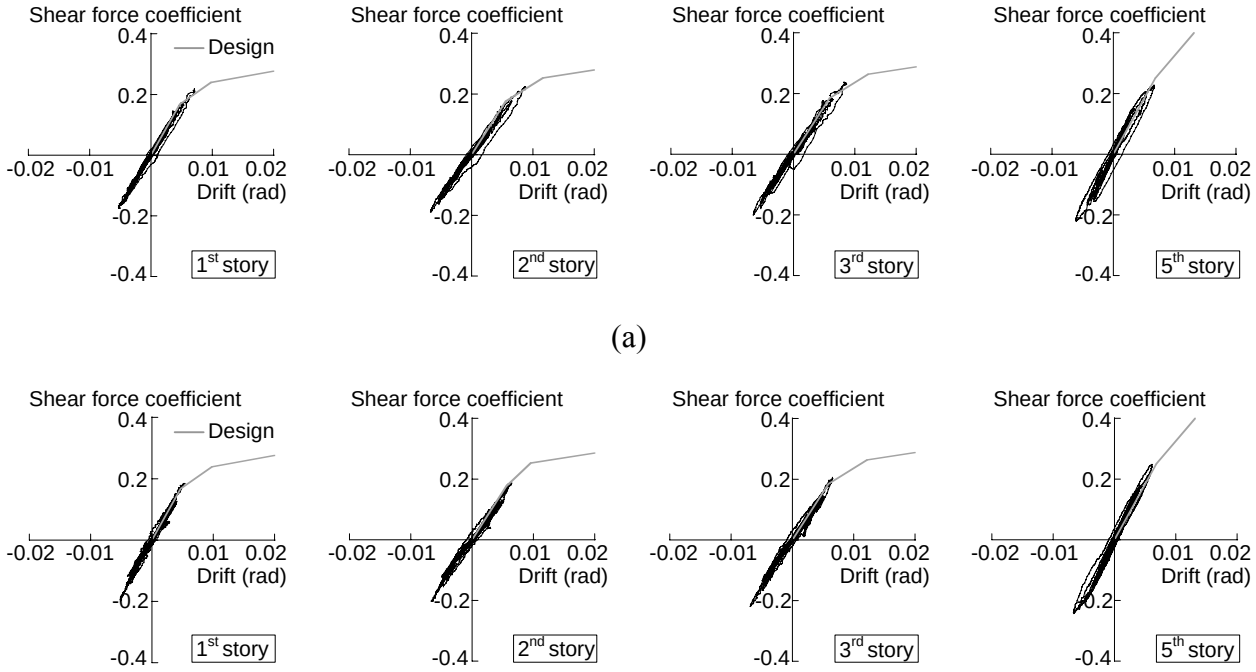

(a)

(b)

Figure 3.5 Story shear force and drift angle subjected to El Centro Level 2 loading:
(a) Longitudinal direction; (b) Transverse direction

Figure 3.6 shows the responses obtained from the first San wave (San-1) to the third San wave (San-3) loadings. The test specimen showed results that are commensurate with the design curve. The resistance of the longitudinal test frame is about 15% larger than the design value. In the longitudinal direction response of the San-3 wave, four fractures made the story stiffness decreased to 17.2 from 22.7. The story stiffness decreased about 25%. Here the stiffness was evaluated as the secant stiffness of the story shear force and drift angle relationship measured from the origin to the 0.005 rad drift angle. In the transverse direction, fractures at the bottom flange of connections made the story stiffness decreased significantly in the positive direction (while the fractured connections were subjected to positive bending). The story stiffness decreased to 15.7 and 18.6 in the positive and negative directions from the initial story stiffness of 28.3, meaning the reduction by 44 and 34% after the four fractures. Most fractures in the transverse direction located in the same position but in different floors. This might have made the story stiffness decreased more notably than that in the longitudinal direction and cause residual deformations of the test specimen at about 0.1% drift angle (see Figures 3.2 and 3.3).

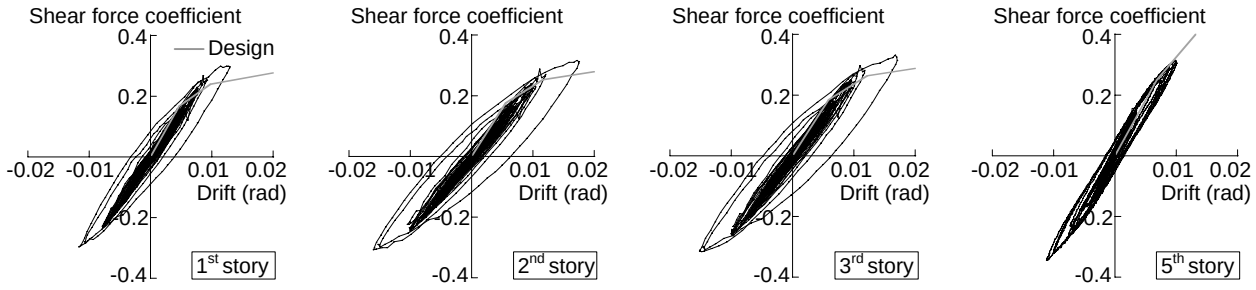

(a)

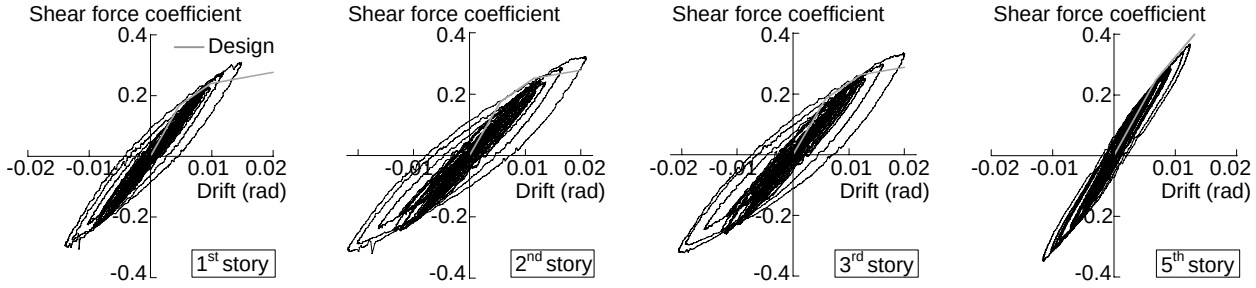

(b)

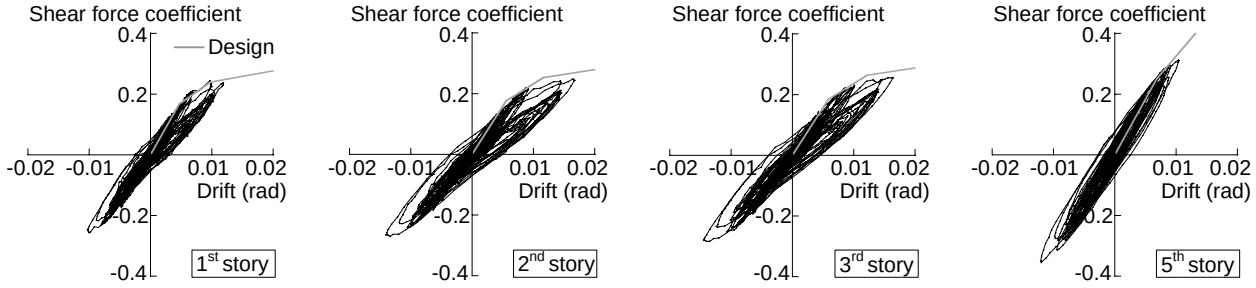

(c)

Figure 3.6 Story shear force and drift angle: (a) Longitudinal (San-1); (b) Longitudinal (San-3); (c) Transverse (San-1)

3.3.2 Change of first natural period

Figure 3.7 shows the first natural period of the test specimen and the pseudo velocity response spectra of the input waves. The first natural periods were obtained by the white-noise inputs applied prior to each main test. The input was with RMS of 0.4 m/s^2, 250 s in duration, and 0.2 to 20 Hz in frequency bandwidth. The initial first natural period was 2.13 and 2.07 s in the longitudinal and transverse directions, respectively. The long-period ground motions: Hog and San waves, predominate at about three second. Increase of the period after each test made the test specimen subject to larger energy input in the succeeding test because of the rising shape of the pseudo velocity response spectra of these long-period ground motions. After the level 2 El Centro loading, the period became 2.15 and 2.21 s in the two directions, respectively. The stiffness of the test specimen decreased about 5 and 12% relative to the initial stiffness. To find out the reason to cause

the decrease, the transverse directional story shear forces obtained from two different methods were compared: one was obtained from the story mass times the acceleration (F_m), and the other obtained from the shear forces applied to the columns placed in one story (F_c). The column shear force was obtained from the strain gauges glued at two sections in the middle part of columns. These two forces are shown in Figure 3.8, which indicates that the shear force obtained from these methods are nearly identical. The nonstructural partition walls that were installed in the transverse directions of the second and the third stories were most unlikely attributed to the contribution to lateral resistance under the level 1 and level 2 El Centro wave loadings. The main reason for the stiffness deduction of the test specimen is considered as the development of slab cracks in the vicinity of connections.

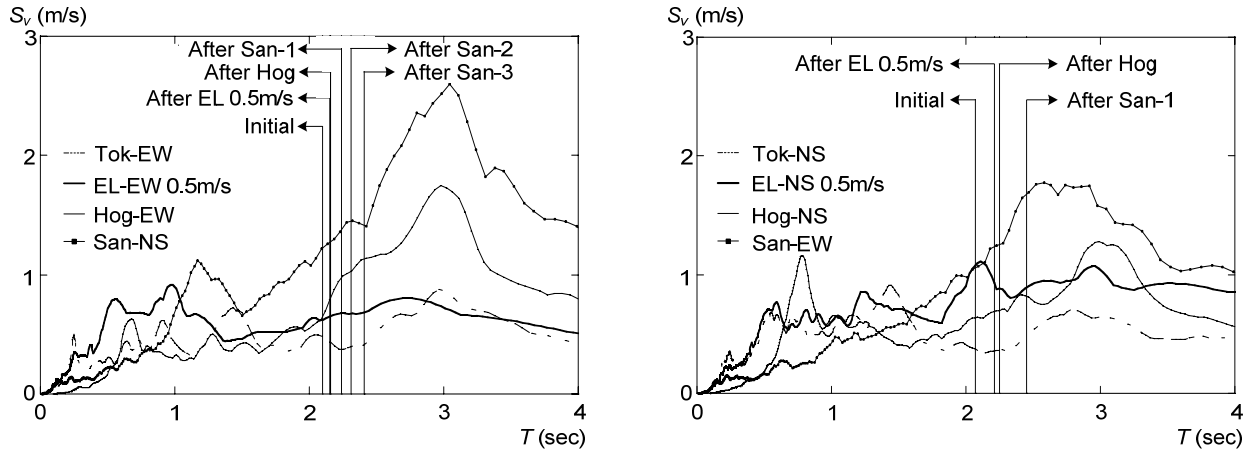

(a) (b)

Figure 3.7 The first natural period and the pseudo velocity response spectra of input waves: (a) Longitudinal direction; (b) Transverse direction

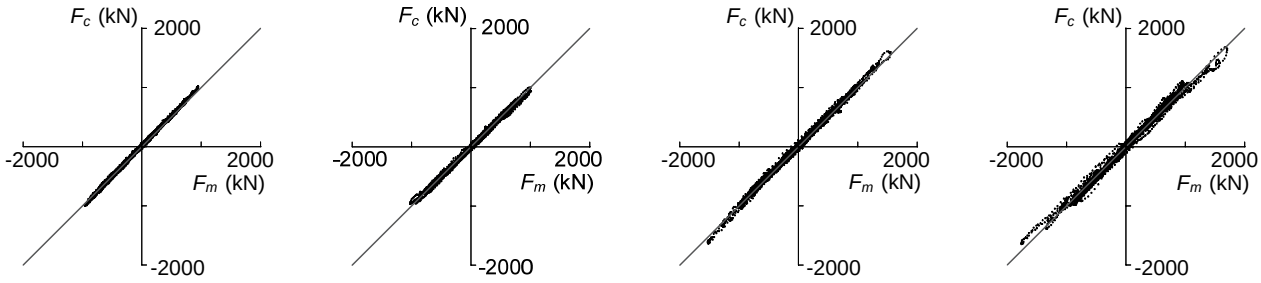

(a) (b) (c) (d)

Figure 3.8 Transverse directional story shear force obtained from columns versus that from the mass times acceleration: (a) Second story (El Centro level1); (b) Third story (El Centro level1); (c) Second story (El Centro level2); (d) Third story (El Centro level2)

After the level 3 San wave loading (San-1), the first mode period increased to 2.25 and 2.45 s in the longitudinal and transverse directions. The stiffness of the test specimen decreased about 8 and 19% in this loading. Four fractures made the stiffness reduction larger in the transverse direction. For the longitudinal direction, the stiffness reduction after San-1 made the test specimen

sustained larger energy input under the second and the third San wave loadings and eventually lead to larger deformations (Figure 3.1 (a)). The first mode period grew to 2.4 s after the third San wave loading (San-3). Fractures of four shop weld connections made the stiffness decreased about 8%. Related to the initial stiffness, the overall stiffness decreased 24 and 28% in the longitudinal and transverse directions after the series of earthquake loadings. Comparing with the story stiffness reduction obtained from the story force and deformation relationship (25% and 44% in the longitudinal (San-3) and transverse (San-1) directions), the stiffness reduction caused by the fractures was more notable in the test frame.

3.4 Floor response and effects of long-period ground motions

3.4.1 Maximum floor response

Figure 3.9 summarizes the maximum floor acceleration, velocity and displacement responses obtained from the level 1 El Centro wave to the third San wave loading (San-3). These maximum values are plotted with respect to the height. The velocity and displacement were obtained by integrating the acceleration record of each floor. Under the level 1 El Centro wave loading, the maximum accelerations in the longitudinal and transverse direction were about 3 and 2 m/s^2. When subjected to the level 2 El Centro wave loading, the accelerations increased to about 7 and 4 m/s^2. The maximum acceleration responses of the Hog wave and San waves, which belonged to level 2 and level 3 earthquakes, were 4 to 5 m/s^2, located between those of the level 1 and level 2 El Centro wave loadings (Figure 3.9(a)). However, the maximum velocity and displacement responses generated by those long-period ground motions became notably larger. The maximum velocity response of the San-1 and San-3 waves were both over 2 m/s, which were about 25% larger than that of the level 2 El Centro wave loading. For the maximum displacement, the difference between the design and long-period ground motions became more notable. The responses in the longitudinal directions were closed to 1 m, which was about two times larger than that of the level 2 El Centro wave loading.

The San-3 wave generated similar responses at the substitute layers with those of the San-1 wave but caused larger displacements in the test frame because of the fractures. To summarize, long-period ground motions were similar in the floor acceleration to that of the design earthquake but generated significant larger floor velocities and displacements. The large floor velocity and displacement are the likely causes for the overturning of unfixed furniture and damage to various nonstructural components **(**Ishiyama et al. 1982, Midorikawa et al. 1995**).**

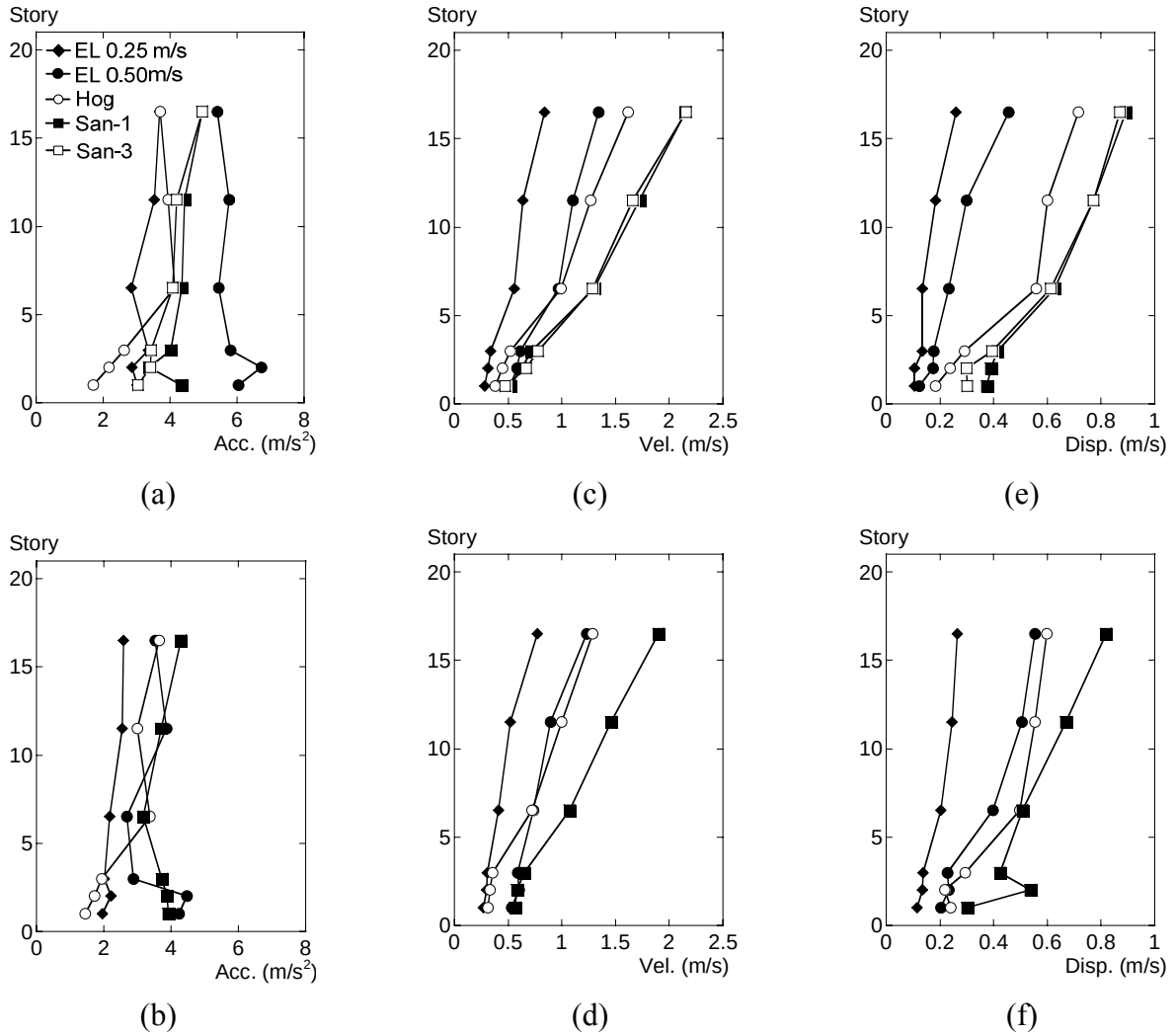

Figure 3.9 Maximum floor response: (a) Longitudinal acceleration; (b) Transverse acceleration; (c) Longitudinal velocity; (d) Transverse velocity; (e) Longitudinal displacement; (b) Transverse displacement

Figure 3.10 shows the acceleration, velocity and displacement responses at the roof of the test specimen subjected to the level 2 El Centro and San-1 waves. Responses of these two waves showed clearer comparison between the design wave and long-period ground motion. The maximum accelerations of these waves were both about 6 m/s^2. The strong shaking duration were significantly different. The shaking while the acceleration exceeded 2 m/s^2 amplitude lasted for about 10 and 120 s in these two waves. The strong shaking duration from the long-period ground motion was about twelve times longer than that of the design wave. From the velocity and displacement time histories, long-period ground motion generated floor velocities over 1.5 m/s and displacements over 0.7 m for over two minutes. Cumulative deformations could be significantly lager than those expected in the design wave.

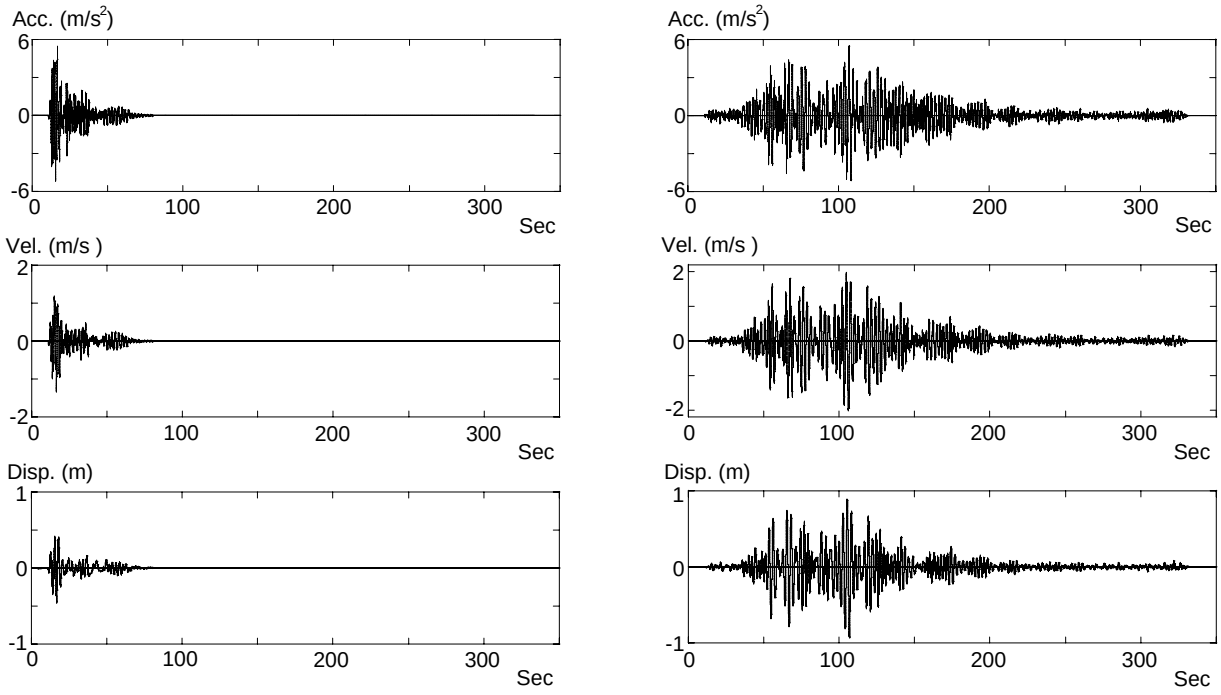

Figure 3.10 Roof floor response in longitudinal direction: (a) Response of El Centro Level 2; (b) Response of San-1

3.4.2 Cumulative inter-story plastic deformation ratio

Figure 3.11 shows the growth of cumulative inter-story ductility ratio of the second story, which sustained the maximum drift angles for all loading cases. These values, obtained after each ground motion, were summed up to the first connection fracture. The yield drift angle was 0.5 % for all stories and used to normalize the cumulative plastic inter-story drift angle. The first San wave (San-1) generated cumulative inter-story plastic deformation ratios of 18 and 37 in the transverse and longitudinal direction, respectively. The level 2 El Centro wave generated cumulative inter-story plastic deformation ratios of 2 in both directions. It is notable that the long-period ground motion generated more than ten times the cumulative plastic deformation than what was expected by the design wave.

After the 1994 Northridge earthquake, extensive analyses were conducted on the performance of beam-to-column connections (FEMA 350, 2000). Based on numerous tests and analyses at that time, a standard loading protocol by which performance of beam-to-column connections was qualified (AISC 2005) was developed. According to the protocol, the loading history consists of six cycles each for drift angles of 0.375%, 0.5%, and 0.75%, four cycles for drift angles of 1%, and 2%, and two cycles each for drift angles with an increment in drift angle of 1%. The tested connection is qualified if it sustains at least 80% of the full plastic moment, ${}_bM_p$, after the completion of the drift angle of 4%. Suppose that the yield drift angle is 0.5%, the cumulative inter-story plastic deformation ratio reached with this protocol is 161 at the end of loading with the drift angle of 4%. When looking

into the cumulative inter-story plastic deformation ratio obtained from the test, the first San wave generated about 40 in the cumulative ratio, and after all three San waves, the cumulative inter-story plastic deformation ratio reached about 150. The cumulative inter-story plastic deformation ratio of 161 stipulated by the AISC is still larger than the value, meaning more than a value expected for three times the long-period ground motion. The criteria stipulated by AISC may be too stringent for the performance checking of beam-to-column connections of high-rise buildings when they are subjected to long-period ground motions.

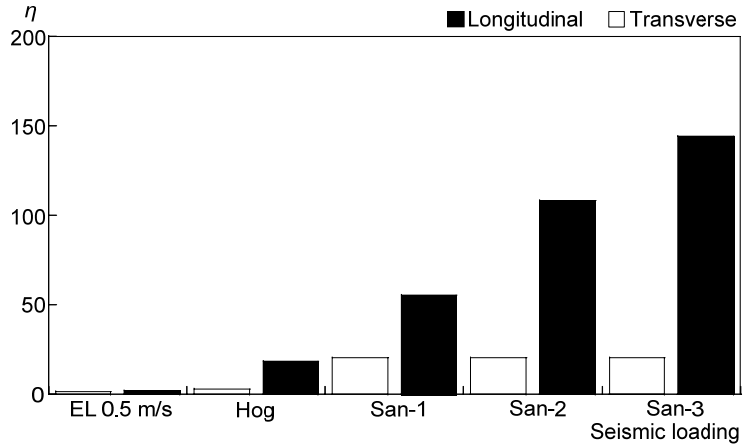

Figure 3.11 Cumulative inter-story plastic deformation ratio

3.4.3 Story ductility ratio and story cumulative ductility ratio

The story ductility ratio, μ, was defined as the maximum inter-story drift divided by the story yield drift. The story yield drift angle was estimated as 0.55 and 0.45% for the longitudinal and transverse directions, respectively. The story cumulative ductility ratio was defined as the total energy dissipation of each story divided by the product of the story yield drift and the corresponding story shear force (Akiyama 2002). Both ductility and cumulative ductility reached their largest values in the second story (Figure 3.12). The ductility ratios observed in both the level 2 El Centro and Hog waves were about two, and that observed in the San-1 wave was about three. On the other hand, the cumulative ductility ratios of the Hog and San-1 waves reached four times and fifteen times that observed in the level 2 El Centro wave. Large values of cumulative ductility ratio relative to ductility ratio are very notable in the long-period input waves.

Under the San-1 wave, the μ value of the transverse direction was enlarged to about 2.5 because of the fractures (Figure 3.3). The value remained smaller than that of the longitudinal direction. However, the fractures caused significantly large cumulative ductility at a ratio of 43 which was 1.7 times of that in the longitudinal direction. The large cumulative ductility caused by a few fractures could become a very high demand to the other unfractured connections in the test frame.

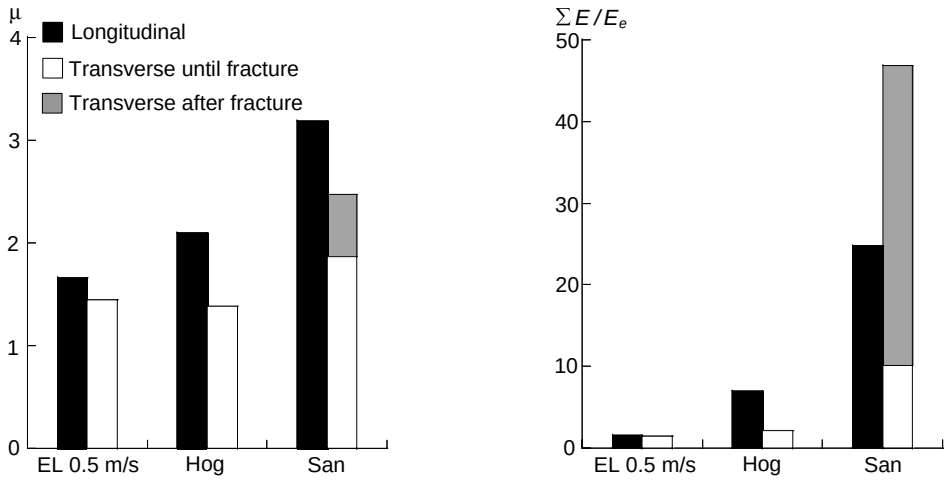

(a) (b)

Figure 3.12 Inter-story deformations: (a) Max. ductility ratio; (b) Cumulative ductility ratio

Figure 3.13 shows the distribution of cumulative ductility ratios with the height of the test specimen. The dotted lines represent the cumulative values measured until the first fracture. This figure showed similar results with the maximum inter-story drift angle distribution (Figure 3.1). Each story of the test specimen sustained similar cumulative ductility ratios when subjected to the level 2 El Centro wave loading. The cumulative ductility ratios started to concentrate on the test frame after this loading. The San-1, San-2 and San-3 waves exhibited significant cumulative ductility ratios at the second and third stories, which were about 15, 20 and 25 times larger than that of the design wave. The large cumulative ductility concentrations in these two stories made most fractures occurred at these two stories (Figure 3.4) and caused the cumulative ductility in the substitute layers reduced after each San wave loading.

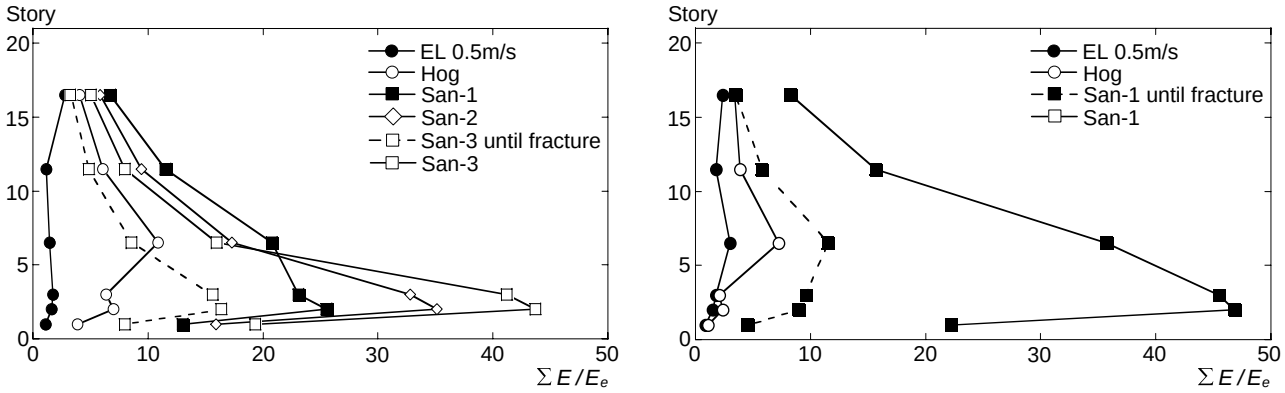

(a) (b)

Figure 3.13 Distribution of inter-story cumulative ductility ratios: (a) Longitudinal direction; (b) Transverse direction

3.5 Nonstructural components

Figure 3.14 shows the plan arrangement of the ALC panels and drywall partitions. These partition walls were arranged in two directions with interior doors inserted. In the transverse directions, larger span partition walls were arranged than in the longitudinal direction. For the level 1 El Centro wave loading (with the maximum drift angle in the transverse direction was 0.4%), rocking of the ALC panels were observed and made the panels cracked at the bottom edge in three locations (Figure 3.15). For the drywall partitions, cracks and deformations of plaster boards were observed along the door frame. No damage was observed in the doors inserted in the ALC panel partition. Floor slabs cracked at the foot of door frame inserted in the drywall partition. For the level 2 El Centro loading (with the maximum drift angle was 0.9%), no further damage of the ALC panel partition was observed except the cracks observed in the level 1 loading. The plaster boards of the drywall started to bump out from the wall because of the compression in the plane. The door frame installed in the drywall was deformed further, but the door remained operational. For the San-1 wave (with the maximum drift angle of 1.5%), no further damage was observed in the ALC panels except those observed in the level 1 and 2 loadings. Rocking of the ALC panels made panels sustain less in plane compression and reduce the damage. The doors installed in the ALC panels had no damage, either. Three plaster boards of the drywall partition dropped off especially at the corner of the wall due to the large inter-story deformations generated by the long-period ground motion. The door frames and panels inserted in the drywall partition was seriously deformed, because the deformed frame bumped into the door panels and made the doors unable to close again. The past full scale shaking table tests that also examined the ALC panel and drywall partitions showed similar results with those obtained in this test (Akazawa et al. 2008, Lee et al. 2006).

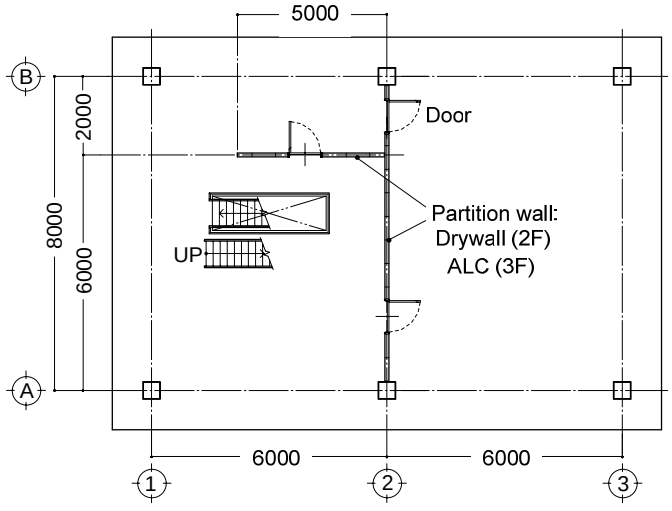

Figure 3.14 Nonstructural component plan

Figure 3.15 Damage to various nonstructural components

3.6 Conclusions

The long-period ground motions were input sequentially until the test specimen sustained serious damage, i.e., fractures of multiple beam-to-column connections. The demands of long-period ground motions, progress of damage, stiffness deterioration of the test frame and the functionality of the interior space were quantitatively evaluated in this chapter. The main observations are summarized below:

1. The maximum drift angles of the test specimen were smaller than 0.5% and 1.0% under the level 1 and level 2 design earthquake loadings. The test specimen remained elastic under the level 1 test, and no serious damage was observed in the level 2 loading. The story shear force distribution along the height was similar to the distribution specified in the Japanese building standard. The story shear force and inter-story drift relationships obtained from the test also showed notable correspondence with the design values. These indicated that the test specimen shaking in this study satisfied the requirements stipulated in the Japanese seismic design code and reasonably represented the actual high-rise buildings.
2. A few beam-to-column connections fractured under the level 3 long-period ground motion loadings, i.e., San-1 to San-3. Connections in the transverse direction of the test specimen fractured in four locations under the first San wave loading (San-1). Connections in the longitudinal direction fractured in four locations when subjected to the third San wave loading (San-3). Fractures made the maximum story drift angle grew to 1.7 and 2.2% in the transverse and longitudinal directions, respectively. Comparing with the initial stiffness (before the tests), stiffness of the two directions of the test specimen decreased 18 and 9%, respectively, in the San-1 and San-3 wave loadings.
3. When subjected to long-period ground motion (Hog wave), the test specimen diclosed cumulative ductility ratios more than four times that considered in the design (level 2 El Centro),

while the maximum story drifts remained nearly the same as the design value. The story cumulative ductility ratio of the level 3 San wave reached fifteen times that given in the Level 2 El Centro wave. This is the most notable behavior that characterizes the responses in the long period ground motions. The long-period ground motion (San wave) generated similar magnitudes of acceleration with the design wave at a value of about 6 m/s^2, but significant larger floor velocity and displacement of about 2 m/s and 1m while those of the design wave were 1.2 m/s and 0.4 m. The large velocity and displacement lasted for over two minutes and generated significantly large cumulative ductility ratio.

4. For the level 1 El Centro wave loading, no damage was observed in the nonstructural components except for small cracks and deformation of the panels in the ALC panel partition and drywall partitions. For the level 2 loading, cracks and deformation of the panel grew, but there were no drops or deformation of the doors that could affect the functionality of the interior space. When subjected to the level 3 San wave loading (with the maximum drift angle of 1.7%), no further damage was observed in the ALC panel partition. Plaster panels of the drywall partition dropped in multiple locations especially at the corner of the wall. Doors which were installed in the drywall partition were seriously deformed and made the doors unable to close again.

REFERENCES

[3.1] Architectural Institute of Japan. (2006). Standard for the Ultrasonic Inspection of Weld Defects in Steel structures. (in Japanese)

[3.2] Japan Society of Civil Engineering. Architectural Institute of Japan. (2006). Report of seismic performance improvement of civil, architectural structures subjected to long-period ground motions generated by subduction zone. (in Japanese).

[3.3] Suita. K., Kitamura, Y., Goto, T., Iwata, T., Kamae, K. (2007) Seismic Response of High-Rise Buildings Constructed in 1970s Subjected to Long-Period Ground Motions. *Journal of structural and construction engineering, Architectural Institute of Japan.* 611, 055-061. (in Japanese with English abstract).

[3.4] Kojika, Y., Mayahara, T., Kawasaki, M., and Kitamura, H. (2007). Damage evaluation of a steel structure super high-rise building for long period earthquake vibration: Part 1 The maximum of a member level, accumulation value. *Architectural Institute of Japan.*, 2007, 0461-0462. (in Japanese).

[3.5] Lee, T.H., Kato, M., Matsumiya, T., Suita, K., and Nakashima, M. (2006). Seismic performance evaluation of non-structural components: Drywall partitions. Journal of Earthquake Engineering and Structural Dynamics, Vol.36, No.3, March 2007, pp.367-382.

[3.6] Akazawa, M., Matsuoka, Y., Suita, K., Yamada, S., and Shimada, Y., (2008).E-Defense experimental for Steel Buildings: Part 26 Behavior of Interior Material on Full-scale 4-story building Collapse Test. *Architectural Institute of Japan.*, 2008, 0843-0844. (in Japanese).

[3.7] Akiyama, H. Collapse modes of structures under strong motions of earthquake. Annals of

Geophysics, Vol. 45, N. 6, December, 2002.

[3.8] Nakashima, M., Roeder, C. W., and Maruoka, Y. (2000). Steel moment frames for earthquakes in United Stated and Japan. *J. Struct. Eng*., 126(8), 861-868.

[3.9] Ishiyama, Y. (1982). Motions of rigid Bodes and Criteria for Overturning by Earthquake Excitations, Vol.10, No.5, 1982, pp.635-650

[3.10] Midorikawa, S., Satoh, T. (1995). Investigation on Overturning of Furniture at Kushiro City Hall and Kushiro Local Meteorological Observatory During the 1993 Kushiro-Oki Earthquake: Relation of overturning rate with floor response. *Journal of structural and construction engineering, Architectural Institute of Japan.* 469, 053-060. (in Japanese with English abstract).

CHAPTER 4

Seismic Capacity of Beam-to-Column Connection of Existing High-rise Building

4.1 Introduction

In this chapter, the seismic capacity of beam-to-column connections in the test specimen are examined from a series of shaking table tests in which a long-period ground motion was applied for multiple times until fractures occurred in the connections. First, fracture reasons were examined by the fracture surface examination. Second, the effect of RC floor slab on the connection behavior is investigated by comparing the results obtained from the tests with those of bare beam tests obtained in the past. Third, the cumulative ductility capacity of these connections is quantified in reference to the test results.

4.2 Damages of beam-to-column connections

Figure 4.1 illustrates the damage distribution of the second to the forth floor connections observed after the end of tests. Damage wildly distributed at these connections and they were categorized as fracture, local bucking, and crack by visual inspection. Fracture was defined as a break of the flange or severe cracks that lead the resistance of connection significantly decrease to at least 80% lower of the experienced maximum strength. Within the fifty-six connections in the test frame, eight fractures occurred in the end and all of them were outer-column connections. Field weld connection and shop weld connection both fractured at four locations. Figure 4.2 shows the close-up of the damages. Local buckling occurred at web and bottom flange and only observed in the shop weld connections (Figure 4.2(a)). Cracks occurred at the bottom flange weld access holes (Figure 4.2(b)). Owing to the shape of weld access holes, the cracks occurred at the bottom flange welding boundary of the field weld connection. For shop weld connection, cracks started from the flange and web medals. Figure 4.2(c), shows a seriously cracked field weld connection. The crack also started from the toe of weld access hole and extended through flange metal and the welding boundary. The connection was qualified as a fracture because the crack lead the resistance decrease to 80% of the maximum strength in the end (illustrated as WL in Figure 4.8(c)).

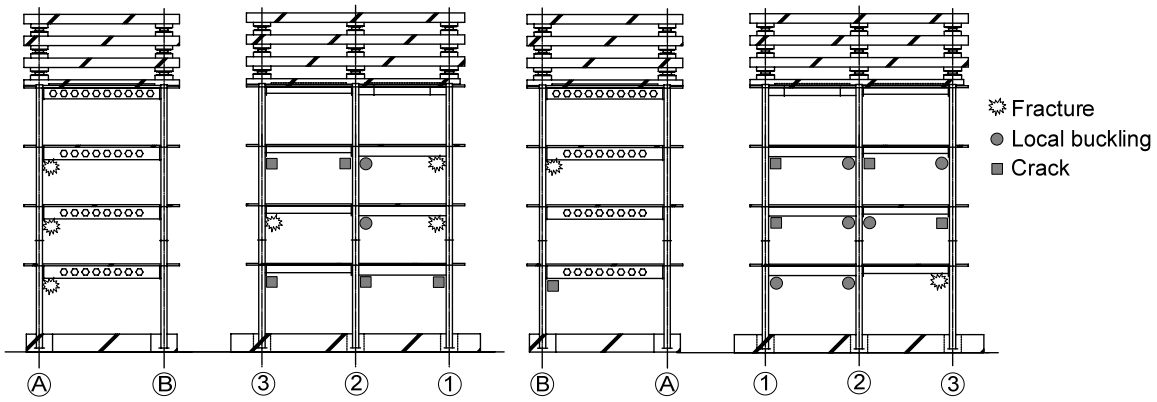

Figure 4.1 Observations of connections

(a) (b) (c)

Figure 4.2 Damage of connections: (a) Local buckling; (b) Cracks; (c) Severe crack

The close-up views of the other three fractured field weld connections were showed in Figure 4.3. Fractures occurred along the weld boundary of the bottom flange without notable deformation or local bucking at web or flange. Several cracks were observed at the same location of other unfractured field weld connections. It's believed that stress was extremely concentrated on the weld access hole end, as initial cracks were formed from here and developed to brittle fracture, eventually.

Many connections fractured in the 1994 Northridge earthquake and 1995 Hyogoken-Nanbu earthquake (FEMA 350; Bertero et al. 1994; Nakashima et al. 2000). The connections adopted in this test, however, differed significantly from the connections damaged in those earthquakes. In this test, box columns with inner-diaphragms were used to replicate Japanese high-rise buildings. In the US, wide-flange columns have been used, while square tube columns with through-diaphragms were adopted in nearly all damaged connections in the Hyogoken-Nanbu earthquake. The shapes of the weld access holes as well as the weld materials were not identical to each other, either. In the Hyogoken-Nanbu earthquake, fracture surfaces were brittle with little sign of plastic deformations, and most of them were observed at the complete joint penetration (CJP) weld between the beam bottom flange and column (Report on the Hanshin-Awaji Earthquake Disaster, 1997). In this test, fractures also occurred at similar locations.

(a) (b) (c)

Figure 4.3 Fractures of field weld connections: (a) The second floor connection; (b) The third floor connection; (c) The forth floor connection

Fractures of shop weld connections are shown in Figure 4.4. Initial cracks at the toe of the weld access hole grew to the fracture of bottom flange metal. The shop welded web connection fractured after the fracture of the bottom flange. After the Hyogoken-Nanbu earthquake, failures of shop weld connections were also observed in the damaged buildings (Report on the Hanshin-Awaji Earthquake Disaster, 1997). The report indicated that 3.3% of the 2396 inspected shop weld connections were damaged including fractures or cracks. 20.5% of the damaged connections were fractured at the flange metal. Shop weld connections in this test showed similar failure mode.

(a) (b) (c)

Figure 4.4 Fractures of shop weld connections: (a) Third floor (NR); (b) Forth floor (NR); (c) Third floor (SL)

4.3 Bending moment versus rotation relationship

Measurement of bending moment

Figure 4.5 shows the typical plan of the specimen. Shop weld and field weld connections were arranged in the longitudinal and transverse direction of test specimen, respectively. In each of the second to forth stories, eight connections were chosen for detailed recording, which resulted in a total of twenty four connections for investigation of detailed hysteretic behavior.

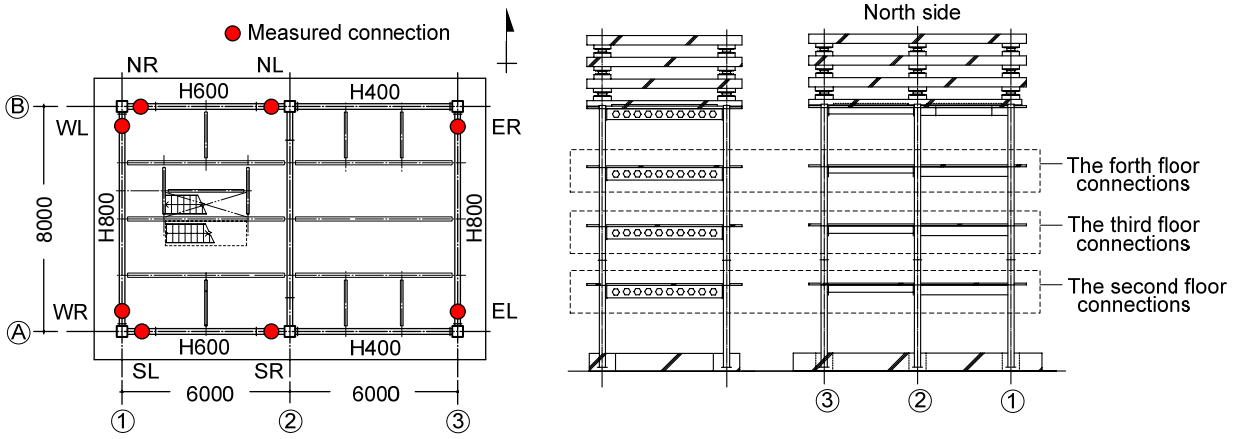

(a) (b)

Figure 4.5 Measurement of connections: (a) Typical specimen plan; (b) Elevation

The bending moment of the beam end was obtained by extrapolating the bending moments measured in two cross-section located in the elastic portion of the beam (L'=1.8 m, Figure 4.6(b)). Moments in the sections were obtained by multiplying the section forces obtain from the measured strain (ε_i) and correspondent area (A_i) by the distance from the gauges to the center of RC floor slab (Figure 4.6(a)). The rotation was the angle measured between the beam end and beam mid-span.

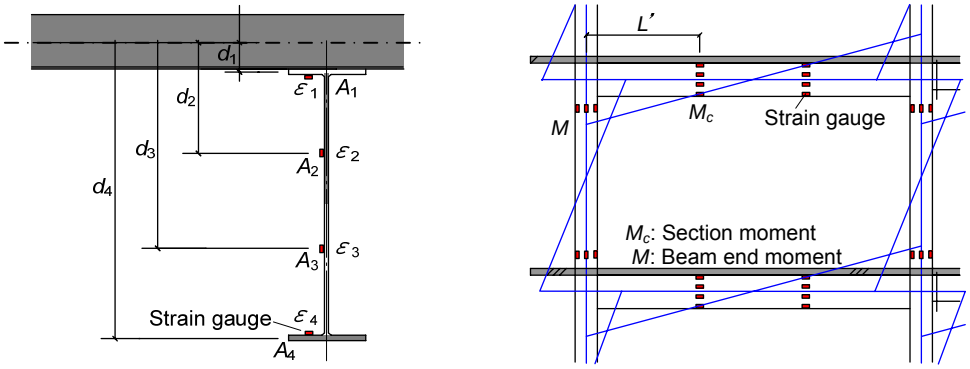

(a) (b)

Figure 4.6 Measurement of the connection strength: (a) Section moment estimation; (b) Estimation of beam end moment

Bending moment versus rotation relationship

Figure 4.7 shows the bending moment versus rotation relationships of the twelve field weld connections under the first San wave loading. The bending moment is normalized by the full plastic moment, ${}_bM_p$, of the bare beam, with the yield strength of steel obtained from the coupon test.

Field weld connections fractured at four locations. Three fractures (illustrated as EL in Figures 4.7(a), (b) and (c)) occurred at the bottom flange at a rotation of about 0.007 rad, while the strength reached about 1.1 ${}_bM_p$ on the average. The other fracture (illustrated as WL in Figure 4.7(c)) occurred at the bottom flange at a larger rotation and strength of 0.012 rad and 1.3 ${}_bM_p$,

respectively. In the positive bending, the resistance decreased rapidly after the fracture, while the bolts connecting the shear plate and web remained unfractured. Resistance recovered from about 1%s rotation because of the contact of slid bolts and web metal. Figure 4.8 shows the deformation of the bolt hole of the shear tab. During the succeeding negative bending, the fracture surface was closed, and the resistance recovered. Connections at ER, where located at the opposite side of the connection at EL (Figure 4.5), sustained large deformation at negative bending owing to the low positive resistance of fractured connections.

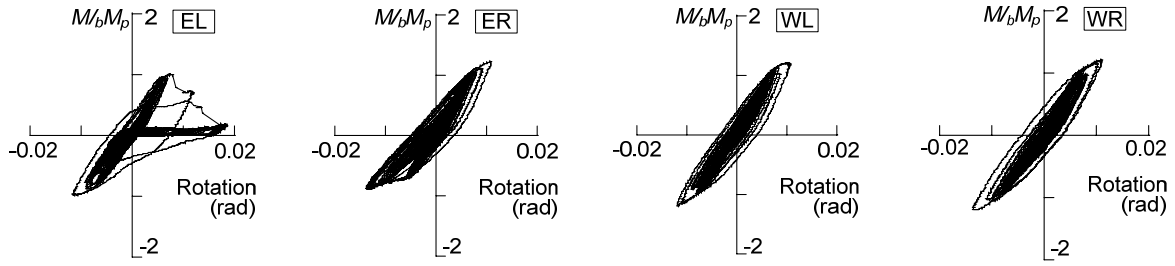

(a)

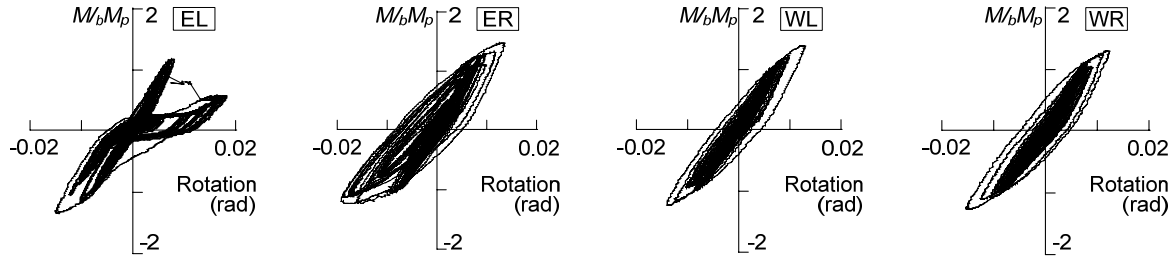

(b)

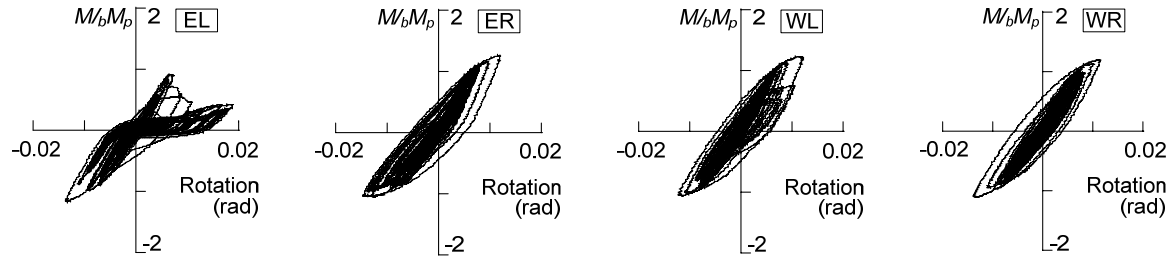

(c)

Figure 4.7 Hysteretic behavior of field weld connections (San-1): (a) Second floor connections; (b) Third floor connections; (c) Forth floor connections

Figure 4.8 Deformation of bolt hole

Figure 4.9 shows the hysteretic behaviors of shop weld connections under the third san wave loading. None of the shop weld connections fractured during the first and second San wave loadings, and all connections exhibited stable behavior. During the third San wave loading, two connections fractured and the others were able to sustain rotation of over 0.02rad stably. From the hysteretic behaviors, fracture at the bottom flange and crack in the web leave very little resistance remain in the positive bending. The two fractures occurred at similar instance while the beam rotation was about 0.015 rad.

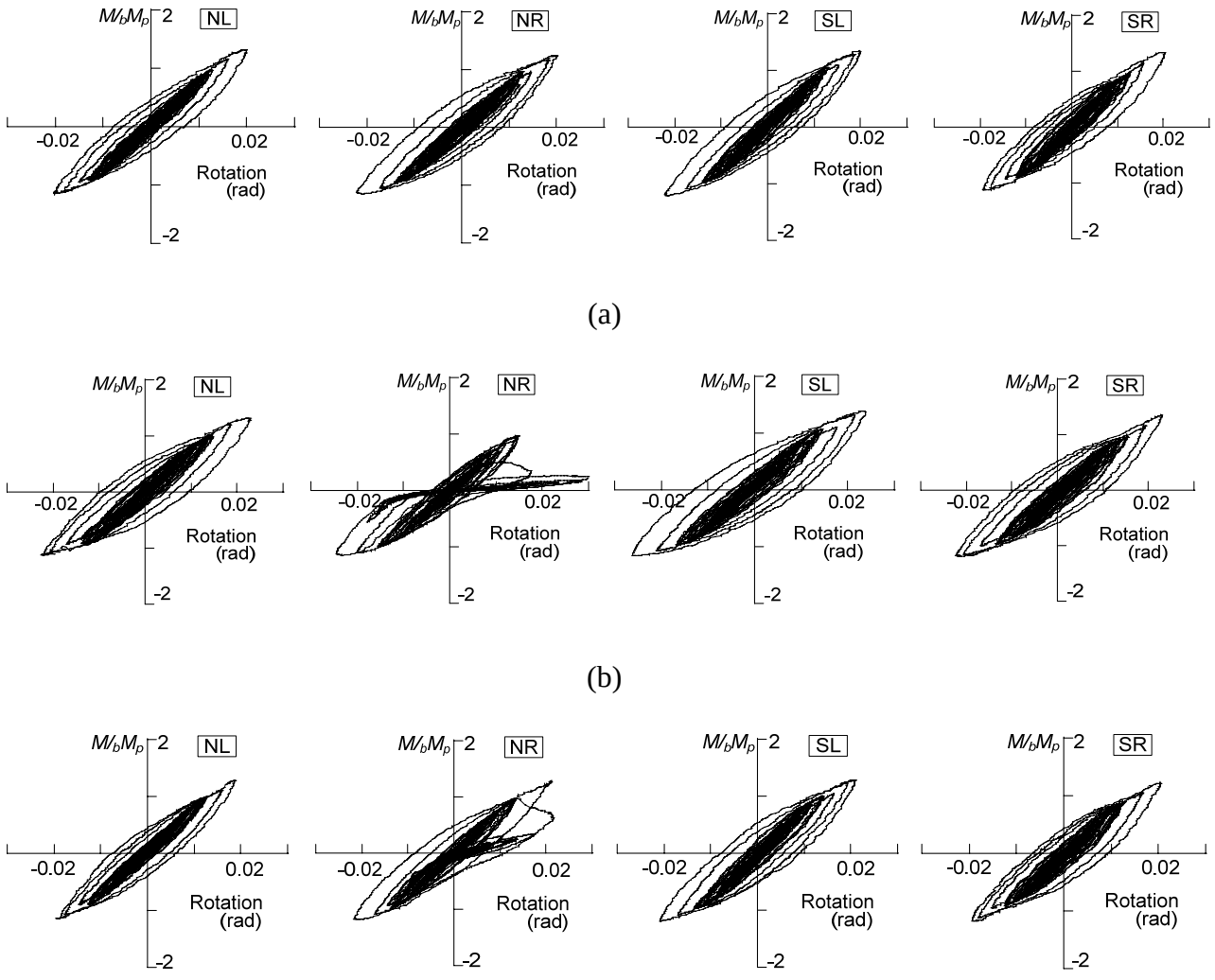

(a)

(b)

(c)

Figure 4.9 Hysteretic behavior of shop weld connections (San-3): (a) Second floor connections; (b) Third floor connections; (c) Forth floor connections

Figure 4.10 shows the hysteretic behaviors of two fractured third floor connections subjected to the level 2 El Centro, Hog and San wave loadings. The connections both sustained the maximum deformation in the test frame (maximum inter-story drift occurred at the second and third stories). Filed weld connection showed slight inelastic behaviors under the level 2 El Centro and Hog wave loading while the maximum beam rotation was about 0.006 rad (Figure 4.10(a)). Connection

fractured under the first San wave loading at the maximum beam rotation of about 0.009 rad. Before fracture, connection experienced fewer plastic cycles than other unfracured ones (Figure 4.8).

Shop weld connection sustained larger deformation than that of field weld connection under the three loadings. Maximum rotation of shop weld connection was 0.008 rad under the level 2 El Centro wave loading while the maximum inter-story drift angle was 0.9%. The fractured shop weld connection was able to sustain the maximum resistance of 1.3 $_bM_p$ in the positive bending and rotation of 0.022 rad under the second San wave loading. Connection showed stable hysteretic loops before the fracture and experienced notable plastic cycles than that of field weld connection.

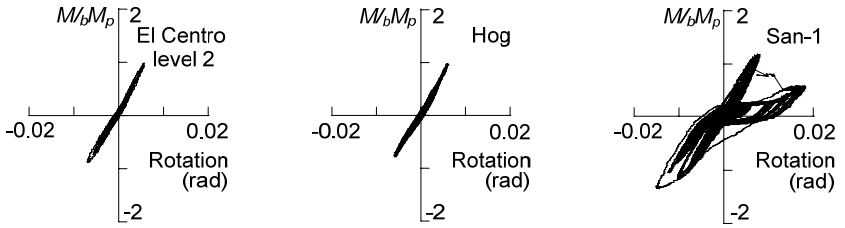

(a)

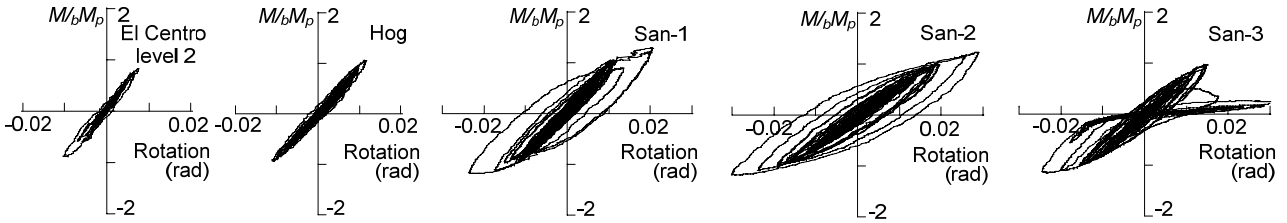

(b)

Figure 4.10 Hysteretic behavior of fractured connections: (a) Field weld connection (the third floor, EL); (b) Shop weld connection (the third floor, NR)

4.4 Examination of fracture surfaces

In the field weld connections, welders have to work on unstable scaffolds in a high altitude. Due to the presence of beam web, welding at the bottom flange have to be interrupted at the web, and the welder have to move to the other side of the beam to weld the next pass every after he/she finishes one pass in the front. In the shop weld connection, all welds are applied in the shop. The full penetration weld at the top flange is finished first; then the connection is overturned by 180 degrees, and the weld of the bottom flange is applied in the same way as that of the top flange. Note that welding in the bottom flange is not interrupted in the middle of the flange. Past tests indicated that weld quality in this area could dominate the capacity of connections (for example, Engelhardt et al. 1993).

In the E-Defense specimen, construction of the specimen and welds of the connections followed as closely as possible the actual situation in the construction field. The welders worked in an altitude of about 15 m. All welders were certified, and all groove welds were ultrasonically tested

and qualified by an independent welding-inspection firm. Nonetheless, the welded surfaces were as shown in Figure 4.11. In comparison with the shop welded fracture surface that showed ductile fracture, multiple weld defaults (the incomplete fusion) were observed in the field weld connection, particularly in the central area, i.e., the vicinity of the toe of the weld access hole. These defaults were not detected in the ultrasonic tests. Although named the field weld connection, almost all previous laboratory tests with the field weld connections were fabricated in the laboratory and in no high altitude. In those tests, the ultra sonic inspection was also implemented in most ideal conditions. The results of this test suggest the difficulties in quantifying the difference in weld quality between the actual site and laboratory and that the quality in actual conditions may be significantly lower than what have been examined extensively in the laboratory. Ultrasonic tests were applied while the workers also have to work on unstable scaffolds in a high altitude, which might have made the detection accuracy lessened.

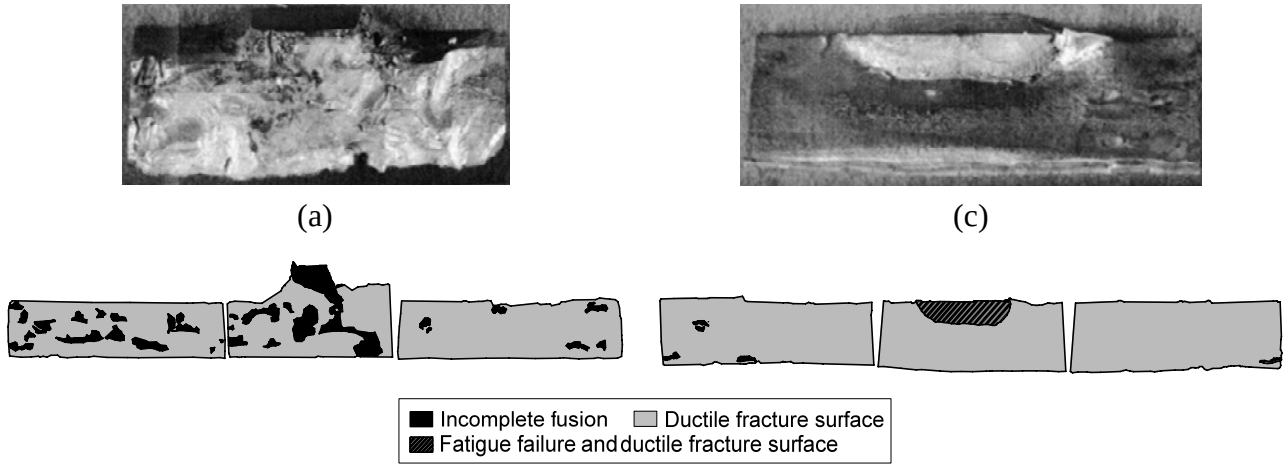

Figure 4.11 Inspection of fractured cross-section: (a), (b) Field weld connection; (c), (d) Shop weld connection

Figure 4.12 shows the microscopic examination of the bottom flange of an unfracured field weld connection. No fault was detected in this connection under the ultrasonic test. However, multiple faults actually existed in the sections especially at the edge and the middle of the flange which were the beginning and ending place of welding. In the sections, faults mostly located at the welding boundary: the boundary between flange metal and welding metal, column metal and the welding metal, and the bottom of the penetration welding. Faults tended to commonly exist in the field weld connections. Although ultrasonic test was conducted at every connection right after the welding, there still have some difficulties to get an accurate result of the inspection especially at the middle of the flange.

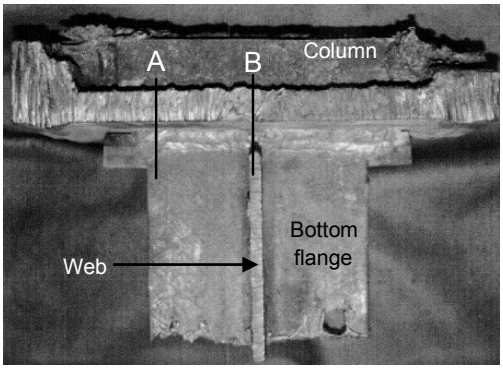

(a)

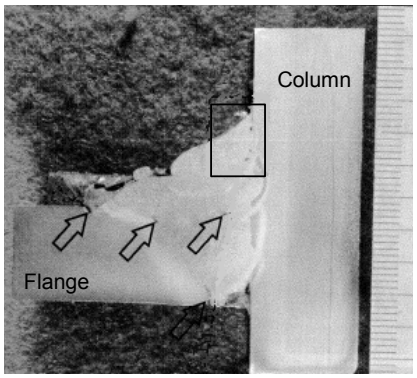

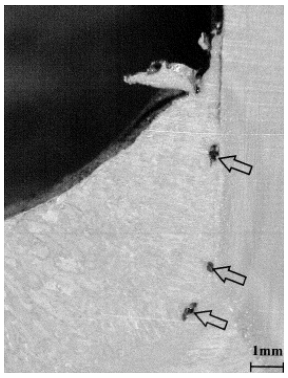

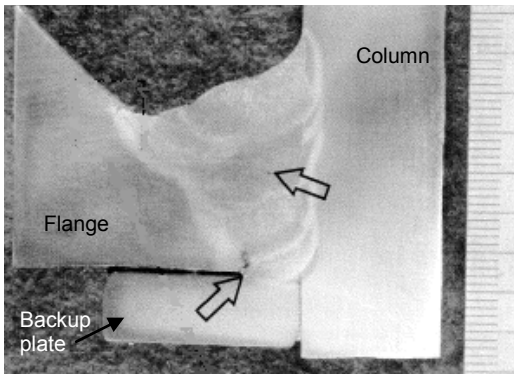

(b) (c) (d)

Figure 4.12 Microscopic examination of an unfractured cross-section: (a) Bottom flange specimen (the third floor, ER); (b) Section A; (c) Detail of section A; (d) Section B

4.5 Increase of strength

Figure 4.13 summarizes the experienced maximum strengths of all connections. Two past bare beam tests (Yamada et al 2008 and Kitamura et al 2008) are also included. The normalized strengths of the bare beams and the E-Defense specimen are at about 1.0 and 1.3 ${}_bM_p$ on the average. The composite beam action exhibited the strength increase in the order of 30% over the corresponding bare beams. Among the field weld connections, one of the four connections with thirteen bolts and three of the eight connections with nine bolts fractured. Although the connections with thirteen bolts were designed to have a 15 % extra strength than those with nine bolts, the results indicated only 5 to 10% increase in the strength.

For the fractured connections, the cumulative plastic rotation of connection remained nearly unchanged (from the 0.15 rad to 0.16 rad on the average) even when the supplemental bolts are arranged. The supplemental bolts increased the ductility only by 5%. The Yamada specimen and Kitamura specimen have identical connection details but with different numbers of bolts (7 bolts and 16 bolts for Yamada and Kitamura, respectively). The normalized maximum strength and cumulative plastic rotation ratio increased from 0.9 ${}_bM_p$ and 32 to 1.0 ${}_bM_p$ and 43 by by the addition of web bolts from 7 to 16. The improvement was 11 and 35% for the maximum strength and cumulative ductility ratio, respectively. Tsai et al (1995) conducted tests on bare beams with the WUF-B connection detail,

in which the number of bolts was the test parameter. Comparing with the baseline connection in which five bolts were used, the normalized maximum strength and cumulative plastic rotation improved from 1.02 ${}_bM_p$ and 0.22 rad to 1.04 ${}_bM_p$ and 0.24 rad if seven bolts were arranged. Neither the maximum strength nor ductility was improved notably with supplemental bolts. From the observation of the E-Defense test, the performance of supplemental bolts at web tended to be unnotable because of the presence of RC floor slab.

The average strength of the fractured and unfractured field weld connections are 1.1 and 1.3 ${}_bM_p$. For the shop weld connections, the averaged values are 1.30 and 1.31, respectively. The shop weld connections show more stable performance, and even if the connections fractured, it occurred after experiencing a larger strength.

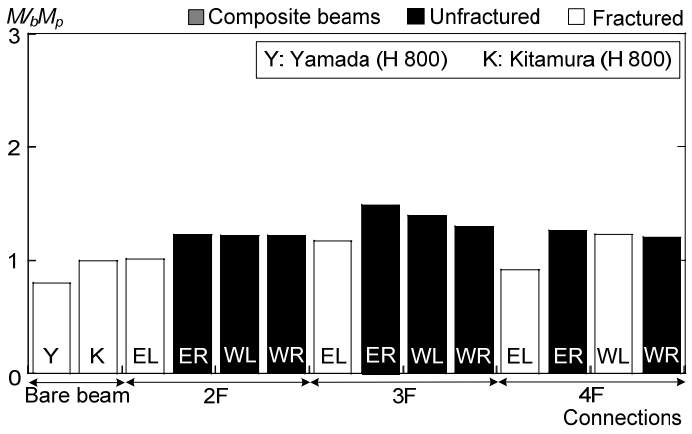

(a)

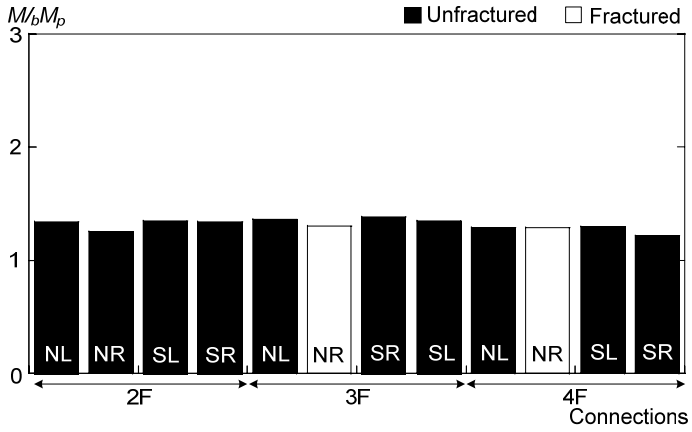

(b)

Figure 4.13 Maximum strength of connections: (a) Field weld connections;
(b) Shop weld connections

4.6 Strain concentration

Figure 4.14 shows the strains at the bottom flange, measured at a location 40 mm farther from the

column face (refer to Figure 2.7) and for various beam rotations. Strains are plotted for positive bending, i.e., when the bottom flange sustained tension. Relationships of the maximum strain and rotation are significantly different between the previous two bare tests (without RC floor slabs) and the E-Defense test. The strains without the RC floor slab are about 1.5% on the average at a rotation of 0.018 rad (drift angle of 1.9%), while that with RC floor slab exceeds 3% at a much smaller rotation of 0.012 rad (drift angle of about 1.4%). The strain at the bottom flange of the field weld connection was greatly amplified over two times by the presence of RC floor slabs, and it was apparently due to the upward shift of the inflection point in the positive bending. In addition, the strain observed at the bottom flange weld access hole of the shop weld connection was 1.4% at a rotation of 0.12rad while that of the field weld connection exceeded 3% under the same rotation. The field weld connection sustained two times larger strain than that of the shop weld connection.

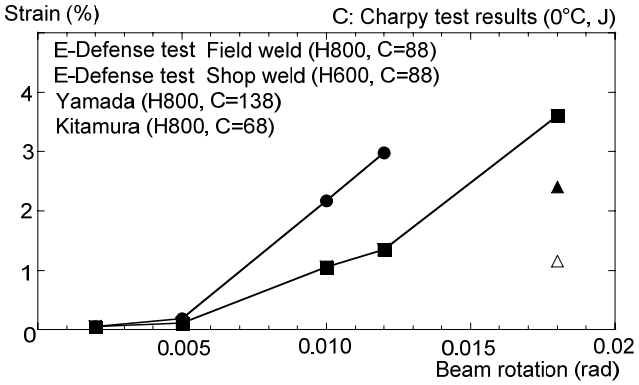

Figure 4.14 Growth of bottom flange strains

4.7 Cumulative plastic rotation

Cumulative plastic rotations are summarized in Figure 4.15. In the connections of the E-Defense test, the rotation was the summed value of those given in the level 2 El Centro wave, the Hog wave, and the San waves up to the fracture.

The rotation shows a large scatter in the field weld connections, primary because fractured connections are included. The averaged rotation of the four fractured E-Defense connection was 0.16 rad, which was only about half of that of the connections without RC floor slabs (Yamada et al 2008 and Kitamura et al 2008). The shop weld connections experienced the San wave for three times. The averaged cumulative plastic rotations of fractured and unfractured shop weld connections are 0.86 rad and 0.94 rad.

Kim et al (2004) conducted a series of tests on shop weld connections with and without RC floor slabs. The specimen with the slab exhibited strains at the bottom flange two times larger than those observed in the bare beam. Strain concentrations made the maximum and cumulative plastic deformation capacity reduced by about 50% of the corresponding bare beam. These observations are similar to what was examined in this study.

A series of beam-to-column connections tests were conducted on various types of connections with and without RC floor slabs after the 1994 Northridge earthquake. Engelhardt et al (2000) conducted tests using the reduced beam sections (RBSs) for seismic rehabilitation of the pre-Northridge steel moment connections. The results indicated that the RBS bare beams specimen buckled at a 0.003 rad plastic beam rotation, and the strength was reduced to less than 80% of ${}_bM_p$. The same beam but with slab delayed the occurrence of buckling, and the composite beam was able to sustain a 0.04 rad rotation and absorb at least two times larger energy than the bare beam. Uang et al (2000) conducted a series tests on RBS and haunch connections with and without RC floor slabs. The RBS connections showed similar results with that of Englhardt et al so that the slab was quite effective in delaying instability of the beam and enhancing the ductility significantly. For the haunch specimens, two bear beam specimens fractured at the top flange under a 0.008 and 0.015 rad plastic rotations. The composite specimens were able to stably sustain a 0.027 rad plastic rotation and absorb at least two times larger energy than the corresponding bare beams.

As discussed above, the floor slab contributes to the enhancement of ductility sometimes, but other times it becomes a factor to reduce the ductility. When the connection, i.e., the toe of the weld access hole, is the weakest spot, the floor slab seems to make the spot even more vulnerable due to the promotion of tensile strain at that spot. When the weakest spot is moved away from the connection and located in the beam section, the floor slab serves as a restrainer to delay the beam instability.

Within the twelve field weld and twelve shop weld connections in the E-Defense specimen, the field weld and shop weld connections fractured in four and two locations, respectively, and the averaged cumulative rotations of those fractured connections were 0.16 rad and 0.86 rad respectively. Considering those numbers, 67% (=8/12) of the field weld connections can sustain the cumulative plastic rotation over 0.16 rad, and 85% (=10/12) of the shop weld connections can sustain cumulative plastic rotation over 0.86 rad. These numbers again indicate the superity of the shop weld connection in terms of the seismic capacity.

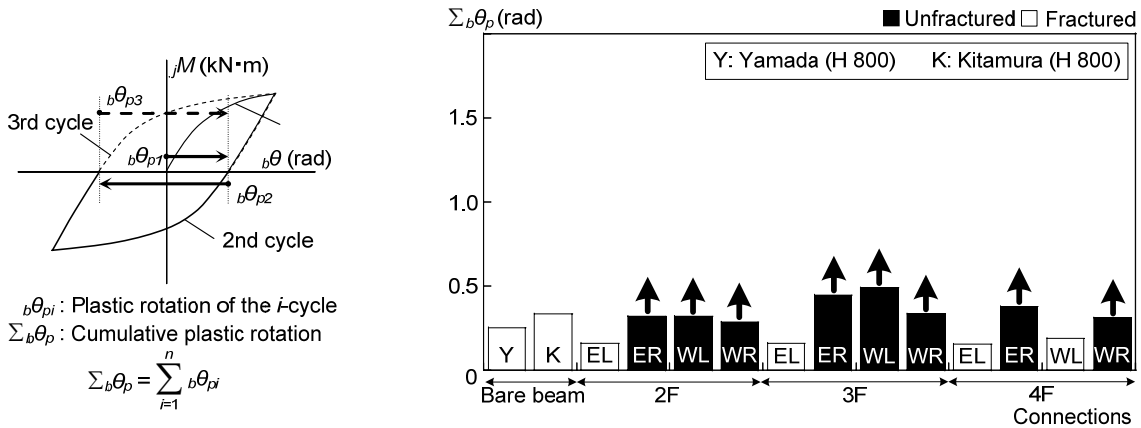

(a)

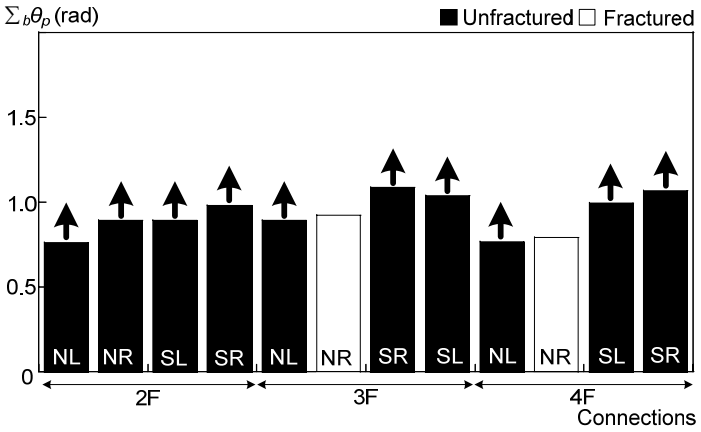

(b)

Figure 4.15 Cumulative plastic rotation of connections: (a) Field weld connections; (b) Shop weld connections

4.8 Cumulative ductility ratio

Figure 4.16 summarizes the cumulative ductility ratios of connections. The cumulative ductility ratio was defined as the total dissipated energy obtained from the hysteretic loops of the connection divided by the product of the full plastic moment and the beam yield rotation of the bare beam. The ratio was the summed value of those given in the level 2 El Centro wave, the Hog wave, and the San waves up to the fracture. The average of fractured field weld connections and shop weld connections were 9 and 71. The minimum cumulative ductility capacity of field weld connection was only 13% of that of shop weld connection. The cumulative ductility demand, which was taken as the average value of the third floor connections of the unretrofitted E-Defense test specimen (as the largest inter-story deformation occurred at the second and the third story) generated by of the level 2 El Centro, Hog and San waves, are illustrated in the figure. The demands of level 2 El Centro and Hog waves were 2 and 6. Although field weld connections show lower capacity than shop weld connections, connections were able to sustain the demand of the level 2 design wave. However, the demand of the level 2 long-period ground motion, Hog wave, was very close to the capacity of the field weld connections. The level 3 San wave demanded cumulative ductility ratio of 19 which was two times larger of the capacity of field weld connections. Connections were unlikely to sustain the demand but shop weld connections remained safety with the difference of 73%. The average cumulative ductility ratio of the two bare beams was 34. Field weld connection which have RC floor slab on the beam only sustained about 30% energy dissipation capacity of that of the corresponding bare beams.

Considering those minimum capacity of fractured connections, 67% (=8/12) of the field weld connections can sustain the cumulative ductility ratio over 9, and 85% (=10/12) of the shop weld connections can sustain cumulative ductility ratio over 71.

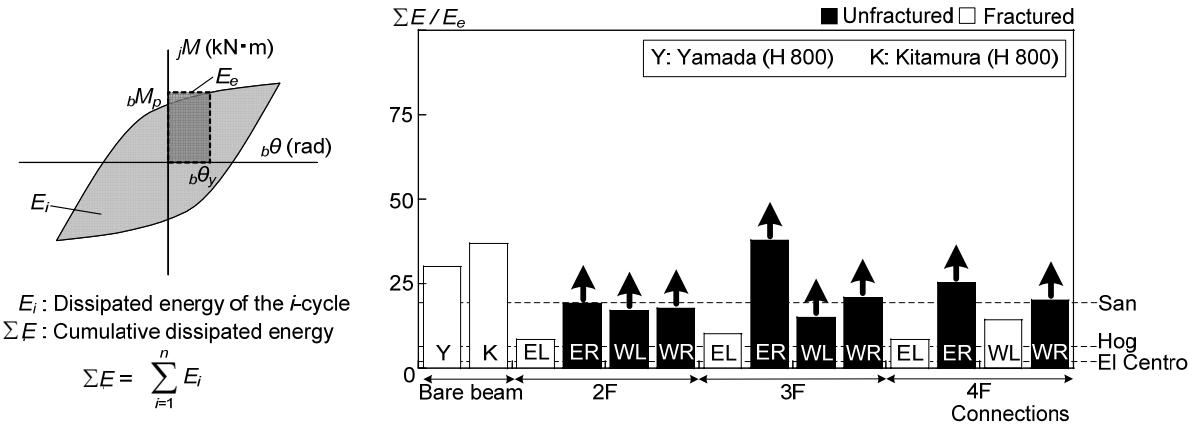

(a)

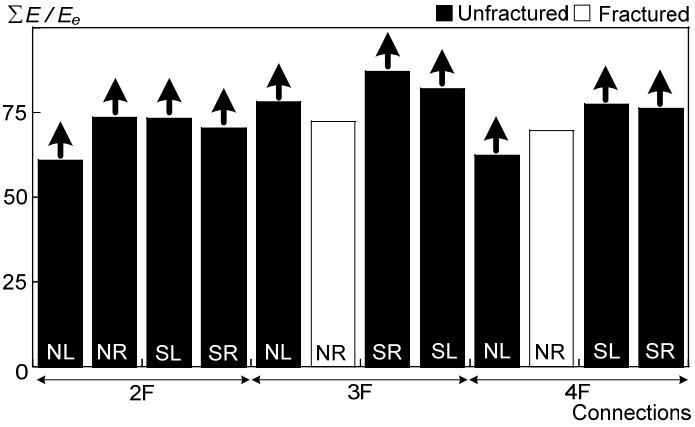

(b)

Figure 4.16 Cumulative ductility ratio of connections: (a) Field weld connections; (b) Shop weld connections

4.9 Maximum ductility ratio

Figure 4.17 summarizes the maximum ductility ratios and the experienced deformation cycles in the test. The ductility ratio is defined as the maximum beam rotation normalized by the beam rotation (θ_p) while the bending moment reached the full plastic moment of the bare beam. The ratios of field weld connection showed a large scatter. The minimum ductility capacity of the fractured field weld connections and shop weld connections were 1.3 and 2.0 on the average.

The numbers of the experienced beam rotation cycles that exceeded 0.005 rad and 0.01 rad of every connection are also plotted in the figure. The deformation cycle was the summed value of those given in the level 2 El Centro wave, the Hog wave, and the San waves up to the fracture. In the field weld connection, connection sustained rotation exceeded 0.01 rad was about 2 cycles on the average. Most experienced plastic deformation cycles concentrated on the range of 0.005 to 0.01 rad. The fractured connections only sustained about 10 cycles and the unfracured connections sustained at least 20 cycles of this range. Shop weld connections sustained two more San wave loadings and lead to significantly large values than those of the field weld connections. Connections sustained about 110 and 30 cycles that exceeded 0.005 and 0.01 rad, respectively. Thus, each San

wave loading generated about 30 and 10 cycles that exceeded 0.005 rad and 0.01 rad with the maximum ductility ratio of about 2.

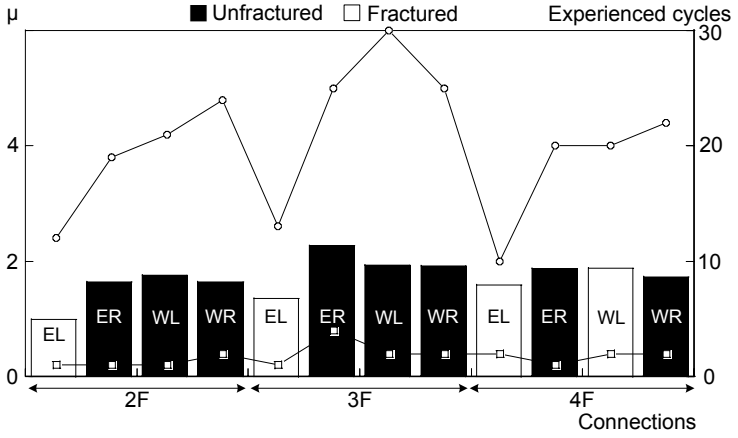

(a)

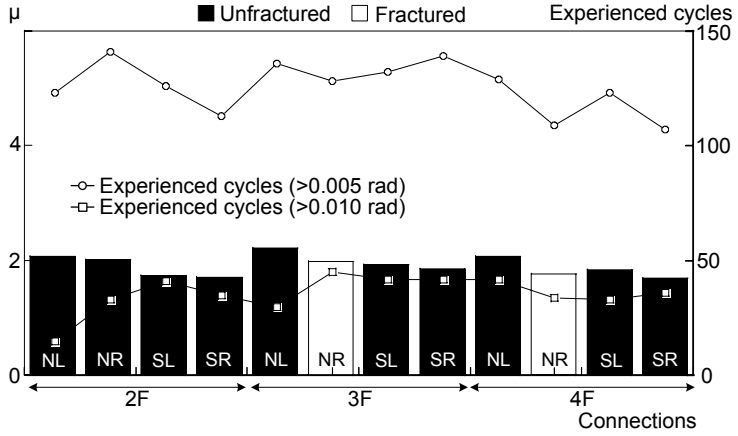

(b)

Figure 4.17 Maximum ductility ratio and experienced cycles: (a) Field weld connections; (b) Shop weld connections

4.10 Effects of R.C. floor slab

Figure 4.19 summarizes the stiffness ratios of the twenty four beam-to-column connections. The ratio was obtained by normalizing the slope of the beam section moment versus the section curvature relationship by the Young's modulus of elasticity and cross-sectional moment of inertia (EI) of the corresponding bare beams. Beam section moment and the section curvature were both measured from the gages glued in the sections of the mid-span (Figure 4.7). The ratios in Figure 4.19 were the response of a white-noise excitation with RMS of 0.4m/s^2 which was conducted before the test. Stiffness ratios of the 600 and 800 mm deep beams, which were arranged in the longitudinal and transverse direction of test specimen, indicated that stiffness of composite beams increased 90% on the average because of the presence of RC floor slab.

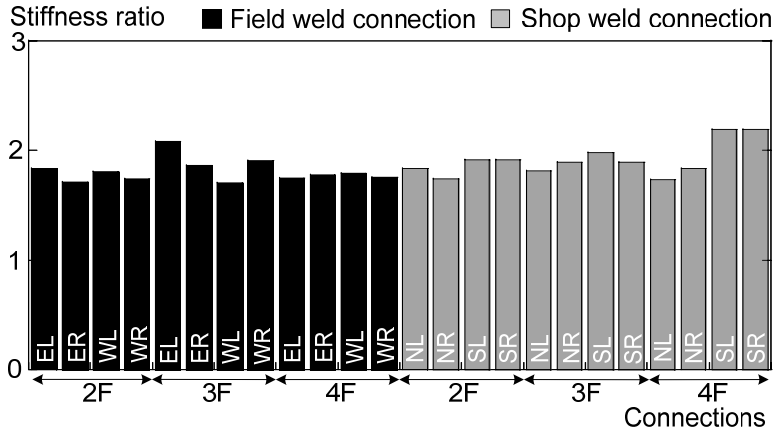

Figure 4.18 Stiffness ratios of the composite beams

Stiffness ratios were measured after each loading and summarized in Figure 4.19(a). Stiffness decreased after each loading and became close to one after the first San wave loading. Effects of RC floor slab became very small under the small excitation (white-noise excitation with RMS of 0.4 m/s^2). Figure 4.19(b) shows the first mode period of the test specimen measured by the same white-noise loading. The periods increased after each level of loading owing to the stiffness decrease of test specimen. Fractures of field weld connections caused a large first mode period increase in the transverse direction. A numerical analysis result was also plotted in the figure to examine the relationship between the decrease of connection stiffness and the increase of periods. This numerical model was built using linear members with rotation springs inserted at all beam-to-column joints. Strength of members was obtained from the measured material properties. The first mode periods of the model were close to those of the test specimen. The initial stiffness of the rotation springs were tuned in reference to the stiffness decrease ratio of each loading (Figure 4.19(a)). The results indicated that the first model periods of the numerical model increased in a very similar trend with those of the test results. Stiffness decrease of the connections mainly attributed to the change of the first mode periods of the test specimen. Cracks developed in the RC floor slab could be the reason to reduce the composite effects after each loading and lead to the increase of the first model period of the test specimen.

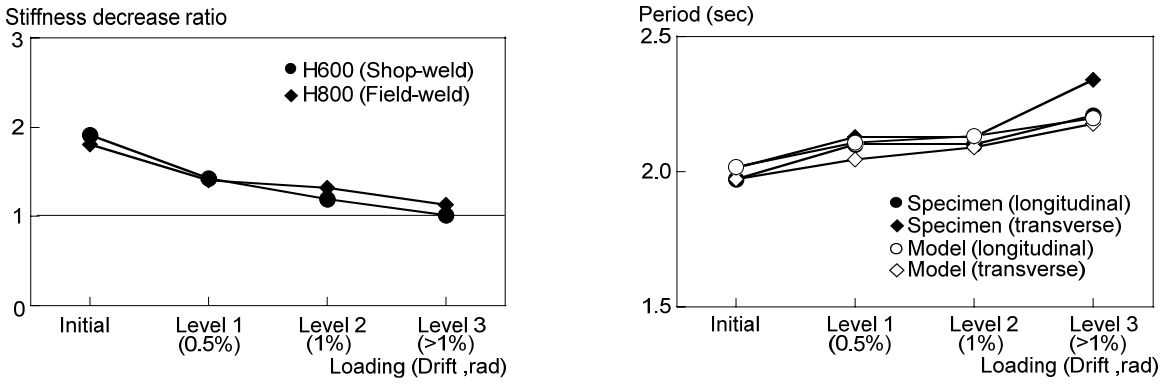

(a) (b)

Figure 4.19 The changes of the composite stiffness of connections and the first model periods of the test specimen: (a) Stiffness decrease; (b) Increase of first mode periods

Figure 4.20(a) shows the cracks of RC floor slab that observed before the first time San wave loading and after the test. Punching failure commonly occurred at connection area after the first San wave loading. Cracks at two connections of each floor were plotted in Figure 4.20(b) to (d). Distribution of the cracks changed after the San wave loadings. The long-period ground motion enlarged the range of cracks and made small cracks be connected. Some cracks extended along the direction of beams which might affect the composite effects of connections.

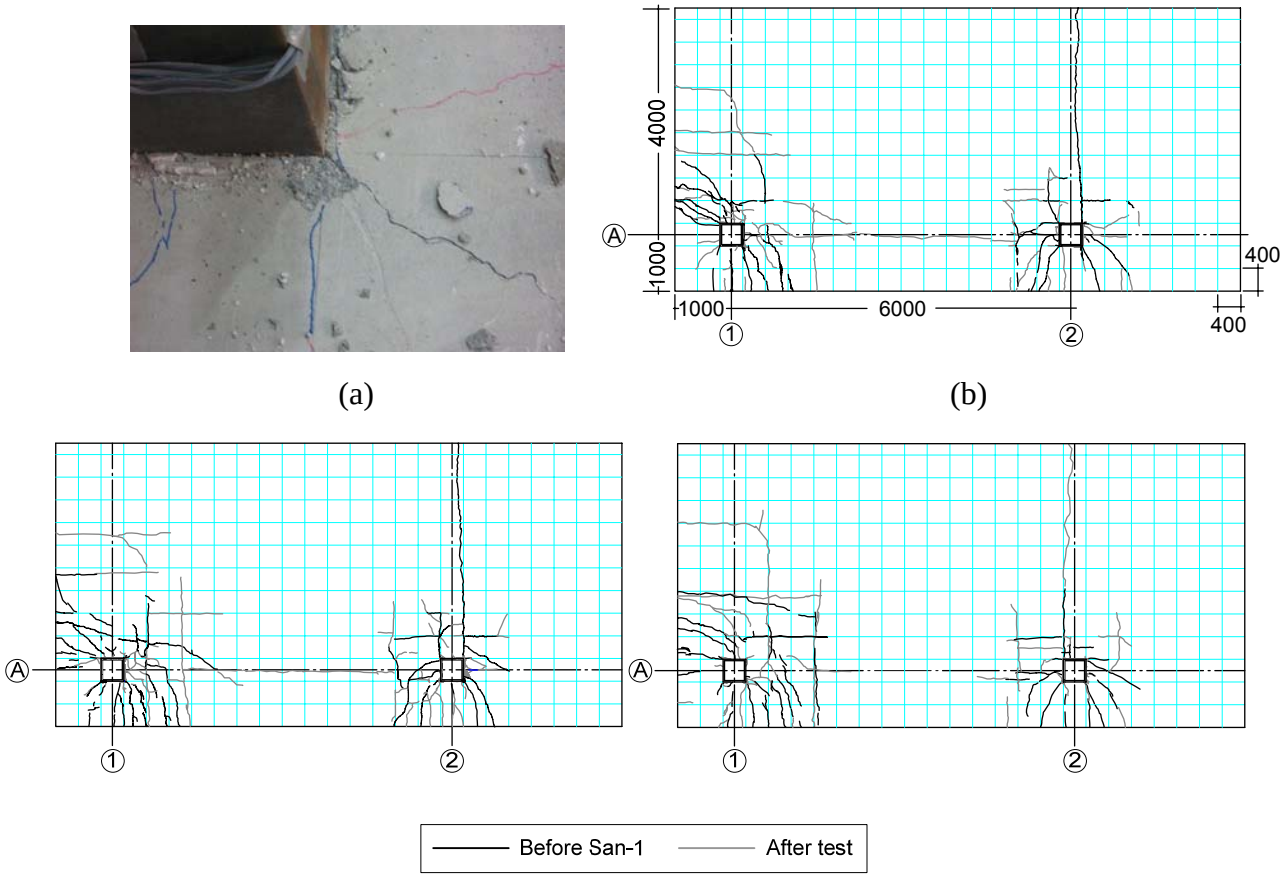

(a) (b)

(c) (d)

Figure 4.20 Cracks at RC floor slab: (a) A close-up of cracks; (b) Second floor slab; (c) Third floor slab; (d) Forth floor slab

4.11 Conclusions

The field weld connection and shop weld connection with early time connection details are adopted in the test frame and tested by input the long-period ground motions sequentially until the test specimen sustained serious damage, i.e., fractures of multiple beam-to-column connections. Major findings obtained from this study are summarized below.

1. Between the two types of beam-to-column connection adopted in the test, i.e., the field weld connection and shop weld connection, the field weld connection tended to have lower ductility, particularly in terms of the cumulative plastic rotation and cumulative ductility. According the

test results of twenty four connections recorded in detail, the field weld connection had the cumulative plastic rotation and ductility ratio of 0.16 rad and 9 in the 67% probability, while the shop weld connection had the plastic rotation and ratio of 0.86 rad and 71 in the 85% probability.

2. The significant difference in ductility capacity was attributed to the combination of difficulty in quality control and greater concentration of strains. The presence of RC floor slab promoted the strain concentration at the toe of weld access hole in the bottom flange by over 100% on the average as compared to the case for bare steel beams, which resulted in a reduction of cumulative plastic rotation by about 50%.

REFERENCES

[4.1] American institute of Steel Construction, Inc.: Seismic Provisions for Structural Steel Buildings, March 2005.

[4.2] Bertero, V. V., Anderson, J. C., Krawinkler, H. (1994): Performance of steel building structures during the Northridge earthquake, Rep. UCB/EERC-94/09, EERC, Univ. of California, Berkely.

[4.3] Editorial Committee for the Report on the Hanshin-Awaji Earthquake Disaster (1997), Report on the Hanshin-Awaji Earthquake Disaster, building Series Volume 3, Structural Damage to Steel Buildings (in Japanese)

[4.4] Engelhardt, M.D., Husain, A. S. (1993). Cyclic loading performance of welded flange-bolted web connections. *J. Struct. Eng.*, 119(12), 3537-3550.

[4.5] Engelhardt, M.D., Fry, G.T., Jones, S.L., Venti, M., Holliday, S. D. Experimental Investigation of Reduced beam Section Connections with Composite Slabs. *Proceedings; Fourth US-Japan Workshop on Steel Fracture Issues*, San Francisco, February 28 to March 1, 2000.

[4.6] Federal Emergency Management Angency: FEMA350, Recommended Seismic Design Criteria for New Steel Moment-Frame buildings, July 2000.

[4.7] Kim, Y.J., Oh, S.H., Moon, T.S. (2004). Seismic behavior and retrofit of steel moment connections considering slab effects. *Eng. Struct.*, 26(13), 1993-2005.

[4.8] Kitamura, Y., Hashida, I., Suita, K. (2008). Seismic performance and retrofit of beam-column connection for early high-rise buildings, Part 1:Experimental Method and Hysteresis Characteristics. *Architectural Institute of Japan.*, 2008, 1001-1002. (in Japanese).

[4.9] Nakashima, M., Roeder, C. W., and Maruoka, Y. (2000). Steel moment frames for earthquakes in United Stated and Japan. *J. Struct. Eng*., 126(8), 861-868.

[4.10] Tsai, K.C., Wu, S., Popov, E.P., (1995). Experimental Performance Seismic Steel Beam-Column Moment Joints. *J. Struct. Eng.*, 121(6), 925-931.

[4.11] Uang, C. M., Yu, Q. S., Noel, A., Gross, J., (2000). Cyclic Testing of Steel Moment Connections Rehabilitated with RBS or Welded Haunch. *J. Struct. Eng.*, 126(1), 057-068.

[4.12] Yamada, S., Kitamura, Y., Suita, K., Nakashima, M. (2008). Experiment investigation on

deformation capacity of beam-to-column connections in early highrise buildings by fullscale tests. *Journal of structural and construction engineering, Architectural Institute of Japan.* 623, 119-126. (in Japanese with English abstract).

CHAPTER 5

Preliminary Member Tests on Retrofitted Field Weld Connection

5.1 Introduction

It has been speculated that long-period ground motions would generate significantly large cumulative deformation to high-rise buildings and may lead to severe structural damage under the shaking (JSCE, AIJ. 2006; AIJ. 2007; Suita et al. 2004; Kawabe et al. 2008; Nakagawa et al. 2008). According to the observation of the 1994 Northridge and 1995 Hyogoken-Nanbu earthquakes, brittle fractured field weld connections spread in the damaged buildings (FEMA 350; Bertero et al. 1994; Nakashima et al. 2000).

In chapter4, large scale E-Defense shaking table test verified the capacity of high-rise buildings subjected to long-period ground motions. The ground motions generated fifteen times larger story cumulative ductility to the tested high-rise building than that obtained from the design wave and caused fractures in connections. Field weld connections fractured at about 0.007 rad beam rotation, while the resistance at that instant was about the estimated full plastic moment of the bare beam. According to the observations, a combination of large cumulative ductility demand from the long-period ground motions, weld quality in the field, and the promotion of strain concentrations at the toe of the bottom flange leaded to the fractures. Thus, retrofitting of the existing filed weld connections is very important to make this type of connection more ductile.

The 1994 Northridge and 1995 Hyogokennabu earthquakes tested the seismic capacity of field weld connections and changed the beam-to-column connection design in U.S. and Japan. In the U.S., the pre-Northridge field weld connection (WUF-B) can only been allowed to be used in the Ordinary Moment Frame (OMF), which demand lower deformation than that required for the Special Moment Frame (SMF). Connections like weld unreinforced flange, weld web (WUF-W), reduced beam section (RBS), welded bottom haunch (WBH) among others have been recommended for the OMF and SMF, and all have been qualified as the ductile connections that can satisfy the maximum deformation of 4% drift angle for two cycle without resistance decrease (FEMA 350). For the retrofit of existing connections, however, these recommended connections have difficulties in application because of the presence of RC floor slab. It is also notable that most of the tests based on which the recommendations were stipulated were for bare beams rather than for beams with RC floor slab. According to the E-Defense test results as well as some past tests (Okada et al. 2001, Kim et al. 2004), the slab could cause two time larger strain concentration at the

bottom and reduce the cumulative deformation capacity by half compared with those experienced by the cases for bare beam. The effects of slab cannot be ignored in the seismic capacity evaluation of connections. In Japan, many tests had been conducted after the 1995 Hyogoken-Nanbu earthquake for the evaluation and enhancement of ductility capacity of beam-to-column connections. New types of connection details like a new shape of weld access hole and construction guidelines for the seismic retrofit of existing steel buildings (AIJ. 1996) were proposed. In these guidelines, however, retrofit mainly focus on the connections in the middle and low-rise buildings. Few data have been available for retrofit of the large size connections used in the high-rise buildings. In addition, most of the connection retrofit tests did not consider the effects of RC slabs, either. The actual data about the seismic performance of retrofitted connections are deemed still very limited.

To characterize the deformation capacity of retrofitted beam-to-column connections of early time high-rise buildings, a series of quasi-static member tests were conducted. In reference to some previous tests on retrofitted connections, three types of retrofit methods were adopted, considering the construction feasibility and the effect of RC slab. The retrofit methods were adopted on the connection that duplicated the field weld connection arranged in the E-Defense specimen. The loading history adopted in the member test was determined in reference to the response obtained from the E-Defense shaking table test.

In this chapter, retrofit performance and capacity of these connections are evaluated by quasi static tests in which multiple plastic cycles were applied until the connection fractured. First, design policies, construction methods, and strength equations of the retrofitted connections are proposed. Second, the adopted retrofit performance was evaluated by comparing the cumulative plastic rotation ratios and cumulative ductility ratios of all connections. Third, maximum strength were compared to the estimated strength to evaluate the accuracy of the design equations. Finally, strain values at the toe of weld access holes were compared to evaluate the strain concentration and retrofit performance of all connections.

5.2 Test outline and design of the test specimen

Figure 5.1(a) to (d) show four types of connections, all arranged with the RC floor slab. The original connection shown in Figure 5.1(a) was designed to duplicate the field weld connection with thirteen bolts of the E-Defense specimen. Connections in Figure 5.1(b) to (d) were identical with the original connection but modified using different retrofit methods. The member sizes were scaled down to three quarters of the E-Defense specimen due to the capacity of loading system. The beam was a built-up wide flange section of H 600×150×9×12 and a square tube column of 300×300×19 (BCR295) was adopted. The column beam strength ratio ($_{column}M_p/_bM_p$) was 1.6. The connection strength ratio, $_jM_u/_bM_p$ was 1.11, which was defined as the maximum moment relative to the full plastic moment of the bare beam. $_{column}M_p$ and $_bM_p$ are the full plastic moment of the column and beam section. $_jM_u$ is the maximum flexural strength of the connection. The column was expected to remain in elastic throughout the loading. The number and arrangement of the bolts were determined

in reference to the following policies. The maximum bending moment obtained from the shear strengths of these bolts should be larger than the estimated full plastic bending moment of the shear plate. The bolts should be able to sustain the beam shear force, while the connection meets the requirement for the combination of maximum strength and long term vertical loadings. Similitude in bolt sizes was also maintained; bolts with a diameter of 16 mm were used instead of the original bolts with a diameter of 20 mm.

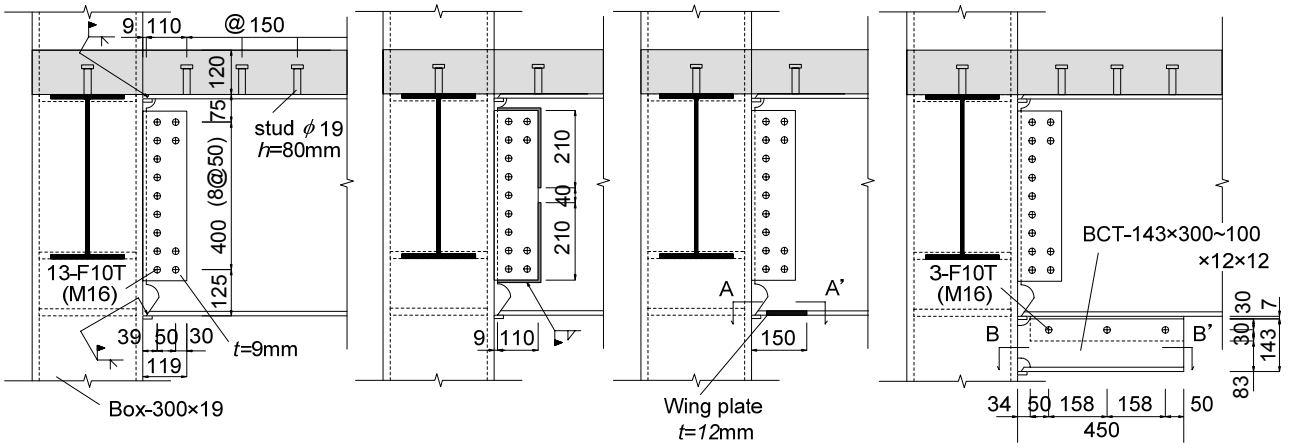

(a) (b) (c) (d)

Figure 5.1 Test connections: (a) Original connection; (b) Connection with supplemental welds; (c) Wing plate connection; (d) Haunch connection

The common connection details applied at all connections are shown in Figure 5.2(a). The top flange weld access hole has a one quarter circle and the toe of the bottom flange weld access hole ends at the boundary of penetration welding. These details were commonly used in early time connections and were identical with that adopted in the E-Defense specimen. The slab thickness was not scaled down, remaining identical with the E-Defense specimen due primarily to the difficulties in reducing the scale of the concrete part including studs. Flat deck plates which were identical with that of the E-Defense test were adopted.

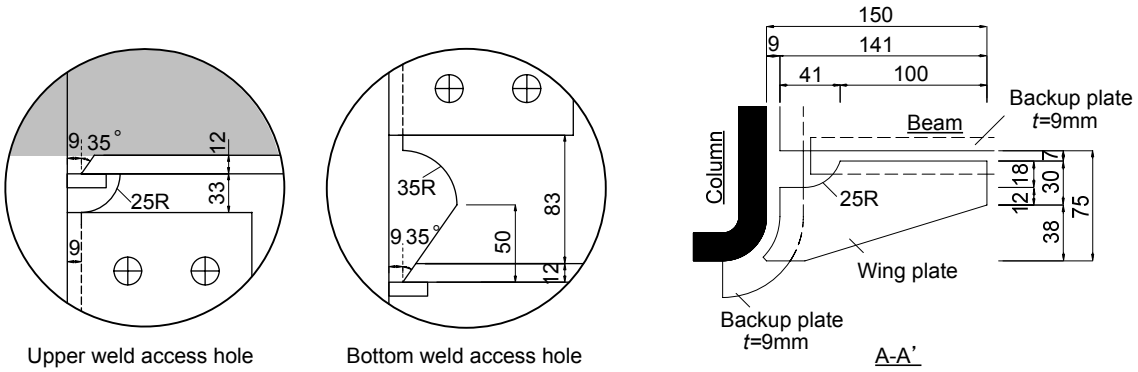

(a) (b)

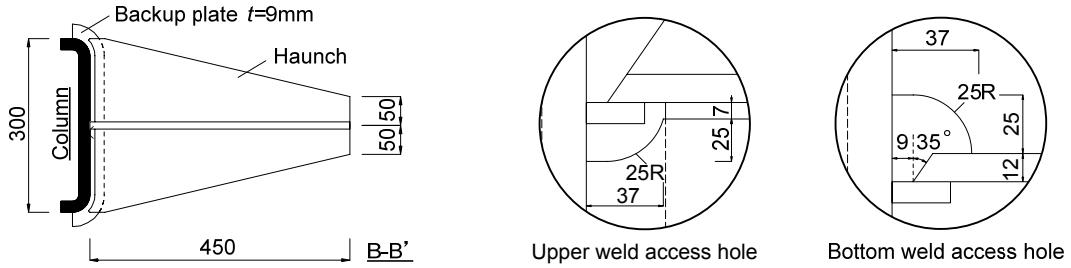

(c)

Figure 5.2 Connection details: (a) Weld access holes of connections; (b) Details of wing plate; (c) Details of straight haunch

To evaluate the performance of retrofitted connections, the original connation was tested as the baseline (Figure 5.1(a)). Base on the connection details, three types of retrofit methods were adopted considering both their retrofit performance and construction feasibility in the filed. The basic policy of the retrofit is to do the best to enhance the seismic capacity with most practical retrofit techniques rather than to set up the required performance for the retrofit.

In the Figure 5.1(b), the connection was modified slightly, and the shear tab was welded to the beam web as a possible retrofit. Tsai and Popov (1988) conducted a series of tests to study the performance of WUF-B connections with supplemental welds at the web. The results indicated that the supplemental welds provided between the beam web and the shear tab improved the cyclic inelastic behavior of the beam; the maximum plastic rotation was improved to 1.3 to 2.4% from 0.9% of its counterpart with no web welding. As a result of this study, U.S. model seismic codes at that time (NEHRP 1991; Seismic 1992; Uniform 1991) stipulated that supplemental welds at the web be applied for beam sections with $Z_f/Z \leq 0.70$ and must be designed to develop at least 20% of the beam's flexural strength. Here, Z is the beam's plastic section modulus, and Z_f is the plastic section modulus of the beam flanges only. This connection was classified as one of the standard connections employed for ductile moment frames before the 1994 Northridge earthquake. For further investigating the effect of supplemental welds, another series of tests were conducted by Engelhardt and Husain (1993). The results showed that for specimens with $Z_f/Z \leq 0.70$ the beam plastic rotations were 0.5 and 1.2% without supplemental welds. With the supplemental welds, the plastic rotations increased to 1 and 1.5%. The specimen with supplemental welds performed at most somewhat better than their counterparts with no web welds. After the 1994 Northridge earthquake, the ductility demand for beam-to-column connections was raised significantly to a level such that the connection endure the maximum drift angle of 4%, with the maintenance of at least 80% of the maximum strength (AISC 2005). Since that time, the supplemental weld connection has been considered unable to satisfy the demand.

Although the supplemental weld is no longer considered as a reliable alternative for the improvement of ductility, the possibility was explored once again in this study to examine how much (or less) the supplemental weld would be effective, this time against cyclic rotations characterized by many cycles, say, more than ten times, but with relatively smaller amplitudes of about 1.0 to 1.5% in the story drift angle. In this test, the shear tab was all welded to the beam web to increase the web

resistance as much as possible. The all welded web connection was capable of sustaining about 35% of the beam's flexural strength. Table 5.1 shows the member sizes and material properties adopted in the test. The SM 490A steel was adopted in all beams to represent the material behavior of the E-Defense specimen.

Table 5.1. Specimen specifications and material properties

Member		σ_y (MPa)	σ_u (MPa)
Box-300×19		435	455
H-600×150×9×12	Flange	350	508
	Web	358	509
Haunch		344	508
Concrete		F_c=21.1 MPa	

According to the E-Defense test results, high strain concentration observed at the toe of the bottom flange weld access hole and weld quality of the field weld connection were the main reason to have made the penetration welds area most vulnerable and lead to a fracture with a lower deformation capacity. Similar fracture situation was also observed in the 1994 Northridge earthquake. To improve the connection ductility, new types of connections were proposed and prequalified based on many tests (FEMA 2000). Tsai et al (1996) conducted a bare beam test on typical pre-Northridge field weld connection with wing plates attached on the top and bottom flanges. The column had a box section column of 450×450×32 and the beam was W21×62. The flanges were widened to the column width using the wing plates. The test results indicated that the connection buckled at the tip of the wing plates and the crack was observed at the top flange under the 0.028 rad plastic beam rotation. The counterpart connection that had no retrofit fractured under the maximum plastic rotation of 0.0168 rad. The plastic rotation capacity was improved to 1.7 times relative to the unretrofitted connection. Uang et al. (2000) conducted a test on a welded haunch connection with the presence of RC floor slab. The W14×426 column and W36×150 beam were connected using the pre-Northridge field weld connection. The composite specimen was able to stably sustain a 4% story drift angle when the beam plastic rotation was 0.027 rad. The resistance decreased gradually after the buckle at the tip of the welded haunch. Lee et al. (2003) conducted a series of bare beam tests on the welded straight haunch connections. The column was H-400×408 ×21×21, and the beam was H-600×200×11×17, which happened to have had an identical beam depth with the member test conducted in this study. Under the SAC standard seismic loading protocol (FEMA 2000), three haunched connections were able to stably sustain the 4 % story drift angle when the beam plastic rotation was about 0.03 rad. All connections buckled at the tip of the haunches. Comparing with the connection without a haunch, the plastic energy dissipation of the haunched connections were about 2.5 times larger. The concept of the wing plate and haunch connections are to move the weakest spot from the beam end where welds and weld access holes were present to a continuous beam without geometrical discontinuities.

The design of retrofitted connections adopted in this test followed those previous studies. Because of the presence of RC floor slabs, retrofit was mostly limited to the bottom flange or to the web (Figure 5.1(b)). Besides, the constructability was very critical particularly in high-rise buildings. Along this line, two types of retrofit methods shown in Figure 5.1(c) and (d) were adopted in this test. In Figure 5.1(c) and Figure 5.2(b), the wing plates were only attached at the bottom flange. In Figure 5.1(d) and Figure 5.2(c), the haunch was designed to create a reasonable mechanism for the box column.

5.3 Estimated strength and construction

Table 5.2 summarizes the estimated strengths of connections based on the measured material properties. ${}_bM_p$ is the full plastic moment of the bare beam (638kN・m). ${}_jM_u$ is the maximum strength of connection (AIJ 2006). Effect of RC floor slab was not considered in the calculation. For the original and connection with supplemental welds, ${}_{cb}M_p$ is the full plastic moment of the composite connection which was estimated as 0.85 times of the compress strength of the concrete ($0.85F_c$), and taking the effective width of the slab equal to the column width (300 mm) (Matsumiya et al. 2005, AIJ. 2002). In both the wing plate and haunch connections, if the plastic hinge occurs at the tip of wing plates or the haunch (150 mm and 450 mm away from the column face), the corresponding resistance at the beam end were 1.05 and 1.19 ${}_bM_p$,respectively. These values were smaller than the estimated strengths of the connections, meaning that the plastification would occur in the beam rather in the beam end. Thus, the ${}_{cb}M_p$ of the two connections were the beam end moment while the composite section at the tip of wing plates and haunch reached the full-plastic moment. The effect width of slab at the location was equal to the column width (300 mm). The haunch improved the maximum strength significantly. The full plastic moment of the column and panel zone were 980kN・m and 996 kN・m based on the material tests.

Table 5.2. Estimated strength of connections

Specimen	${}_jM_u/{}_bM_p$	${}_{bc}M_p/{}_bM_p$
Original	1.11	1.33
Supplemental welds	1.27	1.33
Wing plates	1.39	1.41
Haunch	1.50	1.81

5.3.1 Original connection

The maximum flexural strength of the web connection was controlled by the strength of the shear plate. The connection strength ratio (${}_jM_u$ / ${}_bM_p$) was 1.11, which was identical with that of the E-defense specimen. The Japanese code (AIJ 2006) recommends the connection strength ratio of

not smaller than 1.2. The ratio in this test was slightly smaller than the recommended value. Figure 5.3 shows the field weld situation of this connection.

(a)

(b)

Figure 5.3 Field weld situation: (a) Top flange; (b) Bottom flange

5.3.2 Connection with supplemental welds

Basing on the design for the original connection, supplemental welds were applied to the web. To improve the moment transfer of the web as large as possible, the shear plate was all fillet welded to the beam web (Figure 5.1(b)). The length dimension of horizontal weld at both the top and bottom sides of the shear plate were 110 mm long. The vertical weld was interrupted in the middle by a 40 mm clearance to prevent excessive heat input and residual stresses resulting from a long distance welding.

The maximum flexural strength of the web was determined as the sum of the full plastic moment of shear plate section and the bending moment resistance provided by the horizontal and vertical welds in the web. The connection strength ratio ($_jM_u$ / $_bM_p$) was 1.27. In the meantime, the bending moment resistance from the horizontal welding $_hM_u$ and vertical welding $_vM_u$ were obtained by multiplying the shear strengths of the welds by the distance to the center of shear plate. The equations are showed below.

$$ {}_hM_u = \frac{F_{wy}}{\sqrt{3}} \cdot a\left(l_h - s\right) \cdot D_s \tag{5.1} $$

$$ {}_vM_u = \frac{F_{wy}}{\sqrt{3}} \cdot \frac{a\left\{D_s^2 - \left(l_v' + 2s\right)^2\right\}}{4} \tag{5.2} $$

F_{wy} is the yield strength of web; s is the size of the fillet weld (7 mm); a is the throat of the fillet weld; l_h is the length of the horizontal weld; D_s is the height of the shear plate; and l_v' is the distance of the clearance in the middle of the vertical welding. Figure 5.4 shows the vertical welding applied

to the web.

Figure 5.4 Vertical welding in web

5.3.3 Wing plate connection

Dimensions of the wing plates were determined using the following policies. The thickness of the plate was 120 mm, which was identical with the thickness of the beam flange. This ensured the alignment between the flange and wing plate that were welded together. The width of the wing plate was 75 mm to widen the bottom flange to the column width (A-A' in the Figure 5.2(b)). Because of the presence of the end tab that commonly existed in the field weld connection, one 1/4 circle hole with a radius of 25 mm was adopted in the plates. The length between the wing plate and column (50 mm for each side) could be token as the effect width without considering the out of plane deformation of the square tube column, owing to the presence of the inner-diaphragm in the column. The weld length between the wing plate and beam bottom flange (l_1=100 mm) was determined to ensure the shear force transfer from the wing plate to the beam flange, while the weld between the wing plate and column (l_2=50 mm) arrived at its maximum tensile strength (Figure 5.5).

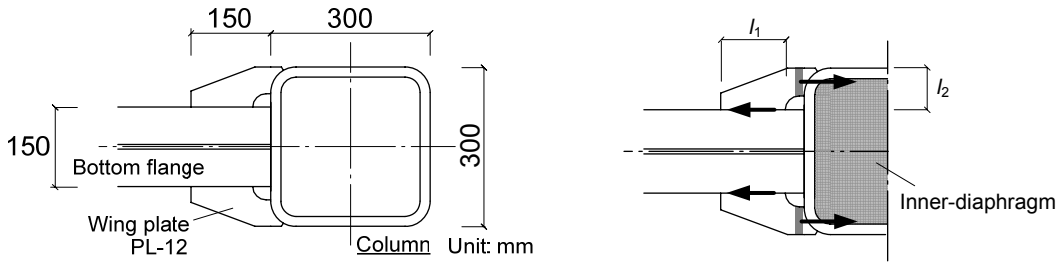

Figure 5.5 Design concept of wing plate

In the fabrication work, the edge of the wing plate was cut to a bevel for groove welding. The wing plate was spot welded to the beam flange and the column with a backup plate to position the

wing plate for welding. Then the welder started to apply the welds.

Comparing with the original connection, the wing plates widened the section of the bottom flange and increased the maximum bending moment. The extra strength supplied by the wing plates ${}_jM'_{fu}$ can be calculated by the following equation when the neutral axial was assumed to locate at the gravity center of the beam.

$$ {}_jM'_{fu} = 2w_e \cdot t_f \frac{d_b}{2} F_{fu} \tag{5.3} $$

w_e is the effect width of the wing plates (totally 100 mm); t_f is the plate thickness of the flange; d_b is the distance between the centers of the two flanges; and F_{fu} is the maximum tensile force of the flange metal. According to the calculation, the connection strength ratio ${}_jM_u / {}_bM_p$ of the wing plate connection was 1.39. Figure 5.6 shows the welding situation and the detail of the wing plate.

(a) (b)

Figure 5.6 Field weld situation of wing plates: (a) Welding; (b) Wing plate

5.3.4 Haunch connection

In the past test (Tsai et al. 1996), attaching wing plates at the top and bottom flanges showed significant improvement in the deformation capacity of field weld connections. For the retrofit of connections, only attaching wing plates at the bottom flange sometime meets difficulties. The presence of the end tab and/or a small size column section would leave very limit space for attaching the wing plates. Attaching a haunch below the bottom flange is another choice for retrofit. The design policies and construction situation of the haunch retrofit are described below.

The haunch member (BCT-143×300~100×12×12) weighed about 3 kg, which was able to be carried by a single human power. The thickness of the bottom flange of the haunch was 12 mm that was identical with the thickness of the beam flange. The flange of the haunch was widened to the column width (300 mm) to transfer the force to the column (Figure 5.2(c)). Because there is no inner-diaphragm at the location where the haunch flange is connected to the column, an effective

width (l_3, showed in Figure 5.7) of the haunch flange was taken to be 3.5 times of the thickness of the column plate (66.5 mm), measured from each side of the edge (AIJ. 2001). The length of the haunch (l_4=450 mm, showed in Figure 5.7) was determined to ensure the shear force transfer between the haunch web and the bottom flange of beam when the haunch flange reaches its maximum tensile force.

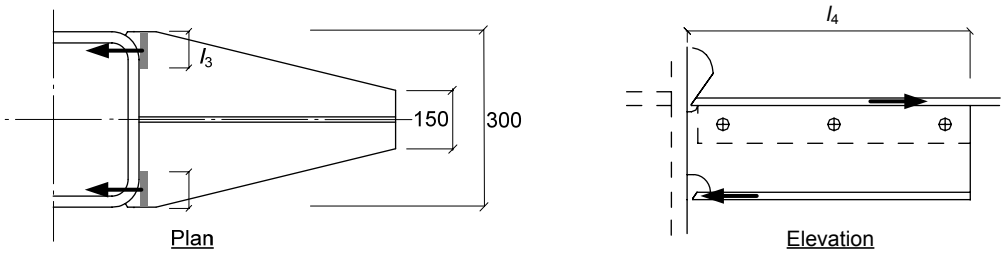

Figure 5.7 Design concept of haunch

In the fabrication work, the haunch was first bolted to the shear tab, which was pre-welded to the bottom flange of the beam. The shear tab also worked as a backup plate when the penetration weld was applied between the haunch web and bottom flange of beam. Then, the welder applied the horizontal, vertical and downward welding at the web and flange of the haunch (Figure 5.8).

The distance from the top of the beam to the neutral axial χ_n was determined by the following formula.

$$x_n = \frac{A_f \cdot D_b + A_h \cdot \left(D_b + D_h - t_{hf}/2\right)}{2A_f + A_h} \tag{5.4}$$

A_f is the area of the beam flange; A_h is the area of the haunch flange; D_b is the depth of the beam; D_h is the depth of the haunch; and t_{hf} is the thickness of the haunch flange. Then the maximum flexural strength of the haunch connection was determined as the sum of the plastic section modular of the beam and haunch. The strength ratio of the connection ${}_jM_u$ / ${}_bM_p$ reached 1.50.

(a) (b)

Figure 5.8 Field weld situation of Haunch: (a) Haunch; (b) Welding situation

All welds of all four connections fabricated in this study were ultrasonically tested by qualified inspectors, and no default was inspected.

5.4 Loading system, loading program and measurement

Loading system

The test setup and test specimen are shown in Figures 5.9 and 5.10. The specimen consists in one column and two beams with respective beam-to-column connections. In one of the specimens, one side of the beam was arranged with the original connection. On the other side of the beam, the connection was modified slightly, and the shear tab was welded to the beam web as a possible retrofit. In the other specimen, the wing plates and haunch connections were arranged on each side of the beams. The top and bottom of the column and the two ends of the beams were pin supported. The horizontal load was applied at the top of the column by the 1,500kN oil jack. A RC floor slab with the thickness of 120 mm was placed on top of the beams. The dimension of the RC slab was limited to 1 m in width and 1.9 m in length on each side. The left and right beams were loaded independently by releasing the pin at the other beam. The column was 3 m long from the jack to the pin support. The beam was 3 m from the center of the column to the pin support. The entire specimen was 3 m in height and 6 m in width, which was three quarters of the E-Defense test frame in the transverse direction.

Figure 5.9 Member test specimen and setup

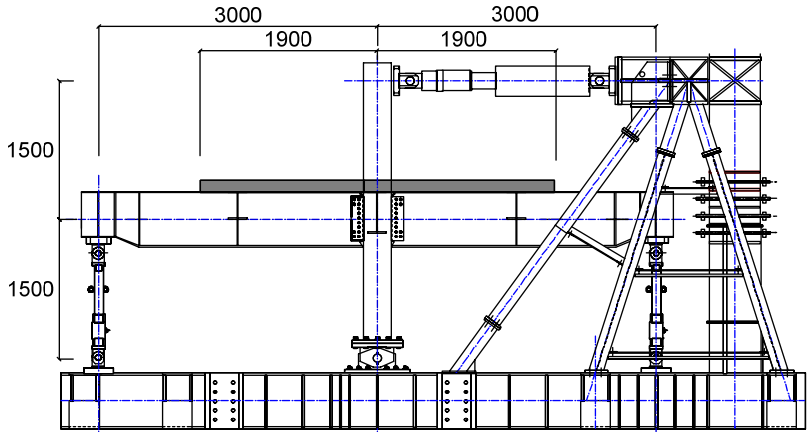

Figure 5.10 Quasi-static loading test setup (unit: mm)

Loading program

The loading history adopted in the member test was determined in reference to the response obtained from the E-Defense shaking table test (Figure 5.11(a)). According to the story drift angle history subjected to the first time San wave (San-1) in the second story in which the story drift angle was the largest, the specimen experienced cycles between 0.4 to 0.6% drift angle amplitudes for fifteen times, cycles between the 0.6 to 0.9% drift angle amplitude for eight times, cycles between the 0.9 to 1.1% drift angle amplitudes for nine times, and cycles between 1.1% to 2.0% for three times. To make the experienced amplitudes as close as possible between the E-Defense test and the member test, the following loading history was adopted for the member test: elastic loading with the 0.2% drift angle for two cycles, followed by the 0.5 % drift angle for two more cycles and inelastic loading, with the 1 % drift angle for eleven cycles, followed by the 2% drift angle for two cycles and 3 % drift angle until the connection fractured (Figure 5.12). Yamada et al. (2008), and Kitamura et al. (2008) conducted two full-scale beam-to-column connection tests considering the effects of long-period ground motions. Those tests had depth and connection details very similar to the field weld connections adopted in the E-Defense test, except that the previous tests did not have RC floor slab on top of the beam. Their loading histories also included multiple plastic cycles to simulate the large cumulative plastic deformation demands from the long-period ground motions (Figure 5.11 (b)). Comparison of those tests with this member test enabled us to observe directly the effect of RC floor slabs on the connection behavior.

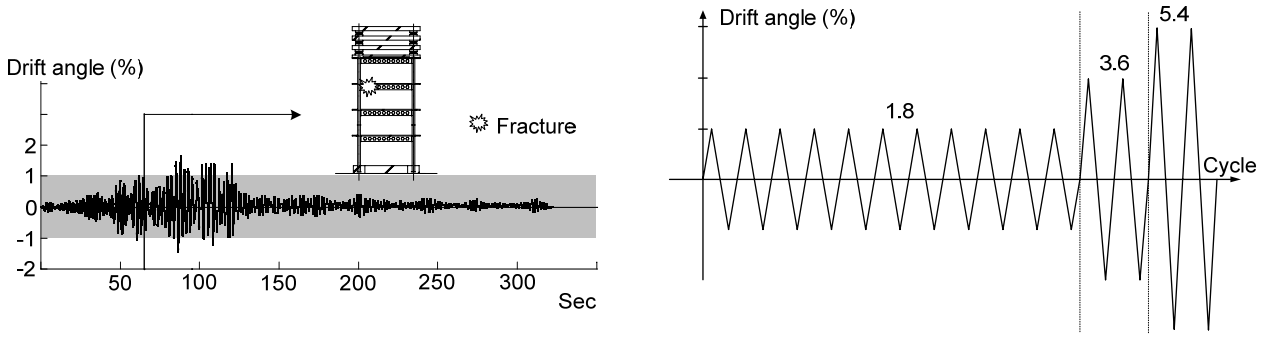

(a) (b)

Figure 5.11 Referenced loading program: (a) Inter-story drift time history of the E-Defense test; (b) Past bare beam test

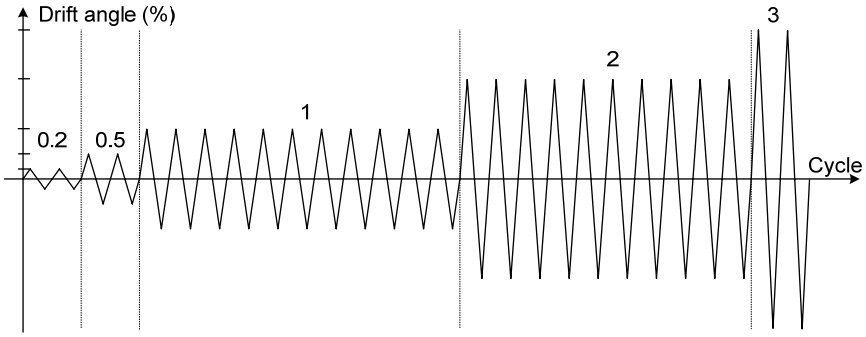

Figure 5.12 Loading program

Measurement

Forty-five channels of data were collected during the loading of each connection, including strains (by strain gauges) and displacements (by displacement transducers). Figure 5.13 shows the measurement detail. Plastic gauges, which were able to measure a strain value to 15%, were placed at both sides of the weld access holes to measure the strain concentration at that location (Figure 5.13(b)).

The beam rotation θ_b as obtained by subtracting the deformations of the column and panel zone from the story drift angle (loading amplitude). Because of the presence of the orthogonal beams (H-446×199×8×12 (SS400)) at the panel zone, the panel zone deformation was unable to measure by displacement transducers. The deformation was obtained by dividing the moment acted at the panel zone using the elastic stiffness of the panel zone. The moment acted at the panel zone was determined by multiplying the jack loading by the distance from the jack to the gravity center of the panel zone. The elastic stiffness of the panel zone was estimated by following the design code (AIJ. 2006).

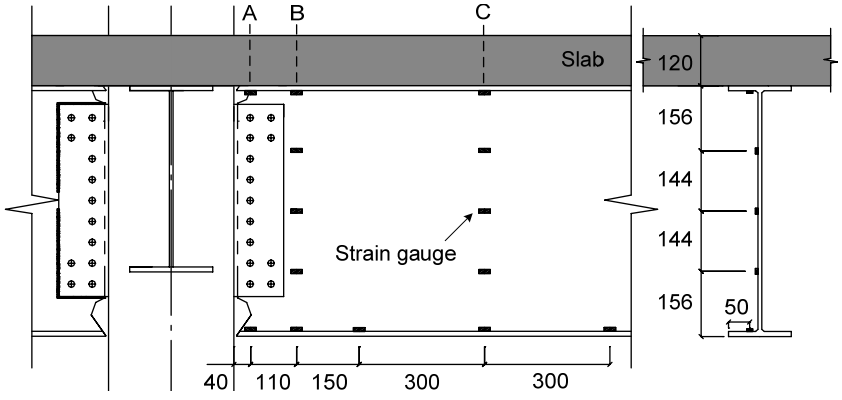

(a)

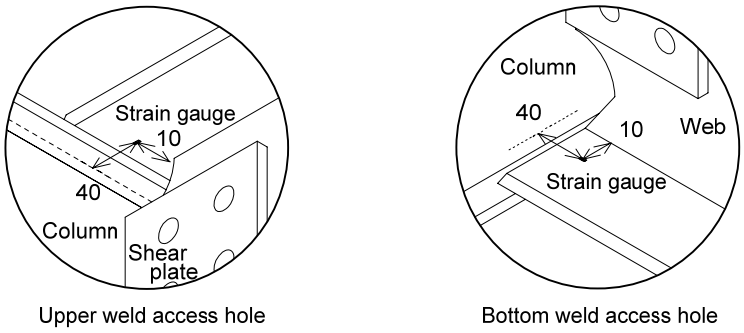

(b)

Figure 5.13 Measurement: (a) Gauges at beam end; (b) Locations of the gauges at Section A

5.5 Observations and hysteretic behaviors

Original connection

The normalized bending moment versus rotation relationship are shown in Figure 5.14(a). The rotation represents the rotation angle between the beam end to the pin support. The hysteretic behavior shows stable loops under the 11 cycles of 1% drift angle loadings (beam rotation was about 0.006 rad). A crack extended from the toe of the weld access hole in the first positive cycle of the 2% drift angle, with the beam rotation of 0.018 rad (Figure 5.14(b)). The crack leaded to fracture of the bottom flange in the next positive bending and made the resistance reduced significantly in the positive bending. Figure 5.14(c) shows a close-up of fracture. Most of the fracture surface was in the base metal of the flange.

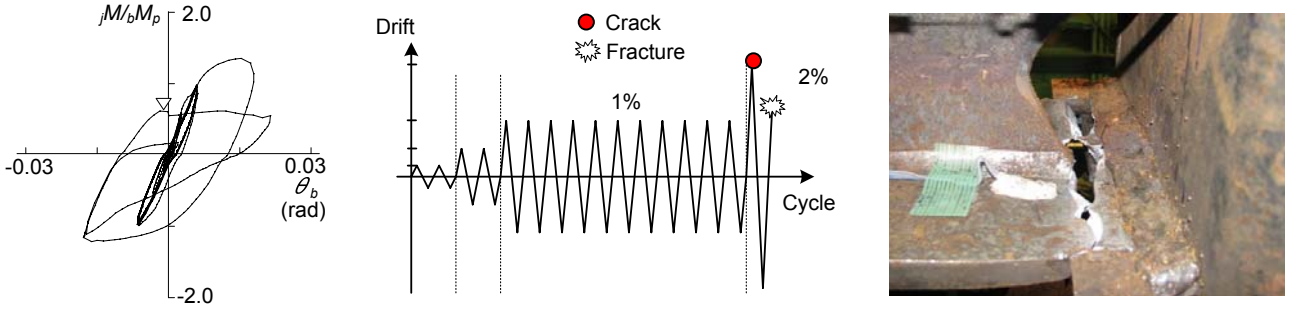

(a) (b) (c)

Figure 5.14 Test result of the original connection: (a) Moment and rotation relationship; (b) Loading history; (c) Fracture situation

Connection with supplemental welds

In the connection with supplemental welds, a crack was observed at the toe of the bottom flange weld access hole during the first positive bending of the 2% drift angle (Figure 5.15(a) and (b)), with the beam rotation of 0.017 rad. In the negative bending, local buckling was formed in the bottom flange, while fractured in the second cycle of the 2% drift angle (Figure 5.15(c)). The connection fractured at nearly the same instant with the original connection. Both the maximum deformation capacity and

fracture pattern were very similar between these two connections. However, the maximum strength of the connection with supplemental welds increased to 1.55 ${}_bM_p$ from 1.36 ${}_bM_p$ of the original connection, and the cumulative ductility ratio increased to 19 from 13 of the original connection. The supplemental welds increased the maximum strength at a value of 14%, and fattened the hysteresis loops, which resulted in an increase in the cumulative ductility. Here, the cumulative ductility ratio was defined as the total dissipated energy obtained from the hysteretic loops of the connection divided by the product of the full plastic moment and the beam yield rotation of the bare beam. It was also observed in the connection with supplemental welds that the measured strain reached about 1.5% at the bottom flange weld access hole (in the positive loading) and 3% at the top flange weld access hole (in the negative bending), respectively, during the amplitude of 1% drift angle. In the original connection, the strain was about 1.5% at the bottom flange weld access hole (in the positive loading) and 0.1% at the top flange weld access hole (in the negative bending), during the 1 % drift angle. It is notable that the strain at the top flange increased 30 times (from 0.1% to 3%) by the application of all-weld in the shear tab.

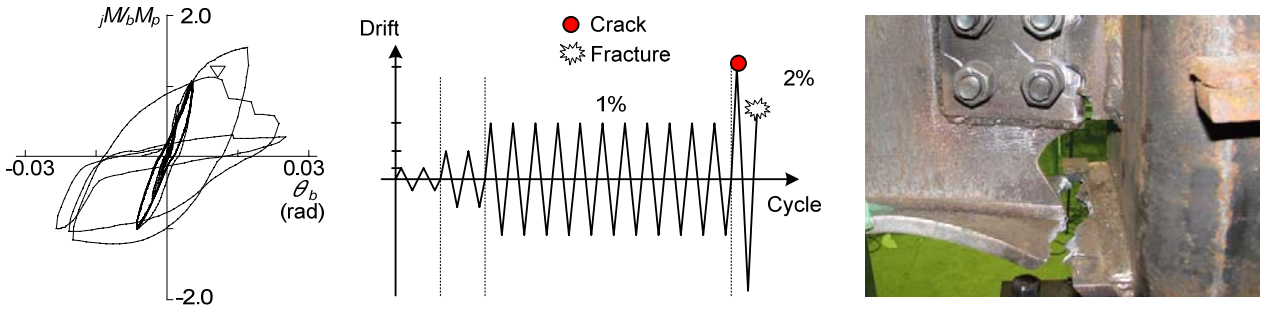

(a) (b) (c)

Figure 5.15 Test result of the connection with supplemental welds:
(a) Moment and rotation relationship; (b) Loading history; (c) Fracture situation

Wing plate connection

The connection was able to sustain more cycles than the previous two connections (Figure 5.16(a) and (b)). Local buckling occurred at the tip of the wing plates under the first negative bending of the 2% drift angle, with the beam rotation of 0.015 rad. A crack initiating from the toe of weld access holes of the top flange was observed in the next 2% drift angle cycle and lead to an eventual fracture after experiencing 10 cycles of the 2% drift angle loading. The fracture at the top flange lead a rapid strength loss in the negative bending. Figure 5.16(c) shows the close-ups of the local buckling and fracture. In the past bare beam test (Tsai et al. 1996), attaching wing plates on the top and bottom flanges enhanced the connection to be able to sustain a 4% drift angle deformation and buckled at the tip of the wing plates. Comparing with that, retrofitting the bottom flange only could caused the top flange sustain high strain in the negative bending and fracture under half of the deformation level.

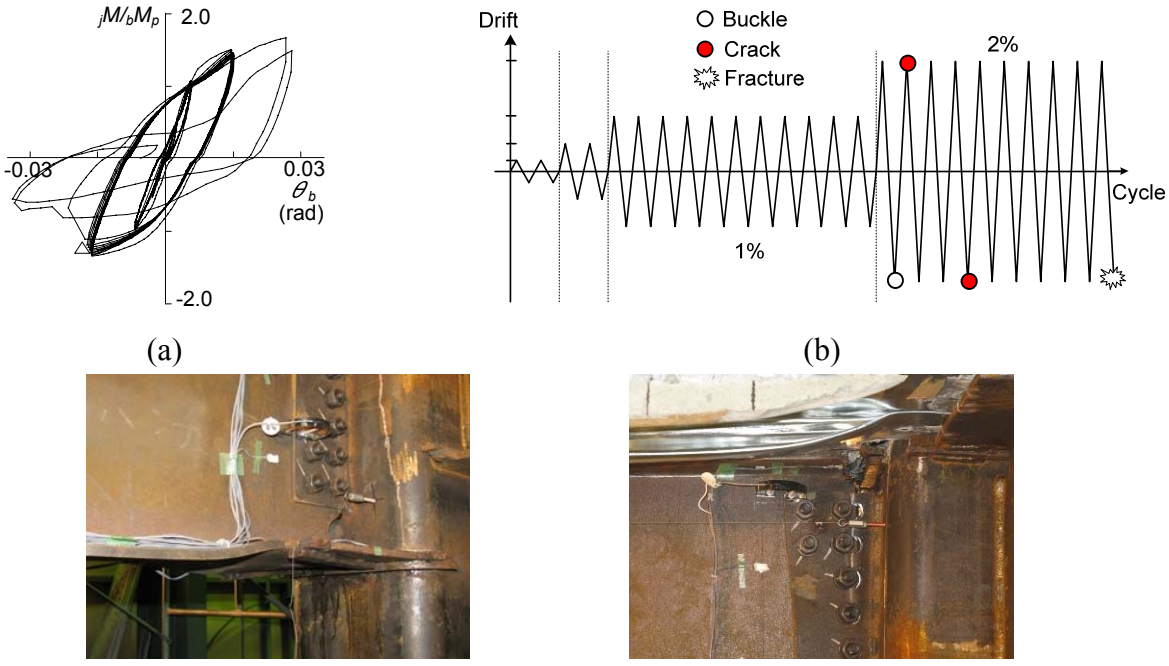

Figure 5.16 Test result of wing plate connection: (a) Moment and rotation relationship; (b) Loading history; (c) Local buckling and fracture

Haunch connection

Both the strength and deformation capacity were greatly improved by attaching the haunch. A crack at the top flange and buckling at the tip of the haunch (450 mm from the column face) were observed at the first 2% drift angle loading (Figure 5.17(a) and (b)). The strength and stiffness gradually decreased after the buckling. The negative bending moment decreased to 70% of the maximum strength under the 3% drift angle amplitude. After the second cycle of the 3% drift angle, the test was terminated due to severe buckling. Figure 5.17(c) shows a close-up of the buckling at the end of loading. The haunch enhanced the resistance and ductility of the bottom and made the crack to have occurred only at the top flange weld access hole, which was similar to the crack observed in the wing plate connection. The crack of the top flange, however, did not lead to fracture in this connection. No crack was observed either at the bottom flange or the haunch. Compared with the past test results (Uang et al. 2000, Lee et al. 2003) which both showed the connection was able to sustain 4% story drift angle, the haunched connections were able to sustain at least 3% drift angle. The presence of the hunch effectively moved the plastic hinge of the beam outside the haunch region as intended in the design.

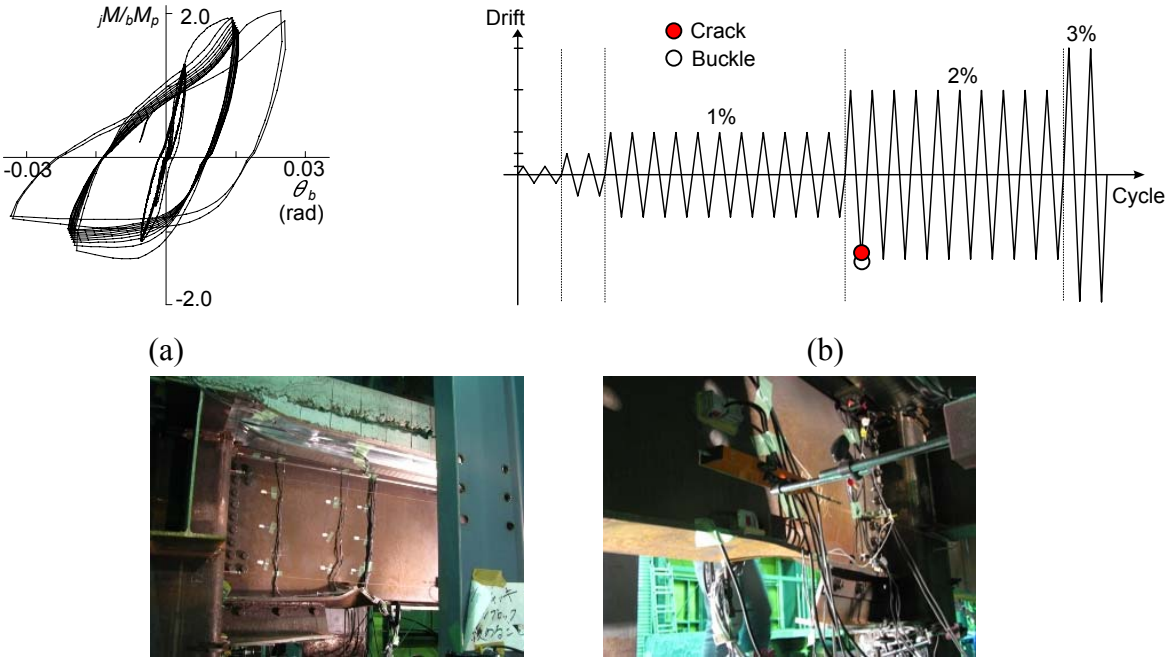

Figure 5.17 Test result of haunch connection: (a) Moment and rotation relationship; (b) Loading history; (c) Plastic hinge formation

5.6 Retrofit performance

5.6.1 Maximum strength

E-Defense connection versus the original connection

The original connection was designed to duplicate the field weld connection with thirteen bolts adopted in the E-Defense specimen. Figure 5.18 shows the hysteresis loops of the original connection and the corresponding E-Defense connections. The connections exhibited similar resistance under the same deformation level. In terms of crack formation, cracks of the two tests all started from the toe of weld access holes and fractured at the bottom flange.

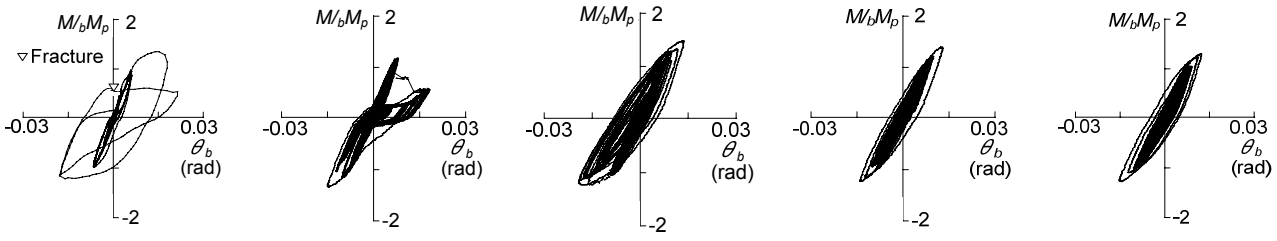

Figure 5.18 Hysteresis loops of original connection and E-Defense connections: (a) Original connection; (b) E-Defense connections

The initial stiffness, maximum strength and yielding strength of the connections are

summarized in Table 5.3, together with the corresponding E-Defense connections. The maximum strength in the positive and negative bending was normalized by the full plastic strength ${}_bM_p$ of the corresponding bare beam. The initial stiffness was taken as the secant stiffness between the origin and the 0.005 rad beam rotation and normalized by the stiffness of the bare beam. The yield strength was determined when the strain at the toe of the weld access hole exceeded the material's yield strain (Section A in Figure 5.13). In both the E-Defense and original connection, maximum strength and stiffness showed notable coordination. The presence of RC floor slabs apparently increased both the strength and initial stiffness in the positive loading to about 1.3 and 1.2 times those of the corresponding bare beams. Yielding strengths are about 70% of expected full plastic moment.

Member test

In the test, the maximum strength, initial stiffness and yield strength varied according to the respective retrofit methods. The haunch connection was able to sustain about two times the full plastic moment of the bare beam. Comparing the maximum negative flexural strength ratio ($M_{max}^-/{}_bM_p$) with the connection strength ratio ${}_jM_u/{}_bM_p$ estimated in the design stage, the test result of each connection shows good correlation (Table 5.2). The maximum strength of the original connection is 8% larger than the estimated value. For the connection with supplemental welds, the wing plate connection, and the haunch connection, the test results are 4, 4 and 9% smaller than the corresponding estimated values, respectively.

Comparing the maximum positive bending $M_{max}^+/{}_bM_p$ with the ${}_{cb}M_p/{}_bM_p$ shown in Table 5.2, the original connection had a 2% difference, connection with supplemental welds had a 14% difference, wing plate connection had a 10% difference, and the haunch connection had a 11% difference with respect to the estimated value. When the effects of RC slab was taken into consideration, the estimated strength of composite beam still showed well coordination with the test results. In the retrofitted connections, the maximum strength of the haunch connection was the largest, 1.5 times larger than that of the original connection. The $M_{max}^+/{}_bM_p$ of the connection with supplemental welds and the wing plate connection were 1.1 and 1.2 times of that of the original connection. The strength was not significantly improved by those retrofits. In the haunch connection, however, the greatly enlarged strength might reverse the strong column weak beam mechanism and lead the column failure in the end. Thus, care should be taken for this type of retrofit so that the retrofitted connection might not be too large in the strength increase.

Table 5.3. Maximum strength and initial stiffness of connections

	$M_{max}^+/{}_bM_p$	$M_{max}^-/{}_bM_p$	K^+/K_b	K^-/K_b	$M_y/{}_bM_p$
E-Defense	1.33	1.22	1.15	1.05	0.77
Original	1.36	1.16	1.21	1.15	0.72
Supplemental welds	1.55	1.22	1.43	1.28	0.65
Wing plates	1.67	1.34	1.47	1.21	0.90
Haunch	2.04	1.34	1.47	1.50	1.28

1. ${}_bM_p$, K_b : Full plastic moment and stiffness of bare beam, M_{max}^+ : Positive bending, M_{max}^- : Negative bending, K_c^+ : Positive stiffness, K_c^- : Negative stiffness

Strain concentration

Figure 5.19 shows the strains at the bottom flange, measured at a location 40 mm farther from the column face (section A in Figure 5.13) and for various beam rotations. Strains are plotted for positive bending, i.e., when the bottom flange sustained tension. The thirteen bolts filed weld connections in E-Defense test was also illustrated. The original connection exhibited about twice as large strains as the corresponding field weld connections of the E-Defense specimen. The slab thickness adopted in these two tests was identical, although the steel beam and column was scaled to 3/4 in the original connection. This was due to the difficulties in reducing the scale of the concrete part including studs, and this disparity generated a larger composite effect on the original connection. Incidentally, the shop weld connections of the E-Defense test were identical in the beam depth (600 mm) and slab thickness (120 mm) with the original connection in the member test. Comparison of those indicates that the field weld connection caused about four times larger strain values at the bottom flange, suggesting that the field weld connection would promote strains at the bottom flange most likely because of the lesser constraint in the web to the column than the corresponding shop weld connection.

Both bare beam specimens tested in the Yamada (2008) and Kitamura (2008) tests were subjected to the loading history; eleven cycles with the 1.8% drift angle amplitude, which was twice the elastic rotation corresponding to the full plastic moment, and two cycles with the amplitudes of 3.6% and 5.4%. In the Yamada specimen, initial cracks started in the forth cycle of the 1.8% amplitude, and the connections fractured in the tenth cycle of this amplitude. In the Kitamura specimen, initial cracks started in the ninth cycle of the 1.8% amplitude, and the connection experienced two more cycles of 1.8% and one cycle of 3.6% amplitudes before fracture. Comparing with those bare beam connections, the original connection in the member test fractured in the cycle immediately after cracks were developed in the 2% amplitude. It appears that the presence of RC floor slab promoted fracture after initial cracks because of high strains induced in the bottom flange.

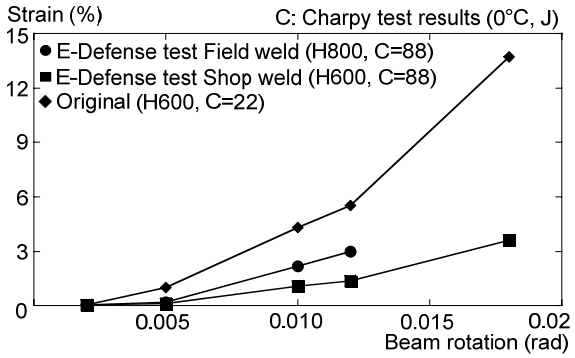

Fig. 5.19 Growth of bottom flange strains

5.6.2 Cumulative plastic rotation

To evaluate the cumulative deformation capacity of the retrofitted connections, the cumulative plastic rotation ($\Sigma_b\theta_p$) of all connections are shown in Figure 5.20. The cumulative plastic rotation

was calculated until the fracture of the connection. The connection with supplemental welds fractured at the same instant with the original connection and caused very similar cumulative plastic rotation. Retrofit performance in terms of the cumulative plastic rotation capacity was not notably improved using the supplemental welds at web. For the haunch connection, the rotation was calculated until the strength was reduced to 90% of the maximum strength. The cumulative deformation capacity of the wing plate and haunch connections were both at least four times larger than those of the original connection and connection with supplemental welds.

Two past bare beam tests that had the same loading cycles but with a little difference in the amplitude was included in the figure (Yamada et al 2008 and Kitamura et al 2008). The specimen by Yamada et al. (7 bolts) and the specimen by Kitamura et al. (16 bolts) had identical connection details but with different numbers of bolts. Comparing with the original connection that represented the thirteen bolt E-Defense specimen, the effect of slab decreased the cumulative plastic rotation ratio to about 40% of the bare beams. The wing plate and haunch connections were able to sustain larger cumulative plastic rotations than the bare beams.

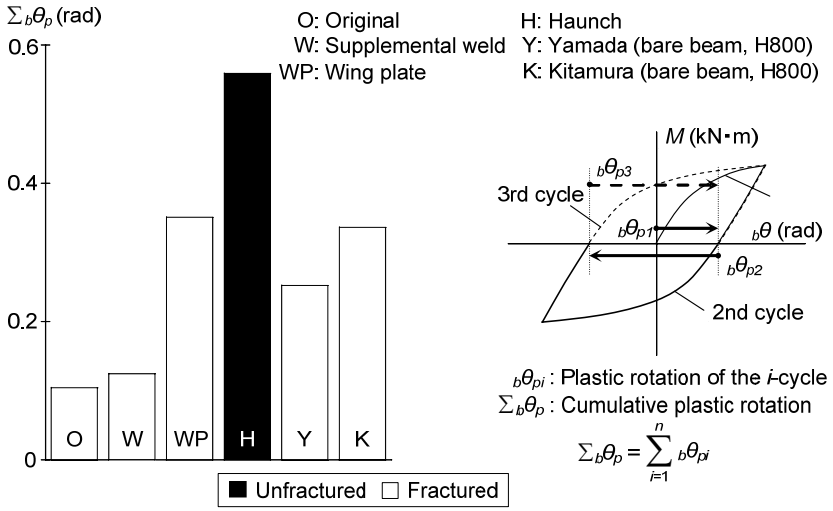

Figure 5.20 Cumulative plastic rotation

5.6.3 Cumulative ductility ratio

Figure 5.21 summarizes the cumulative ductility ratio of the four connections and the E-Defense specimen. The cumulative ratios of these connections were the sum up to fracture. The ratio of the original connection was 13, which was larger than the average value of the four fractured E-Defense connections (with the averaged ratio of 9) but smaller than those of other unfractured E-Defense connections (with the averaged ratio of 19). The ratio of the connection with supplemental welds increased to 19, which is identical with the averaged cumulative ductility ratio of the unfractured E-Defense field weld connections. The cumulative ductility ratio increased 46%. The supplemental welds did not increase the plastic rotation capacity but enlarge the maximum strength and the hysteretic loop and leaded to larger energy dissipation than that of the original connection. If supplemental welds had been applied, the field weld connections might have been able to sustain the

San wave loading. For the wing plate and haunch connections, the capacity was about 1.5 and 2.5 times of the average ratio of the unfracutred E-Defense specimen. The cumulative ductility was significantly improved by attaching the wing plates and haunch at the bottom flange.

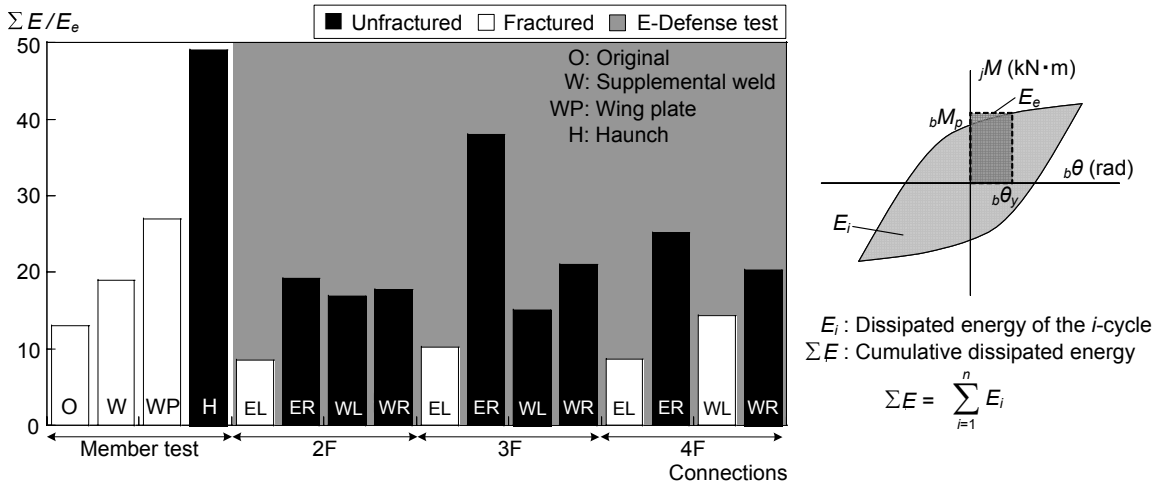

Figure 5.21 Cumulative ductility ratio

5.6.4 Strain values at the beam end

Figure 5.22 summarizes the maximum strain history at the top and bottom flange weld access hole under the positive and negative bending (section A in Figure 5.13). The yield strain (ε_y) was estimated from the measured material properties. Under the 0.2 and 0.5% drift angle amplitudes, the strains remained elastic except for the connection with supplemental welds. The bottom flange yielded at the 0.5% drift angle amplitude.

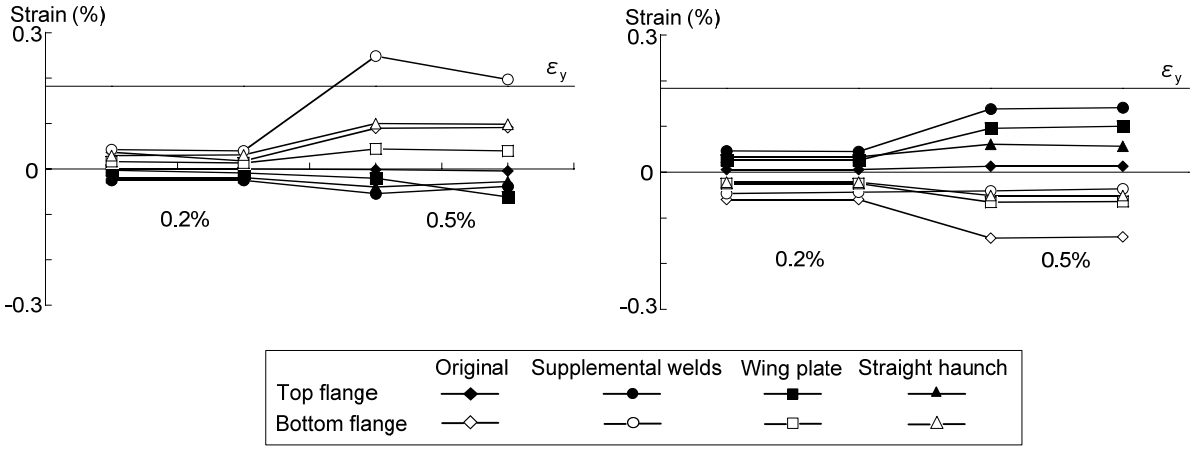

(a) (b)

Figure 5.22 Strains at weld access holes under 0.2 and 0.5% drift angle amplitude:
(a) Positive bending; (b) Negative bending

Figure 5.23 shows the strain history of the connections under the 1 and 2% drift angle loading. Strain history at the top and bottom flanges (section A in Figure 5.13) of each connection were plotted separately.

Effects of the supplemental welds

Under the 1% positive bending, the strain values at the bottom flange of the original connection and the connection with supplemental welds were about 1.0 to 1.5%. Under the first cycle of the 2% drift angle loading, the strains all exceeded 100 times of the yield strain (ε_y). The supplemental weld at web was not likely to reduce the strain at the bottom flange and made the connection fractured at the same cycle as in the original connection. The ductility capacity did not improve. It is notable that the supplemental weld significantly increased the strain at top flange to about 2.5%, which was about 25 times of that of the original connection (Figure 5.23(a) and (b)). Similar results were also observed under the 2% drift angle amplitude. The welds at web significantly altered the strain distribution.

Effects of the wing plates and haunch

Under the 1% drift angle amplitude, the maximum strain at the bottom flange of the wing plate and straight haunch connections were about 1/5 of that of the original connection and the connection with supplemental welds (Figure 5.6(c) and (d)). Retrofit of the bottom flange apparently lessened the strain concentration and made the most vulnerable spot, i.e., the vicinity of the toe of the weld access hole, remained elastic. Under the 2% drift angle amplitude, strain concentration at the wing plate and straight haunch connections were still smaller than the other two connections and did not bring any fracture, while they experienced the same cycle with the original connection. On the other hand, attaching wing plates and straight haunch at the bottom flanges made the strains at the top flange increased to twenty times larger than that of the original connection under the 1% drift angle amplitude. The wing plates and straight haunch effectively decreased strain concentration at the bottom flange; instead they caused larger strains in the top flange. The wing plate connection finally fractured at the top flange after experiencing ten cycles of this large strain value. As the result, deformation capacity was significantly improved in the two connections. After the second cycle of the 2% drift angle loading, strains at the top flange of the wing plate and straight haunch connections decreased because of the buckling at the tip of wing plates and haunch.

Strain at the top and the bottom flange

In the comparison between the strain at the bottom flange of the original connection and the strain at the top flange of the wing plate connection, the strain value of the wing plate connection was about 30% larger than that of the original connection under the 1% drift angle loading (Figure 5.23(a) and (c)). However, the strain at the bottom flange of the original connection exceeded 10% when it was subjected to the 2% drift angle and fractured along the base metal of the bottom flange. The top flange of the wing plate connection sustained a strain of about 4% under the 2% drift angle loading. The connection fractured at the top flange after experiencing ten cycles of the 2% loading. Until the fracture, the cumulative strain value of the top flange of the wing plate connection was 1.7 times larger than that of the fractured bottom flange of the original connection.

This suggests that the top flange was more capable to sustain higher strains than the bottom flange. In the field weld connection with the early time connection details, the weld access hole is

significantly larger in the bottom flange than in the top flange. The toe of the bottom weld access hole is also located at the weld boundary between the weld metal and bottom flange, which is considered as one of the reasons to make the fracture strain of the bottom flange smaller than that of the top flange.

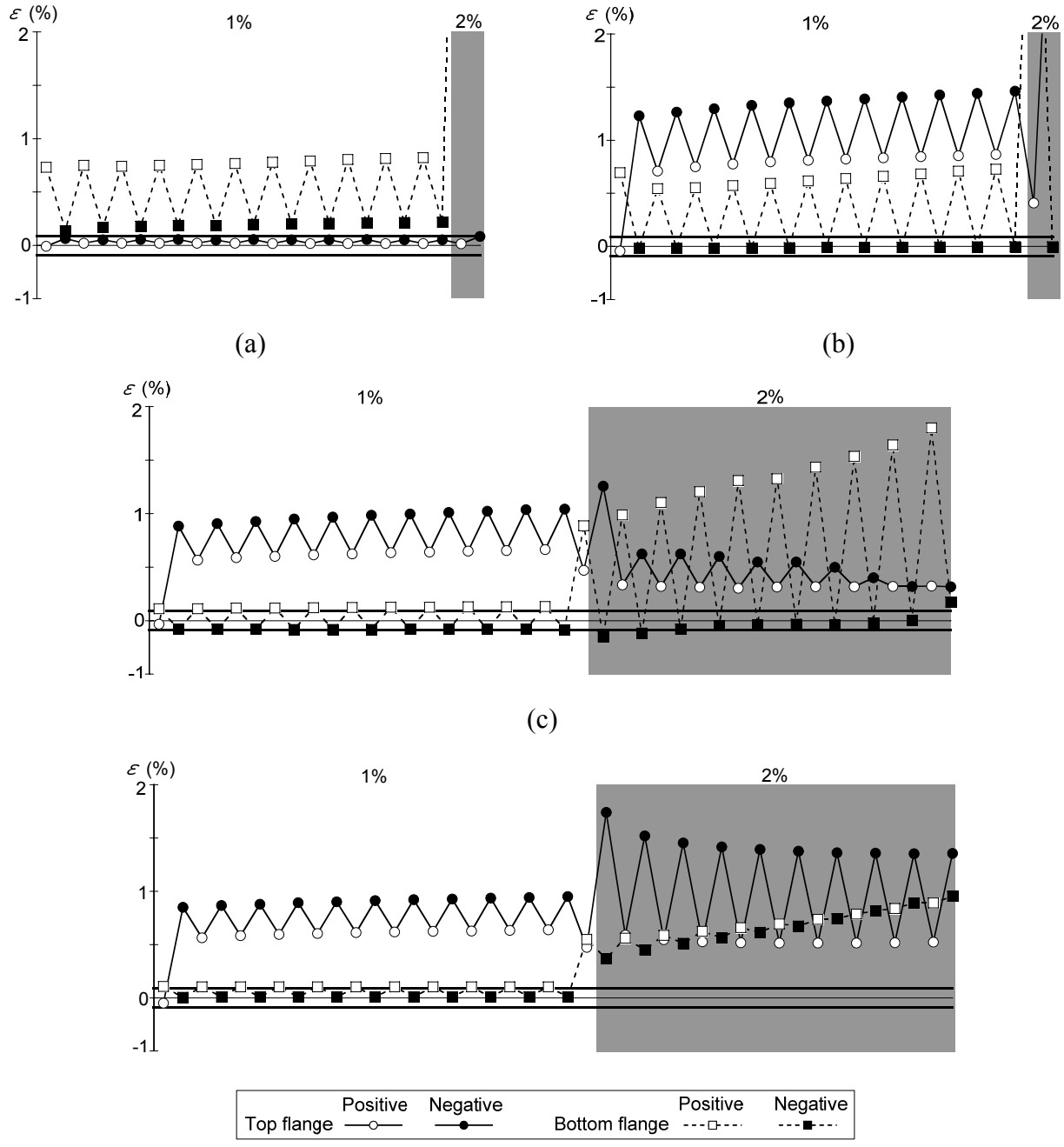

Figure 5.23 Strain values at flange weld access holes in top and bottom flanges:
(a) Original connection; (b) Connection with supplemental welds; (c) Wing plate connection;
(d) Haunch connection

5.6.5 Strain distribution

Figure 5.24 shows the strain values at different locations along the beam length for the bottom flange and under the 1 and 2% drift angle loadings. Comparing with the original connection and connection with supplemental welds, the wing plate and straight haunch connections effectively spread the plastic zone to a longer distance from the column instead of highly concentrated plastic zone near the weld access hole. In the 2% drift angle loading, the highest strain of the wing plate connection stayed at the bottom flange weld access hole, which was similar in the strain distribution to the original connection. In the design, when the beam section at the tip of the wing plates reached the full plastic moment, the resistance at beam end was 1.05 $_bM_p$, which was close to the connection strength ratio ($_jM_u/_bM_p$=1.11). Small local buckling occurred at the tip of the wing plates. The highest strain remained at the beam end, the weakest spot, and lead to fracture at the top flange instead of the strengthened bottom flange. The strain concentration region were distributed to the beam end and the tip of the haunch (450 mm from the column face), and caused a smaller value at about 1%.

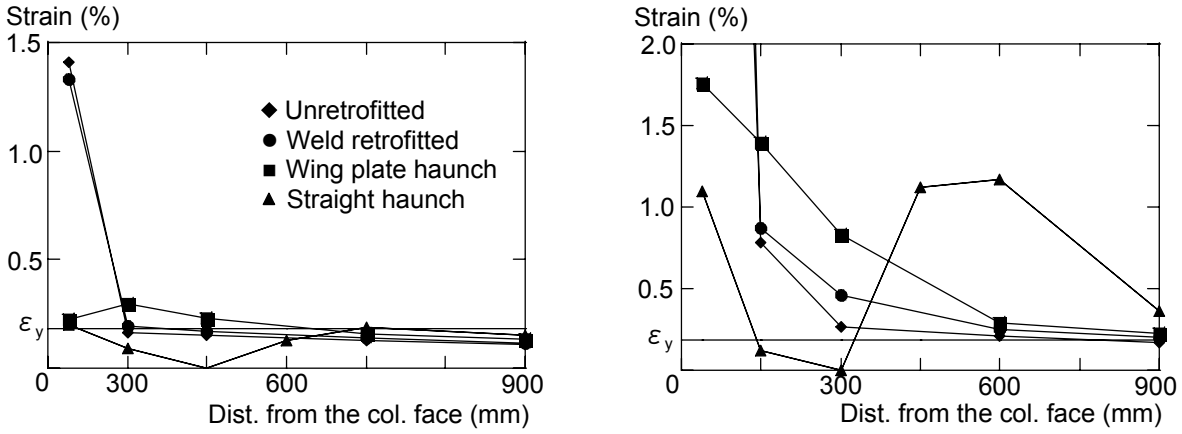

(a) (b)

Figure 5.24 Strain at bottom flange: (a) 1% drift angle; (b) 2% drift angle

5.6.6 Section moment calculation from the measured strains

The three retrofitted connections changed the strain distributions of the connection significantly. Beam moment sustained by the flanges, web and slab might change and lead to three types of failure modes: fractured at the bottom flange (connection with supplemental welds), fractured at the top flange (wing plate connection) and plastic hinge at beam (haunch connection). To evaluate the effect retrofit on the section moment transfer in the connection, the measured strains at B and C sections (located 150 and 600 mm away from the column face as shown in Figure 5.13) were used. Here, considered was the distribution of the moment resistance by the beam flanges, the beam web, and the floor slab with respect to the total moment resistance. Figure 5.25(a) shows the method to estimate the strength from the strain distribution at the section. By linearly connecting the strain

values at different positions along the depth of the section, the location of the neutral axial was determined. In this test, the location was confirmed to be located in the web for all specimens. Then, the section force ${}_sF_1$~${}_sF_7$ were obtained as the product of the sectional area between the two strains, the average strain and Young's modulus. For example, ${}_sF_2$ was the product of the area of Section 2, the average of ε_1 and ε_2, and Young's modulus. Thus, the force acting at the concrete slab section and the entire section moment could be determined by the following equations.

$$ {}_cF = \sum_{j=1}^{7} {}_sF_j \tag{5.5} $$

$$ {}_bM = \sum_{j=1}^{7} d_j \cdot {}_sF_j + {}_cd \cdot {}_cF \tag{5.6} $$

The beam section moment at B can also be obtained from the reaction force measured at the pin support at the end of the beam. Figure 5.25(b) shows the correlation between the section moment obtained from the measured beam section strains and that measured from the reaction force. The difference between the two values becomes larger when the connection sustained deformation larger than the 1 % drift angle amplitude (with the maximum error of about 20%). For the 1 % drift angle and smaller deformation, the results mostly located along the 45 degree line (with the error not greater than 10%). Thus, the estimate method remained reasonable when loading was up to the 1% drift angle.

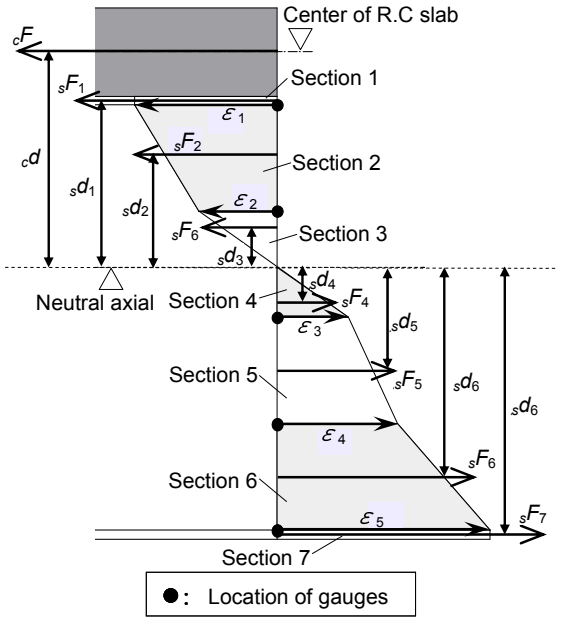

(a)

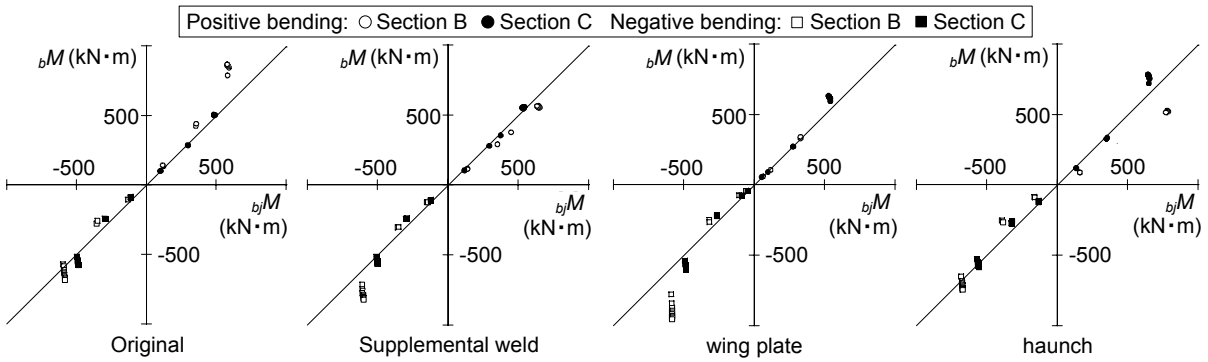

(b)

Figure 5.25 Section moment calculation: (a) Section moment measurement scheme; (b) Correlation with directly measured moment

5.6.7 Effective width of slab

Figure 5.26 shows the equivalent effective width of the RC slab for the original connection, connections with supplemental welds, and wing plate connection when subjected to the 0.2, 0.5 and 1 % drift angle loadings. The haunch connection was not listed, because the haunch changed the beam depth and made the plastic area more complicated than the other three connections. The effective widths at Sections C (Figure 5.13) were obtained by dividing the section force of the RC slab ($_cF$) by 0.85 times of concrete compress strength ($0.85F_c$) and the thickness of the slab (120 mm). The section force of RC slab was the resistance when the connection sustained the maximum positive deformation in each cycle.

The effective widths were very small under the 0.2 and 0.5% drift angle loadings, because the compression force at RC slab was over estimated under this deformation. According to the Japanese design criteria, the estimation of the full plastic moment of the composite beam should consider the column width as the effective width when the plastic hinge is expected to occur at the beam end (AIJ. 2002). In this test, the results at the section showed correspondence with the criteria in the 1 % drift angle loading.

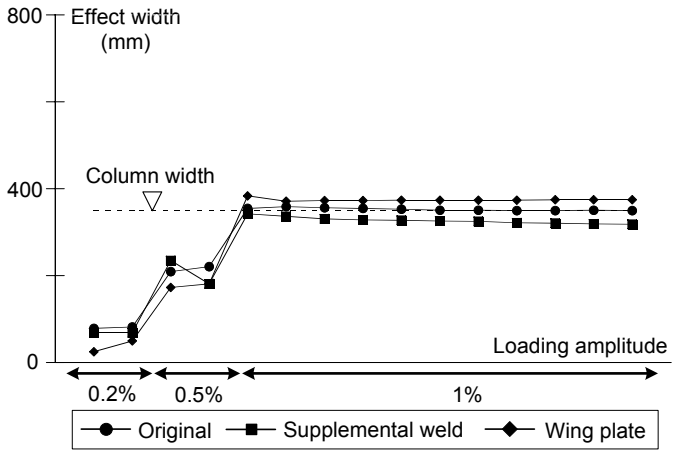

Figure 5.26 Equivalent effect widths of the RC slab

5.6.8 Section moment transfer ratio

Figure 5.27 shows the section moment transfer ratio at Sections B and C when the connections were subjected to the 0.2, 0.5 and 1% drift angles. Values in the figure were obtained when the connections reached the maximum deformation in each cycle. The moments of the RC slab, flanges and web at the positive and negative bending were obtained by section forces ($_sF_1$~$_sF_7$, proposed in the previous section) and normalized by the estimated section moment $_bM$. When the beam yielded, the yielded section force was obtained by using the measured yield strain.

In the negative bending of Section C, the original and connection with supplemental welds showed similar distribution of the section moment transfer. The tension side of the section (rebar, top flange and upper part of web, illustrated as ■, ▧ and ▩ in the figure) sustained about 60% and the compression side of beam section (bottom flange and bottom part of web, illustrated as ▫ and ▨ in the figure) sustained about 40% of the section moment. For the wing plate connection, the tension and the compression sides of the section sustained about 65 and 35% of the section moment. Retrofit of the bottom flange increased the moment transfer of the steel rebar, top flange and the tension side web under negative bending.

Under positive bending, the moment transfer at the top flange of the connection with supplemental welds was significantly different with the other two connections. In Section B, the moment transfer at the top flange of the connection with supplemental welds was about 20% which was larger than 5% of the original and wing plate connections under the 1% drift angle loading. The high stress at the top flange corresponded with the observation of high strain concentration at the top flange (Figure 5.23(d)). The ratio of the web moment (the sum of that of the top and bottom part of web) versus flange moment of the original, connection with supplemental welds and wing plate haunch connections were 1.0, 0.3 and 0.6, respectively. Supplemental welds reduced the moment transfer at web. In Section C, the moment transfer at the top flange of the connection with supplemental welds decreased to 7% and the moment transfer at web increased to 22% which both were similar with those of the other two connections. Supplemental welds made the top and bottom flange of the beam end sustain high strain end.

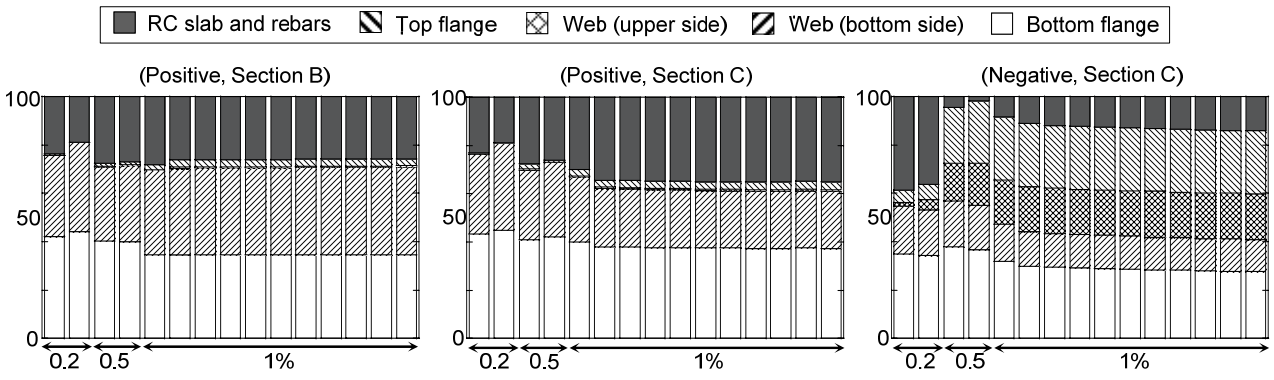

(a)

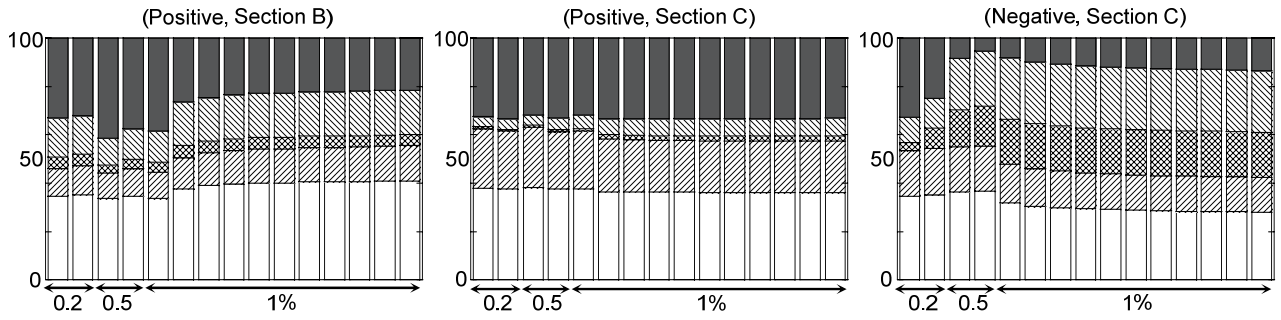

(b)

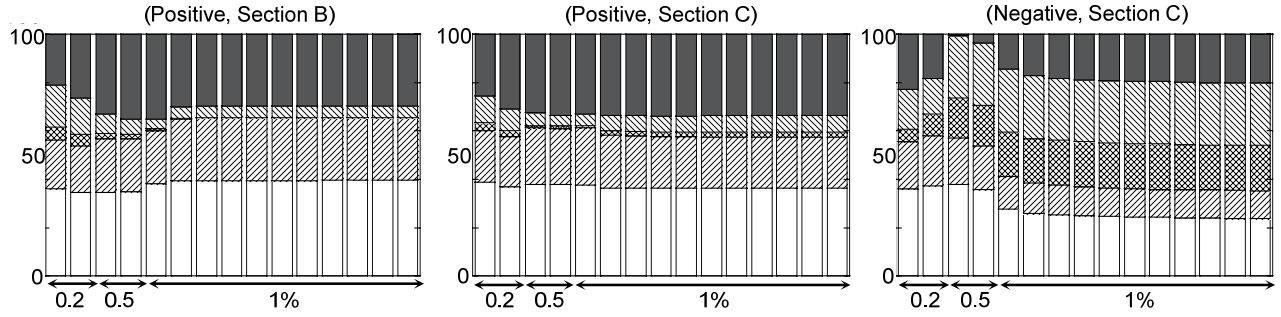

(c)

Figure 5.27 Moment transfer at different sections of beams: (a) Original connection; (b) Connection with supplemental welds; (c) Wing plate connection

5.6.9 Deterioration of stiffness

Figure 5.28 shows the stiffness decrease of the connections after each cycle of loading. The stiffness was obtained from the unloading stiffness of each positive bending and normalized by the estimated bare beam stiffness K_b. The secant stiffness was measured at the final 0.005 rad beam rotation interval before the loading force returned to zero. The stiffness of original connection was about 70% larger than the estimated stiffness of the bear beam. For the connection with supplemental welds, wing plate and haunch connections, the initial stiffness increased by about 80, 90 and 150%, respectively. Stiffness decreased in the first cycle of the 1 and 2% drift angle loading and kept constant under loading with the same amplitude. Cracks of RC slab developed under the first cycle was considered as the main source to decrease the stiffness, and the stiffness remained constant after the cracks were deformed. Figure 5.29 shows the cracks of slab after the 2% drift angle loading. Cracks along the beam direction were mostly connected after the first cycle of 2% drift angle and lead to significant stiffness decrease (Figure 5.28).

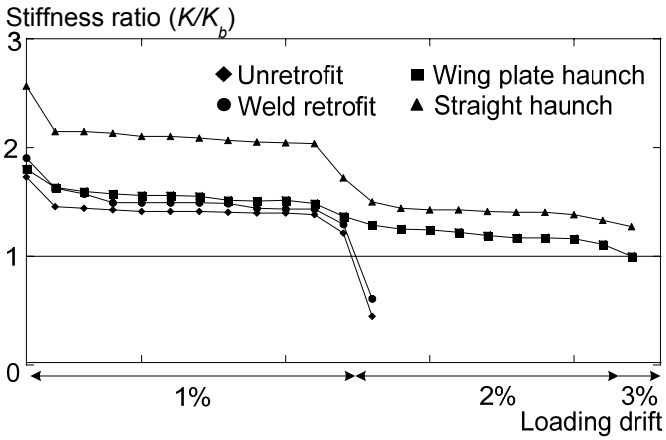

Figure 5.28 Stiffness reduction with increasing amplitudes

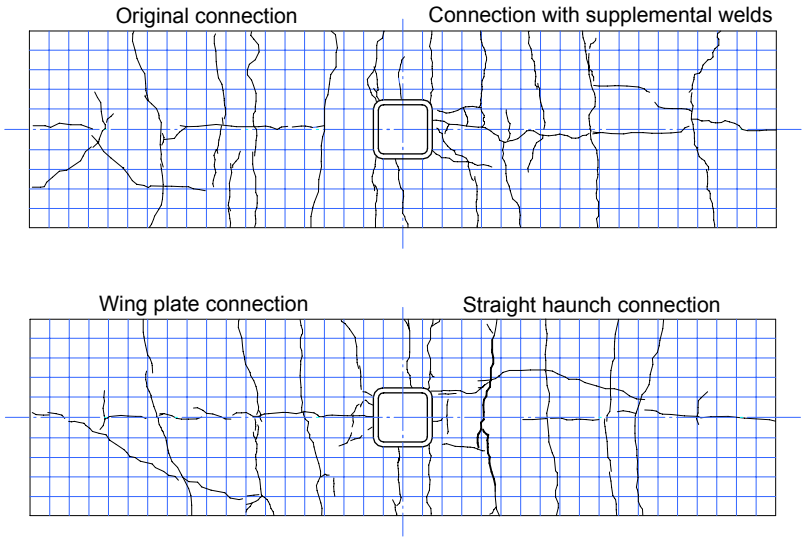

Figure 5.29 Cracks of RC slab

5.6.10 Strain distribution in the RC slab

Figure 5.30 shows the strains of steel rebars arranged in the longitudinal direction of the RC slab. Locations of the strain gauges were aligned with the strain gauges mounted on the steel beam, i.e., 40 mm away from the column face (Section A in Figure 5.13). In the figure, the horizontal axial is the strain value of connection. The vertical axial shows the locations of the strain gauges in the slab plane. In positive bending, all rebars (ϕ13) remained elastic. The whole section of RC slab sustained compression force under the loading. When the deformation became larger, the stains increased especially in the rebar close to the column. In negative bending, tensile stains of the rebars were distributed equally. The rebar sustained similar tensile forces and remained elastic under the 1% drift angle. For the haunch connection, the rebars had to sustain larger tensile forces because of the significant increase of the beam's moment of inertia.

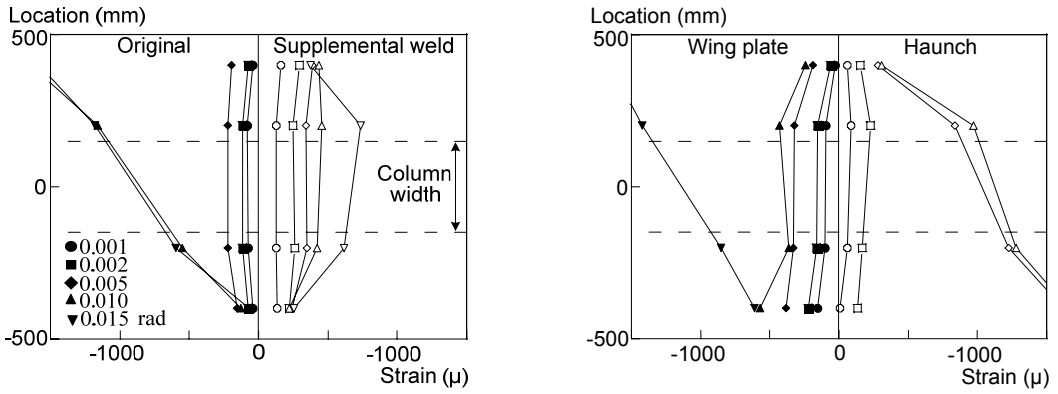

(a)

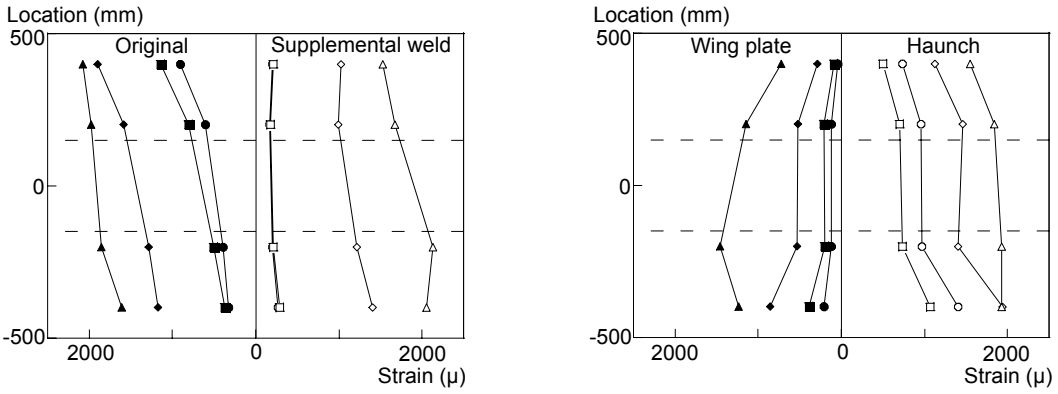

(b)

Figure 5.30 Strain distributions in steel rebars: (a) Positive bending; (b) Negative bending

5.7 Conclusions

A quasi-static test on beam-to-column subassemblages that mimicked the E-Defense connections was conducted. Retrofit was considered, and the original connection was modified by three types of retrofit particularly in consideration of constructability. The loading history included cyclic plastic deformations determined in reference to the seismic response of the E-Defense test when subjected to the long-period ground motion. The connections were tested until fracture or the development of very large plastic deformations. The cumulative ductility capacity of these connections was quantified in reference to the test results. The equations to estimate the strength of the retrofitted connections were proposed and compared to the test results. The main observations are summarized below:

1. The strain at the bottom flange weld access hole of the original connection reached 1.5% under the 1% drift angle and exceeded 10% under the 2% drift angle loading. The high strain concentration made a crack occur at the toe of weld access hole and fractured along the base metal of beam. The cumulative ductility ratio was 13, which was located between that of the fractured and unfracutred field weld connections in the E-Defense test. Comparing with the shop weld connections in the E-Defense test, the field welded original connection generated a strain

value four times as large at the bottom flange, while those two connections had an identical beam depth and slab thickness. The filed weld connection with early time connection details tended to generate larger strain concentration at the bottom flange.

2. The supplemental welds at the web changed the strain distribution at the connection. The strain concentration at the bottom flange was not reduced, but it increased at the top flange instead. The connection cracked at the bottom flange weld access hole and fractured eventually at the same instant with the original connection.
3. The cumulative plastic rotation of the wing plate and haunch connections were at least four times the value obtained for the original connection. The connections were not fractured at the bottom flange at the end of loading, because the strain concentration at the bottom flange was effectively reduced by the retrofit in the bottom flange. Retrofit on the bottom flange increased the strain concentration on the top flange and lead to fracture of the wing plate connection after experiencing ten cycles of the 2% drift angle loading. The cumulative strain at the top flange measured up to fracture was 1.7 times of that at the bottom flange of the original connection. The plastic hinge occurred at the tip of the haunch under the 2% drift angle. The connection was able to sustain a 3% drift angle without fracture.
4. The accuracy of the proposed strength estimation equations developed for the retrofitted composite beams was verified. Comparing with the test results, the estimation were smaller at a difference of about 10%. The equations were able to estimate the strength of the retrofitted connections reasonably.
5. Comparing with the original connection, the supplemental weld at web changed the strain concentration at the top flange and lead the cumulative ductility ratio increased. However, the cumulative plastic rotation remained unchanged. The haunch showed the best performance in this test. However, the maximum strength was increased to two times the full plastic moment of the bare beam, which may make the connection stronger than the column and lead the column failure in the end. The maximum strength of the wing plate connection increased to about 1.6 times of the full plastic moment of the bare beam, and the cumulative plastic rotation was improved to 3.6 times that of the original connection. Considering the performance and constructability, the wing plate haunch connection appears the most efficient retrofit.

REFERENCES

[5.1] Architectural Institute of Japan. (1985). Design Recommendations for Composite Constructions. (in Japanese)

[5.2] Architectural Institute of Japan. (2001). Standard for Structural Calculation of Steel Reinforced Concrete Structures, Allowable Stress Design and Horizontal Load-Carrying Capacity. (in Japanese)

[5.3] Architectural Institute of Japan. (2002). Recommendation for Limit State Design of Steel Structures. (in Japanese)

[5.4] Architectural Institute of Japan. (2006). Recommendation for Design of Connections in

Steel Structures. (in Japanese)

[5.5] Architectural Institute of Japan. (2007). Long-period ground motions and the seismic resistance of buildings. (in Japanese)

[5.6] Bertero, V. V., Anderson, J. C., Krawinkler, H. (1994): Performance of steel building structures during the Northridge earthquake, Rep. UCB/EERC-94/09, EERC, Univ. of California, Berkely.

[5.7] Federal Emergency Management Agency（FEMA-350）Recommended Seismic Design Criteria for New Steel Moment-Frame buildings，2000.7.

[5.8] Harada, Y., Jung, S. M., Morita, K., (2002) Experimental Study on Repair and Modification of Beam-to-Column Connection in Steel Building. *Journal of structural and construction engineering, Architectural Institute of Japan.* 553, 097-104. (in Japanese with English abstract).

[5.9] Japan Society of Civil Engineering. Architectural Institute of Japan. (2006). Report of seismic performance improvement of civil, architectural structures subjected to long-period ground motions generated by subduction zone. (in Japanese).

[5.10] Kawabe, H., Kaname, K., Irikura, K. (2008). Damage prediction of long-period structures during subduction earthquakes-Part 1: Long-period ground motion prediction in the Osaka basin for future Nankai Earthquakes. *Proc. 14th World Conf. Earthq. Eng.*

[5.11] Tsai, K. C., Popov, E. P., (1988) Steel beam-column joints in seismic moment resisting frames，Rep. No. UCB/EERC-88/19, Earthquake Engineering. Research Center, University of California, Berkeley.

[5.12] Kim, Y. J., Oh, S. H., Moon, T. S. (2004) Seismic behavior and retrofit of steel moment connections considering slab effects. *Eng. Struct.*, 26(13), 1993-2005.

[5.13] Matsumiya, T., Suita, K., Nakashima, M., Liu, D., Zhou, F., Mizobuchi, Y. (2005) Effect of RC Floor Slab on Hysteretic Characteristics of Steel Beams Subjected to Large Cyclic Loading. *Journal of structural and construction engineering, Architectural Institute of Japan.* 598, 141-147. (in Japanese with English abstract).

[5.14] Engelhardt, M. D., Husain, A. S., (1993) Cyclic-loading performance of welded flange-bolted web connections，J. Struct. Engrg.，Volume 119，Issue 12，pp.3537-3550.

[5.15] Nakagawa, Y., Kaname, K., Kawabe, H., Irikura, K. (2008) Damage prediction of long-period structures during subduction earthquakes-Part 2: Long-period ground motion prediction in the Osaka basin for future Nankai Earthquakes. *Proc. 14th World Conf. Earthq. Eng.*

[5.16] Nakashima, M., Roeder, C. W., and Maruoka, Y. (2000). Steel moment frames for earthquakes in United Stated and Japan. *J. Struct. Eng*., 126(8), 861-868.

[5.17] Okada, K., Oh, S. H., Yamada, S., Imaeda, T., Yamaguchi, M., Wada, A., (2001) Experimental Study on Deformation capacity of Composite Beams with Conventional Type Beam-to-Column Connections. *Journal of structural and construction engineering, Architectural Institute of Japan.* 547, 161-168. (in Japanese with English abstract).

[5.18] Suita. K., Kitamura, Y., Goto, T., Iwata, T., Kamae, K. (2007) Seismic Response of

High-Rise Buildings Constructed in 1970s Subjected to Long-Period Ground Motions. *Journal of structural and construction engineering, Architectural Institute of Japan.* 611, 055-061. (in Japanese with English abstract).

[5.19] Suita, K., Kitamura, Y., Hashida, I., (2009) Seismic Performance and Retrofit of Beam-to-Column Connection for Early High-Rise Buildings. *Journal of structural and construction engineering, Architectural Institute of Japan.* 636, 367-374. (in Japanese with English abstract).

[5.20] The Japan Building Disaster Prevention Association. Architectural Institute of Japan. (1996) Construction Manual for Seismic Retrofit of Existing Steel Buildings.

[5.21] Tsai, K. C. and Chen, C. Y. (1996) Performance of Ductile Steel Beam-Column Moment Connections, Paper No. 405 in *Eleventh World Conference on Earthquake Engineering*, Acapulco.

[5.22] Uang, C. M., Yu, Q. S., Noel, S., Gross, J., (2000) Cyclic testing of steel moment connections rehabilitated with RBS or welded haunch, J. Struct. Engrg., Volume 126, Issue 1, pp.57-68.

[5.23] Yamada, S., Kitamura, Y., Suita, K. Nakashima, M., (2008) Experimental Investigation on Deformation Capacity of Beam-to-Column Connections in Early High-Rise Buildings by Full-Scale Tests. *Journal of structural and construction engineering, Architectural Institute of Japan.* 632, 119-126. (in Japanese with English abstract).

CHAPTER 6

Seismic Capacity of Retrofitted Frame in Existing Steel High-Rise Building

6.1 Introduction

The member test described in Chapter 5 indicated that the connection with supplemental welds along the shear tab would increase the strength by 14% and the energy dissipation by 46%, while it is unlikely to improve the ductility. The connection fractured at the same instant as the original connection. In the wing plate connection and haunch connection, the cumulative plastic rotation was improved over five times relative to that of the original connection. The retrofit methods were proven to significantly improve the cumulative deformation capacity. In the past static tests, haunch connections have been qualified as a ductile connection (Uang et at. 2000, Lee et al. 2003). To acquire the real data on the retrofit performance by the comparison with the test results obtained from the unretrofitted E-Defense test described in Chapter 4, a full-scale shaking table test was conducted. The test specimen was designed as a four-story, two-span by one-bay frame structure and topped with a concrete mass and rubber bearings system, which was exactly identical with the E-Defense test applied to the original structure except for one difference. All the connections were modified in accordance with the retrofit methods qualified by the member test. The wing plates and haunch were arranged. Besides, the supplemental welds were modified to improve the connection's ductility. More welding works were applied at the web connection. The specimen was tested up to the fractures of multiple connections by the repeated applications of the specified input wave.

In this chapter, the design and construction of the retrofitted connections is presented to supply supplemental information on the retrofit design of existing connections. Second, the response characteristics of the connections are evaluated from the damage observation and corresponding hysteretic behavior. Third, the fracture characteristics are examined in terms of the strain concentrations that appear in beam flanges. Forth, the maximum strength and cumulative plastic rotation of all connections are examined and compared with those obtained for the unretrofitted field weld connections in the last unretrofitted E-Defense test. The quantified retrofitted performance is stated at the end.

6.2 Specimen specification

6.2.1 Design of test specimen

Figure 6.1 shows the global view of the test specimen. Beams with 400 and 600 mm in depth were arranged in the longitudinal direction, and 800 mm deep honeycomb beams were arranged in the transverse direction of test specimen. The 600 mm deep beams in the longitudinal direction were field welded rather than shop welded contrary to the last E-Defense specimen. Twenty four connections arranged from the second to the forth floor beams were modified by using supplemental welds, wing plates and haunches. The connection with supplemental welds was modified to improve the performance and named the connection with modified supplemental welds.

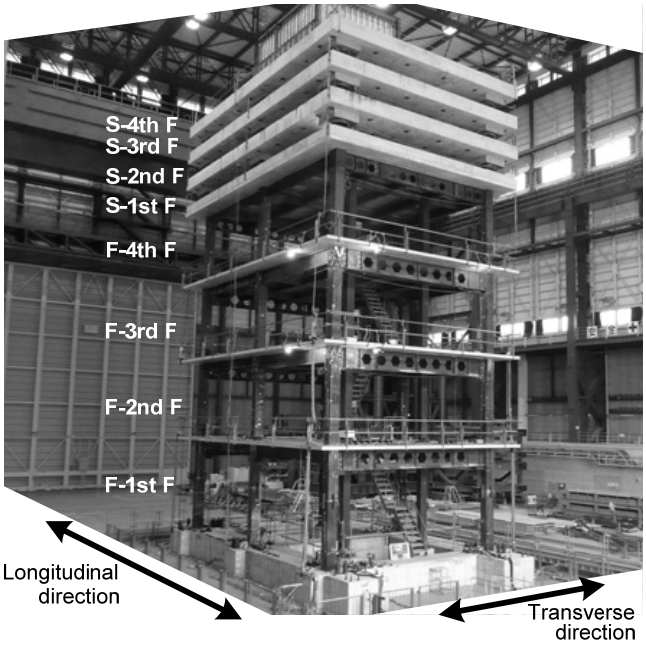

Figure 6.1 Overall view of test specimen

The construction views of the test specimen are shown in Figure 6.2. Construction of the specimen and welds of the connections followed as closely as possible the actual condition in the construction field. The scaffold, which was commonly used for the field welding in high-rise buildings, was adopted (Figure 6.2 (b)). All welders were certified, and all groove welds were ultrasonically tested and qualified by an independent welding-inspection firm. Retrofit of connections was applied after the casting of RC floor slab.

(b)

(c)


(a) (d) (e)



(f) (g) (h)

Figure 6.2 Construction of test specimen: (a), (b) Construction of test frame; (c) Scaffolds for filed weld; (d), (e) Field weld; (f) Ultrasonic test; (g), (h) Ultrasonic test for retrofit welding

6.2.2 Design of beam-to-column connections

The modified supplemental welds, wing plates and haunch were arranged at various locations of the connections (Figure 6.3). The haunch connection that needs the most construction efforts have been regarded as the most ductile connection among the retrofit alternatives. The connection was arranged at the second floor beams, which sustained smaller deformation than the third and forth floor beams in the last unretrofitted E-Defense test. The wing plate connection was arranged at the third and forth floor beams. Connection with the modified supplemental welds was arranged at the third floor beams in the transverse direction. Their retrofit performance was evaluated by inputting a long-period ground motion sequentially until fracture occurs at multiple connections. Within the twenty retrofitted connections, four, twelve, and eight connections were modified with the supplemental welds, haunch and wing plates.

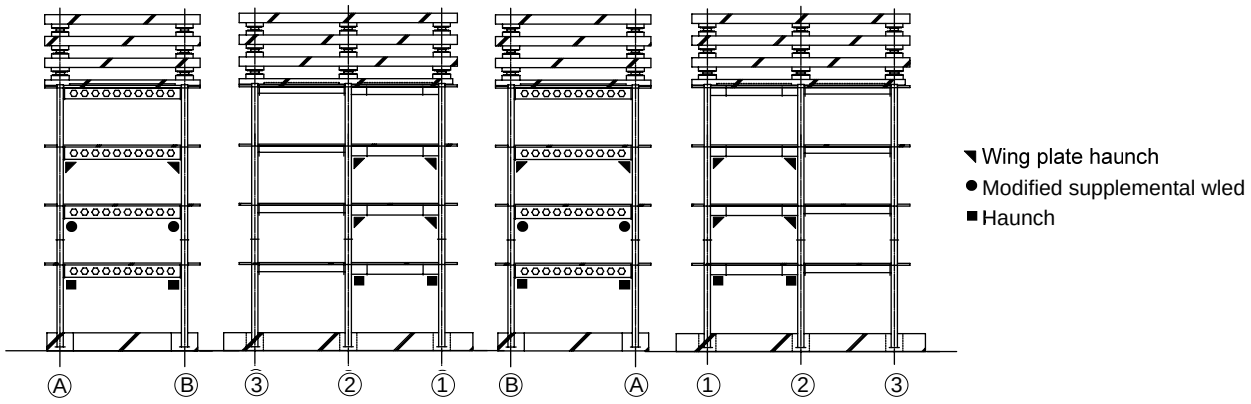

Figure 6.3 Locations of retrofitted connections

Specifications of the structural components and measured material properties are listed in Table 6.1. Material properties were similar with those of the last E-Defense specimen. Charpy V-notch (CVN) impact tests were also conducted for the margin members and deposited metals of welds (Table 6.2). The measured CVN values of the shop weld and field weld deposits were 103 J and 63 J at 0 ^{o}C, respectively.

Table 6.1 Specimen specifications and material properties

		σ_y (MPa)	σ_u (MPa)
Column (SM 490A)	Box-400×400×25	353	522
Beam (SM 490A)	H-600×200×9×19	351	512
	H-400×200×8×13	432	556
	H-500×200×9×16	376	542
	H-800×199×10×15	401	534
	H-650×199×9×14	398	530
Wing plate (PL-19)		396	537
Haunch (PL-16)		356	513
Concrete			29

Table 6.2 Charpy V-notch impact tests results

		CVN values (0 ^{o}C, J)
(1) Base medal-Flange		
Built-up H Beam	H600	73
Rolled H Beam	H800	65
Wing plate	PL-19	130
Haunch	PL-16	261
(2) Weld medal-Flange		
Built-up H Beam	H600	103
Rolled H Beam	H800	63

Estimated strength

Table 6.3 summarizes the estimated strengths of the connections based on the measured material properties. ${}_bM_p$ was the full plastic moment of the bare beam (H-800: 1532kN・m, H-600: 1042 kN・m). ${}_jM_u$ was the maximum strength of connection (AIJ 2006). ${}_{cb}M_p$ was the full plastic moment of the composite connection. The effect of RC floor slab was not considered in ${}_jM_u$. For the connection with modified supplemental welds, ${}_{cb}M_p$ was estimated using the 0.85 times of the compress strength of concrete ($0.85F_c$) and taking the effective width of the slab as the column width (400 mm) (Matsumiya et al. 2005, AIJ 2002). For the wing plate and haunch connections, ${}_{cb}M_p$ was the beam end moment while the composite beam section at the tip of wing plates and haunch reach the full plastic moment. The effect width of slab at the location was equal to the column width (400mm).

Table 6.3 Estimated strength of connections

Specimen	${}_jM_u/{}_bM_p$ (H-600)	${}_{bc}M_p/{}_bM_p$ (H-600)	${}_jM_u/{}_bM_p$ (H-800)	${}_{bc}M_p/{}_bM_p$ (H-800)
Modified supplemental weld	—	—	1.25	1.60
Wing plates	1.42	1.40	1.43	1.35
Haunch	1.65	1.58	1.55	1.48

Connection with modified supplemental weld

In the member test, supplemental welds at the shear tab increased the strength and energy dissipation but did not improve the ductility. Strain concentration at the bottom flange (exceeding 10 % under the 2 % drift angle) was not reduced and lead the connection fracture at the same instant with the connection without such modification. In addition, the comparison between the original connection and the shop weld connections of the unretrofitted E-Defense test, while these two connections had an identical beam depth and slab thickness, generated significantly different strain concentrations. The lesser restraint at the web connection of the original connection generated a four times larger strain than that obtained for the shop weld connection (Figure 5.19).

After the Northridge earthquake, fillet welds at the shear tab corners to beam web is no longer considered as a reliable alternative to improve ductility of WUF-B connection, and is not allowed to be used in the Special Moment Frame (SMF) system. To improve the ductility, the CJP groove weld at the beam web to the column face was further applied on the connection, called welded unreinforced flange, welded web (WUF-W) connection. The CJP weld groove weld at the beam web to the column face and fillet weld at the shear tab to beam web made the WUF-W connection be qualified as a ductile connection based on a serious tests (FEMA 350, 2000). The higher restraint at the web connection was considered to be able to reduce the bending moment sustained by the flanges and lead to higher seismic performance. Ricles et al. (2000) tested the performance of the connections by a serious of static loading tests. Two of them were attached with the RC floor slab. This test adopted the column of H-465×422×45×72 (W14×398) with two beams of

H-912×305×16×24 (W36×150) connected on each side. RC floor slab with a thickness of 165 mm was attached at the top of beam. The displacement history followed the SAC protocol (SAC 1997). The test results indicated that both composite connections were able to sustain a 4% drift angle without strength decrease. The first fracture of the connections occurred at the top flange metal at a distance of 533 mm (21 inch) away from the column face and where severe local flange bucking occurred during the second cycles of the 4% drift angle loading. Fracture of the other connection occurred at the bottom flange metal at a distance of 230 mm (9 inch) away from the column face during the 5% drift angle. Cumulative plastic rotation was 0.37 rad. The supplemental welds at the beam web to column face tended to improve the ductility of connection significantly.

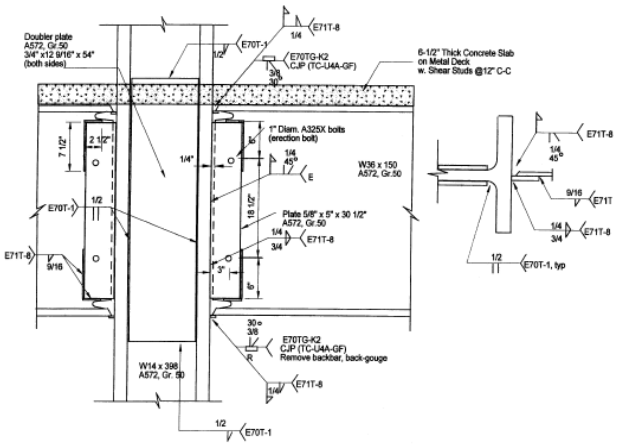

Figure 6.4 Welded unreinforced flange-welded web (WUF-W) connection (Ricles et al. 2000)

In the E-Defense test, the connection with supplemental welds was modified in reference to the WUF-W connection detail. Figure 6.5 shows the details of the connection. Except the supplemental fillet welds at the shear tab, the CJP groove weld was applied at the beam web to column face in the field with a welding length of 630 mm (Figure 6.5(b)). The shear tab worked as the backup plate when the welding was performed. In addition, a plate having the identical thickness of the shear tab (9 mm) was fillet welded to cover the weld access hole and to reduce strain concentration caused at the toe of weld access hole. Figure 6.6 shows the welding situation and close-up views of the connection. The modified supplemental welds in the test provided a higher restraint at the web connection than that of the corresponding member connection.

The maximum flexural strength of the web connection ($_jM_{wu}$) was estimated using the properties of the shear plate and web section which welded to the column. According to the design criteria (AIJ 2006), $_jM_{wu}$ was shown below.

$$_jM_{wu} = m \cdot Z_{wpe} \cdot F_{wy} \tag{5.1}$$

F_{wy} is the yield strength of the web metal. As the web was welded to the column face, the plastic section modulus (Z_{wpe}) of the web connection should be considered as the sum of the shear tab and welded web section (with the presence of weld access holes being considered). The normalized

flexural strength of the web connections (m) became 0.71 when considering the yielding of column face caused by the out-of-plane deformation. Thus, the maximum web flexural strength was the sum of the following strengths: ${}_jM_{wu}$ and the bending moment caused by the fillet weld applied at the supplemental plate. The design strength (${}_jM_u$ / ${}_bM_p$) of the connection was 1.25, which was similar with the 1.27 of the corresponding member connection. The ${}_{bc}M_p/{}_bM_p$ was 1.60 when the effect of RC slab was considered.

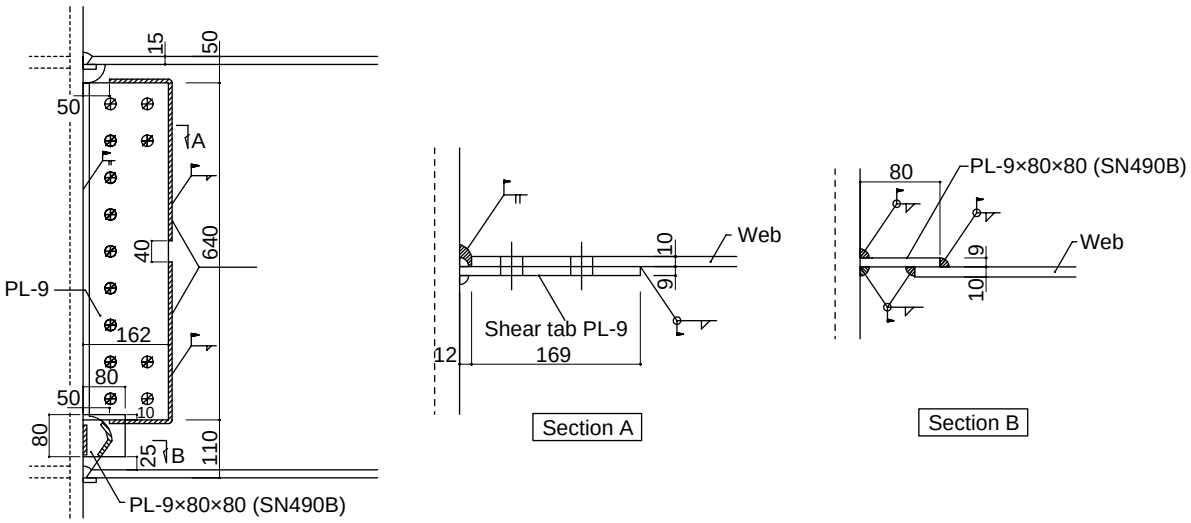

Figure 6.5 Details of the connection with modified supplemental weld

(a) (b) (c)

Figure 6.6 Connection with modified supplemental welds: (a) Welding situation; (b) Supplemental welds; (c) Modified supplemental welds

Wing plate

Figure 6.7 shows the details of the wing plate connection adopted on the 600 and 800 mm deep beams. The thicknesses of the plates were 15 and 19 mm, which was identical with the bottom flanges. The plate width was enlarged to the width of the box section column, i.e., 400 mm. Figure 6.8 shows the welding situation and a close-up view of the connections. Following the strength equations proposed in Chapter 5 (Equation 5-4), the design strength (${}_jM_u$ / ${}_bM_p$) of the connection was 1.42 and 1.43 for the 600 and 800 mm beams. These values were slightly higher than 1.39 designed for the member specimen.

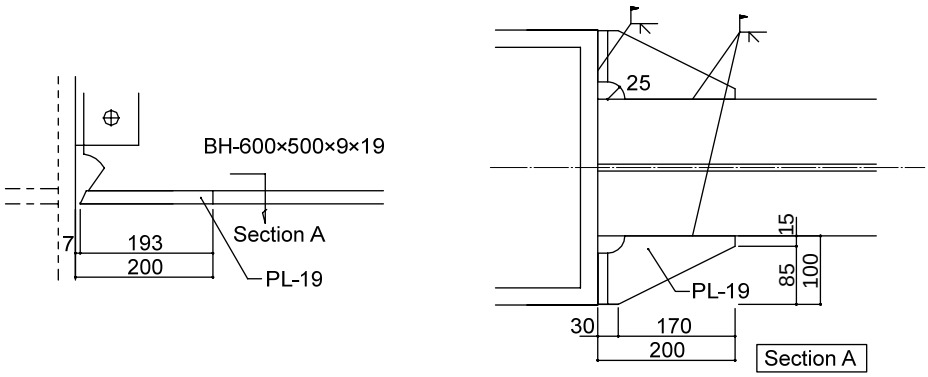

(a)

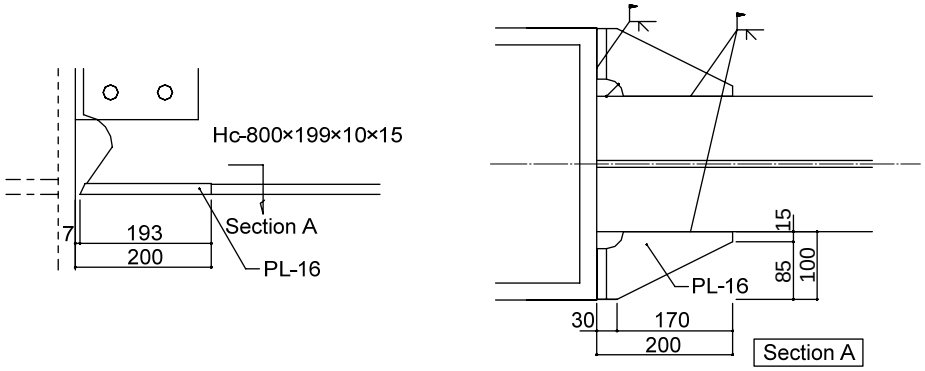

(b)

Figure 6.7 Details of the wing plate connection: (a) 600 mm depth beam; (b) 800 mm depth beam

(a) (b)

Figure 6.8 Wing plate connection: (a) Welding situation; (b) Close-up view

Haunch

Figure 6.9 shows the details of the haunch connection. Haunch of CT-150~400×12×16 and CT-150~400×12×16 were adopted for the 800 and 600 mm deep beams. The filed weld situation and a close-up view of the connection are shown in Figure 6.10. Welds in horizontal and vertical directions were applied at the haunch. The design strength ($_jM_u$ / $_bM_p$) of the connection was 1.65 and 1.55 for the 600 and 800 mm beams, which were slightly higher than 1.50 designed for the member specimen.

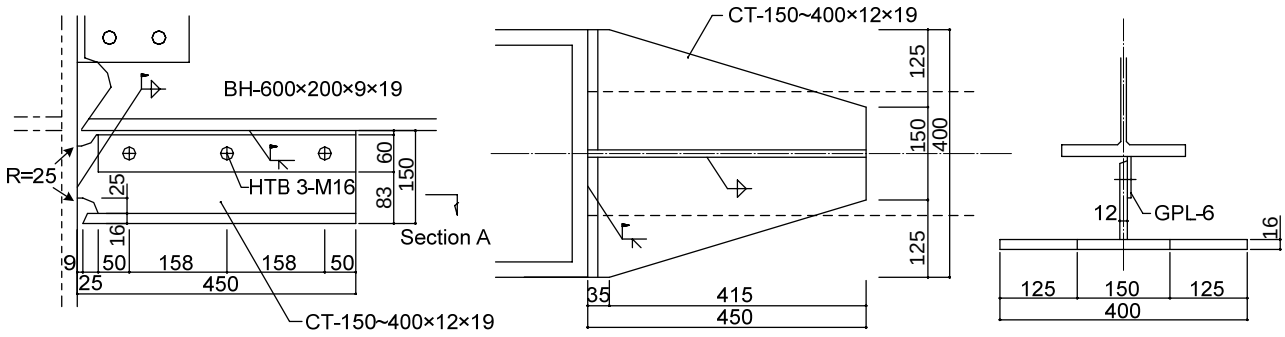

(a)

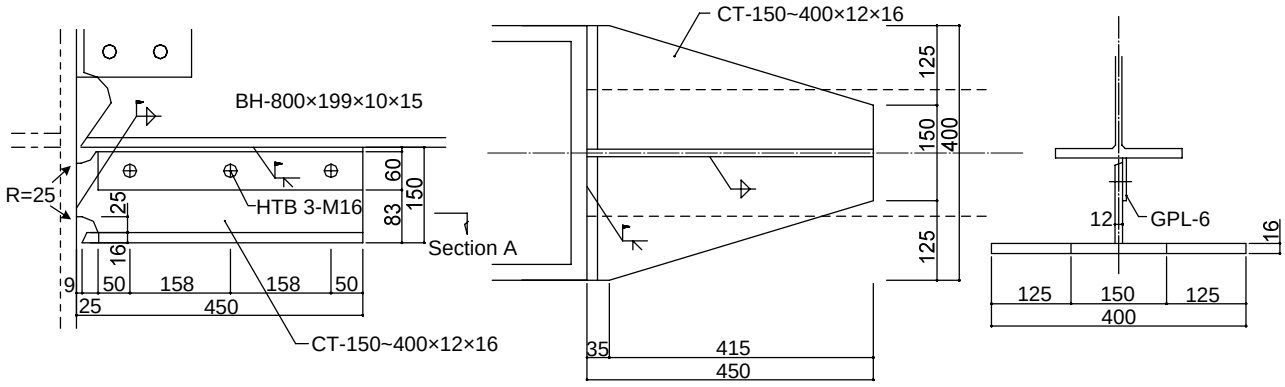

(b)

Figure 6.9 Details of the straight haunch connection: (a) 600 mm depth beam; (b) 800 mm depth beam

(a) (b)

Figure 6.10 Haunch connection: (a) Welding situation; (b) Close-up view

6.3 Measurement plan and loading program

A total of 735 channels of data were collected in the test, including 67 accelerometers, 115 displacement transducers, and 450 strain gauges. The accelerometers were placed on the shaking table and each floor slab to record the accelerations in three directions. The displacement transducers were arranged to measure the inter-story displacements, rotations of beam ends, and shear displacements of connections' panel zones. Bending moment and rotation of twenty four

retrofitted connections were measured in the test. Strain gauges were attached at the top and bottom flange weld access holes and in various locations of beam sections to measure the strain concentration (Figure 6.11).

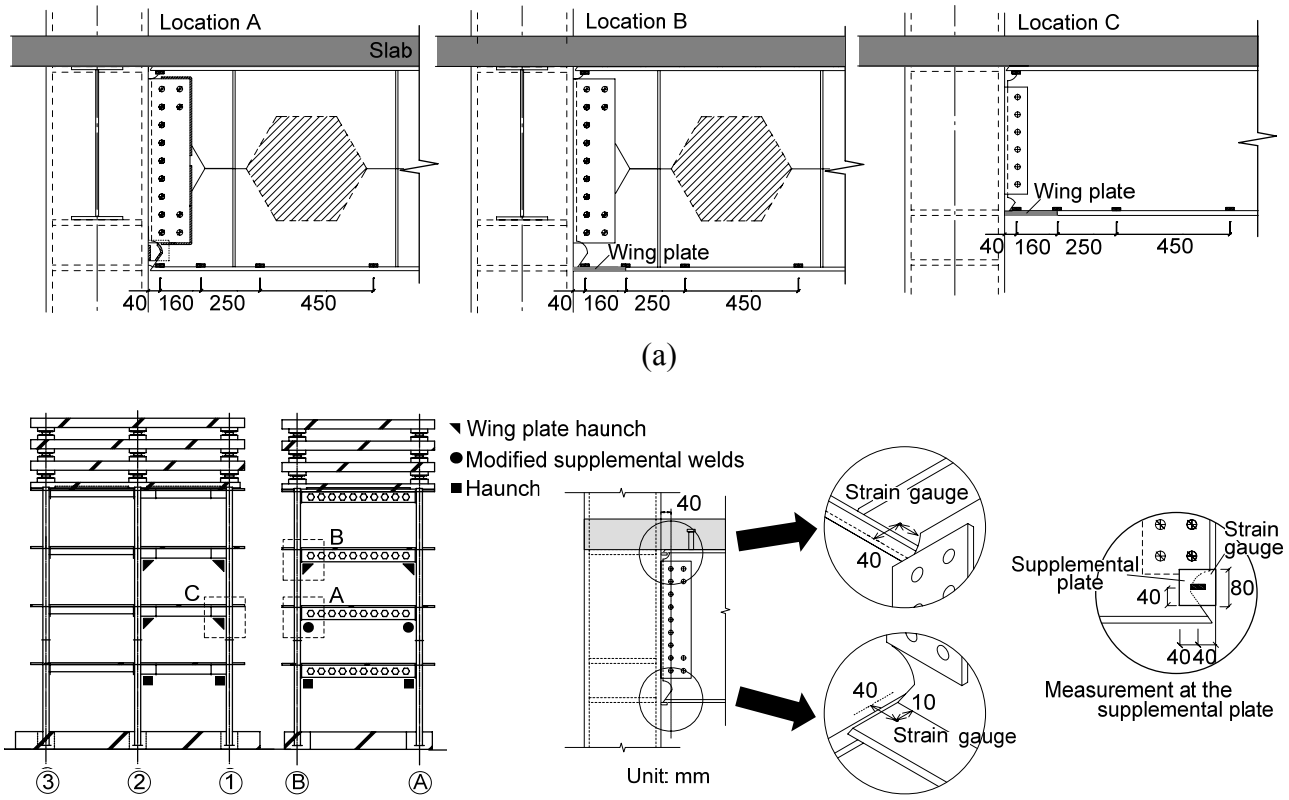

Figure 6.11 Measurement of beam-to-column connections: (a) Measurement at the connections; (b) Locations of three particularly measured connections; (c) Details of the measurement

Shaking table tests in bi-directional input were conducted at three levels with increasing magnitudes of input waves. Three input waves adopted in the last unreftroftitted E-Defense test were applied again in this test, including one near-fault earthquake: El Centro wave, and two synthesized long-period ground motions: Hog and San waves. The El Centro wave was scaled to 0.25 m/s and 0.50 m/s in PGV for the level 1 and level 2 seismic forces in the Japanese design code. The San wave was inputted repeatedly until fractures occurred in multiple beam-to-column connections.

6.4 Test results

6.4.1 Inter-story drifts

Figure 6.12 summarizes the maximum inter-story drift responses from the first to the third story of the test specimen under various levels of loading. The maximum deformation occurred at the second and the third story and increased with increased levels of seismic loading except the Hog

loading in the transverse direction. For the level 1 and level 2 El Centro wave, the maximum inter-story drifts in the second and third stories were slightly smaller than the design limit of 0.5% and 1%, respectively. For the Hog wave, the maximum inter-story drifts in the second and third story were slightly larger than 1%. The maximum strain values measured at the bottom flange reached 0.5% in the level 2 response, but neither cracking nor local buckling was observed.

For the level 3 San wave loading, deformations in the longitudinal direction increased notably than those observed in the transverse direction primarily due to a stronger EW component of the San wave was applied in the longitudinal direction. Under the first time San wave loading, the maximum inter-story drifts in the second and third stories were 1.5% and 1.3% in the longitudinal and transverse directions. The maximum strain value was 0.6% in the beam ends, but no damage was observed in the connections. Deformation of the test specimen started concentrating in the test frame because of the sequential input of the San wave. The maximum inter-story drifts in the second and third stories exceeded a drift angle of 2.2% and 1.4% in the longitudinal and transverse directions under the third San wave loading. The maximum strain value of over 1.3% was observed in the bottom flange of the connection with supplemental welds, but no damage occurred in this connection. Fractures occurred at six connections in the longitudinal direction. After two times of one directional input, the connections in the transverse direction fractured at three locations, and the inter-story drift grew to 1.7%. In the last unrefrofitted E-Defense test, the maximum inter-story drifts of the test specimen were 2.2% and 1.7% in the longitudinal and transverse directions when the specimen sustained fracture during the third time San and the first San wave loading in the two directions. Fractures in the two tests occurred under similar levels of inter-story deformation.

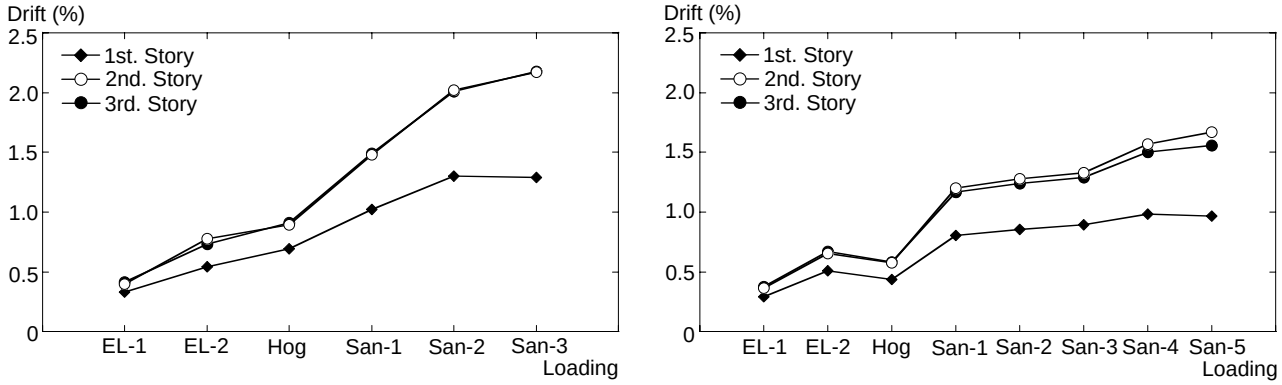

(a) (b)

Figure 6.12 Max. inter-story drift angles: (a) Longitudinal direction; (b) Transverse direction

The wing plate connection in the longitudinal direction fractured during the third San wave loading. The connection with supplemental welds fractured during the fifth San wave loading. The retrofitted connections showed notable increase in the cumulative deformation capacity, compared to that of the unretorfitted field weld connections in the last E-Defense test, in which fracture occurred during the first San wave loading. The locations of the fractures are summarized Figure 6.13. In the recorded connections, the connections with modified supplemental welds and wing

plate connection fractured at two and four locations, respectively. No fracture was observed in the haunch connections.

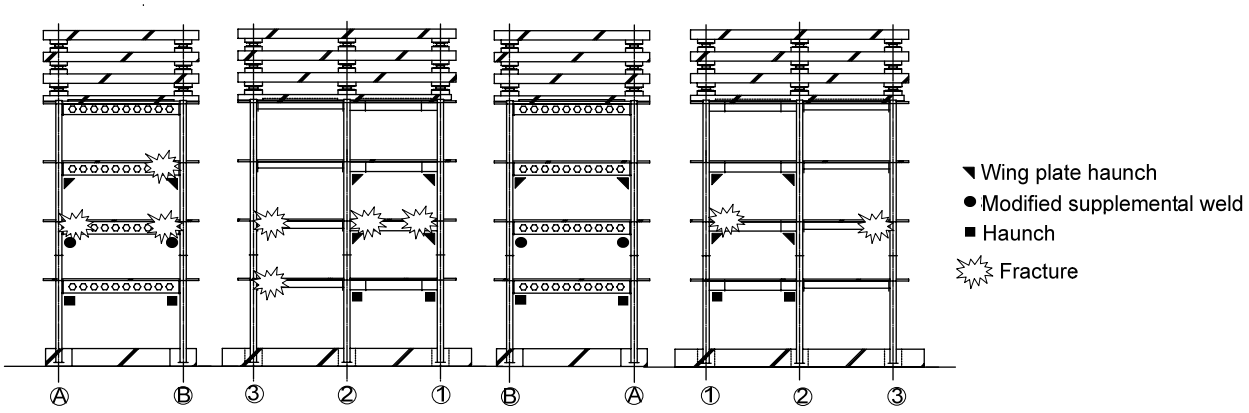

Figure 6.13 Fracture location of connections

6.4.2 Hysteretic behaviors and fracture situations of connections

Figure 6.14 shows the bending moment versus rotation relationships of connection with modified supplemental welds under the fifth San wave loading. The bending moment is normalized by the full plastic moment, ${}_bM_p$, of the bare beam, with the yield strength of steel obtained from the coupon test. Two connections fractured at the bottom flange and lead the resistance to decrease in the positive bending (location of the connections were illustrated in Figure 4.6). Figure 6.15 shows a close-up of the fractured connections. Fractures occurred along the weld boundary between the bottom flange medal and welding medal, which was similar in the observation to the unretrofitted field weld connections in the last E-Defense test. The connections fractured at the rotation of about 0.009 rad and sustained a maximum rotation of 0.016 rad after the fracture. For the connection with supplemental welds in the member test, a crack extended to the shear tab of web connection after the fracture of the bottom flange when the supplemental welds was applied only to the sear tab. In E-Defense test, the CJP weld at the beam web to the column and the supplemental plate provided a limited stiffness loss (about 5%) in the positive bending after the fractures. A 50 mm length crack at the bottom of the shear tab was observed at one of the fractures (EL). No crack nor buckling was observed at the welded web connection in the other three connections. The maximum strain at the weld access holes of the top and bottom flanges were 1.1% and 1.5% before the fracture (Figure 6.11).

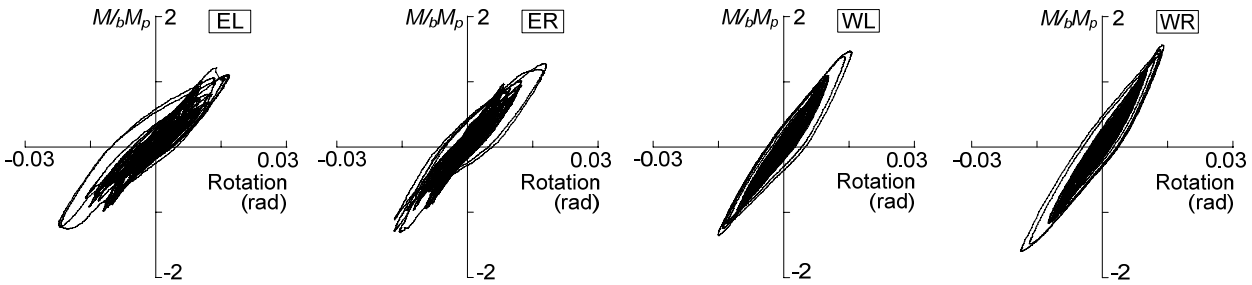

Figure 6.14 Hysteretic behaviors of the connection with modified supplemental welds

(a) (b) (c)

Figure 6.15 Fractures of the connection with modified supplemental welds: (a) Connection in EL; (b) Connection in ER ; (c) Cracking at the shear tab

Figure 6.16 shows the bending moment versus rotation relationships of the twelve wing plate connections. Fracture at the bottom caused a significant resistance decrease in the positive bending. In the negative bending, the fracture surface was closed, and the resistance recovered. Figure 6.17 shows a close-up of the fractures. Fractures of the beam occurred at the tip of the wing plates. Fractures started from the flange metal and extended to the web. Cracks at the tip of the wing plates were also observed in some locations (Figure 6.17(c)). Figure 6.17(d) shows one seriously cracked connection. Cracks extend to most of the bottom flange and web, but no notable stiffness or strength decrease was observed from the hysteretic behaviors (EL of Figure 6.16(a)). The wing plates were able to move the weak spot away from the connection flange and thus avoid brittle fracture caused by defaults possibly developed during the field welding. Before the fractureuy, the maximum strain observed at the bottom flange and the strain at the tip of wing plates were 0.6 and 1.0% (Figure 6.11). In the fractured field weld connection in the last E-Defense test, the maximum strain at the bottom flange weld access hole exceeded 3%. Strain concentration was significantly reduced in the wing plate connection.

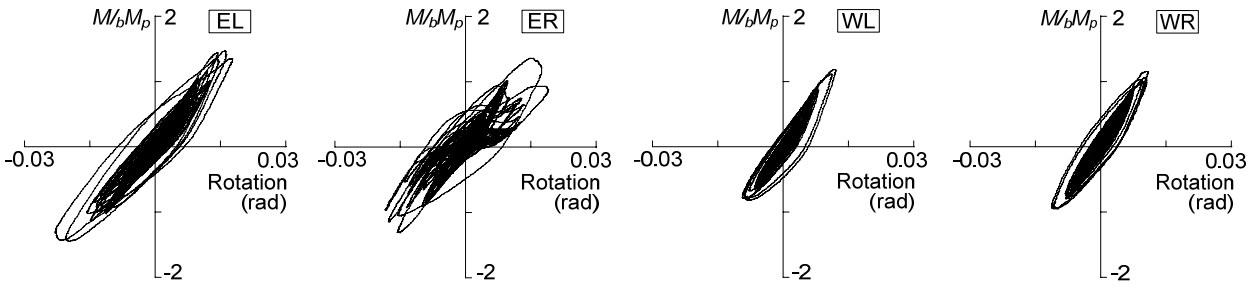

(a)

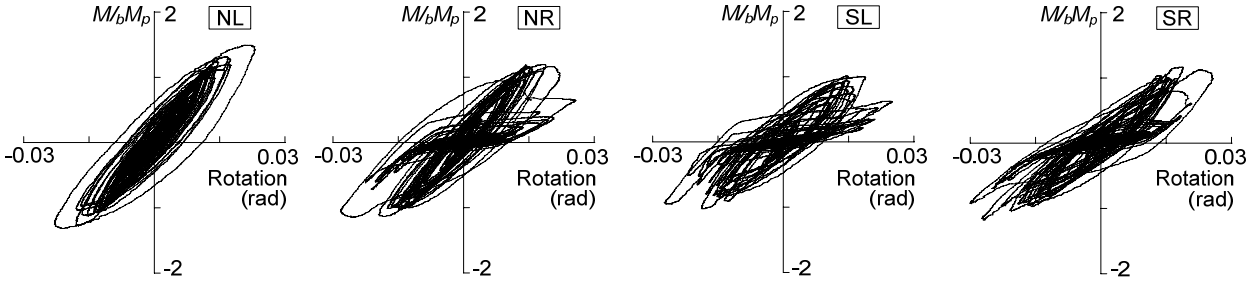

(b)

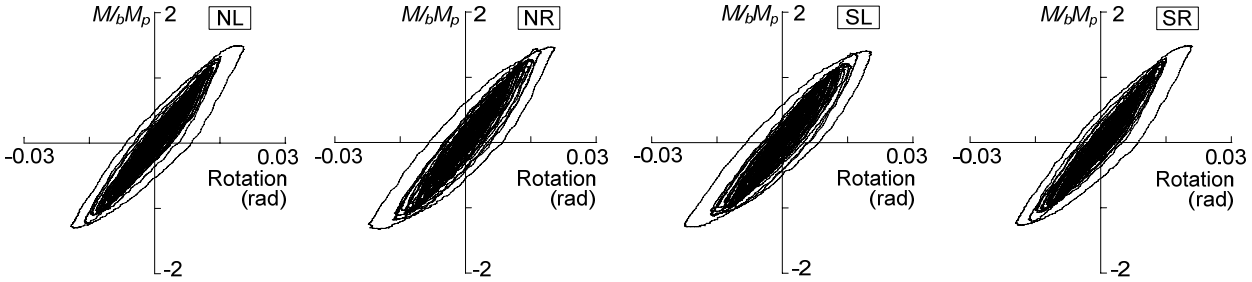

(c)

Figure 6.16 Hysteretic behaviors of the wing plate connections: (a) Connections in the transverse direction (forth floor, H-800); (b) Connections in the longitudinal direction (third floor, H-600); (c) Connections in the longitudinal direction (forth floor, H-600)

(a) (b) (c) (d)

Figure 6.17 Fractures and cracks of the wing plate connections: (a) The third floor connection (SL);(b) The third floor connection (SR);(c) The third floor connection (NL); (d) The forth floor connection (EL)

The bending moment versus rotation relationships of the haunch connections are shown in Figure 6.18. The connections show stable hysteretic loops until the end of loadings. No damage was

observed in the connections excepted one small local buckling that had occurred at the bottom flange and lead the hysteretic behavior loop to become fatter (Figure 6.19). The maximum strain of all haunch connections was 0.6% at the top flange weld access hole (Figure 6.11). Strain values at the same location of the haunch connection in the member test exceeded 2% under the 1% drift angle. Strain concentration at the top flange was reduced. Strain at the bottom flange weld access holes remained elastic during the series of loadings.

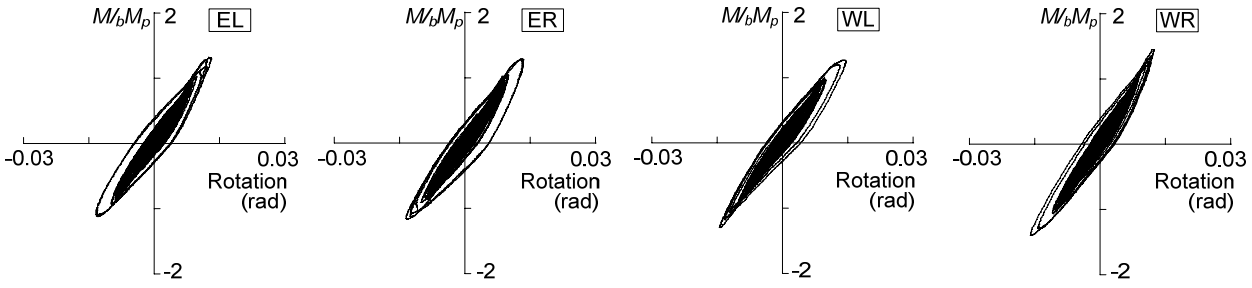

(a)

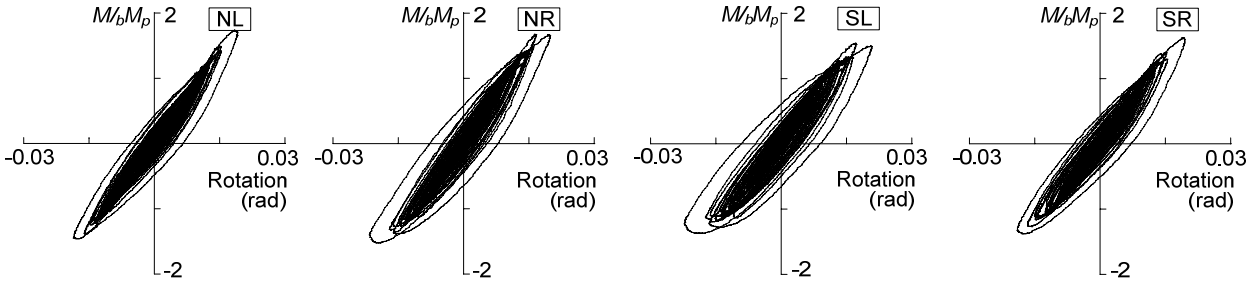

(b)

Figure 6.18 Hysteretic behaviors of the haunch connections: (a) Connections in the transverse direction (H-800); (b) Connections in the longitudinal direction (H-600)

Figure 6.19 Fracture situation of connections (SL)

6.5 Retrofit performance

6.5.1 Maximum strength

The experienced maximum strengths of all connections are shown in Figure 6.20. The maximum strength was normalized by the full plastic strength ${}_bM_p$ of the corresponding unretrofitted bare beam. In the connection with modified supplemental welds, the averaged strength in the fractured and unfracured connections were 1.46 and 1.57 ${}_bM_p$, which were about 9 and 2% smaller the estimated strength (Table 6.3). In the wing plate connections, the average of the fractured and unfracured connections were 1.47 and 1.43 ${}_bM_p$, which were about 7 and 4% larger than the estimated strength (note: the estimate strengths of 600 and 800 mm beams was 1.38 on the average). The average of the haunch connections was 1.53 ${}_bM_p$. The estimate strengths show similar results with the test results (the estimate strengths of 600 and 800 mm beams was 1.53 ${}_bM_p$ on the average). These retrofitted connections exhibited at least 40% increase in strength then that of the bare beams.

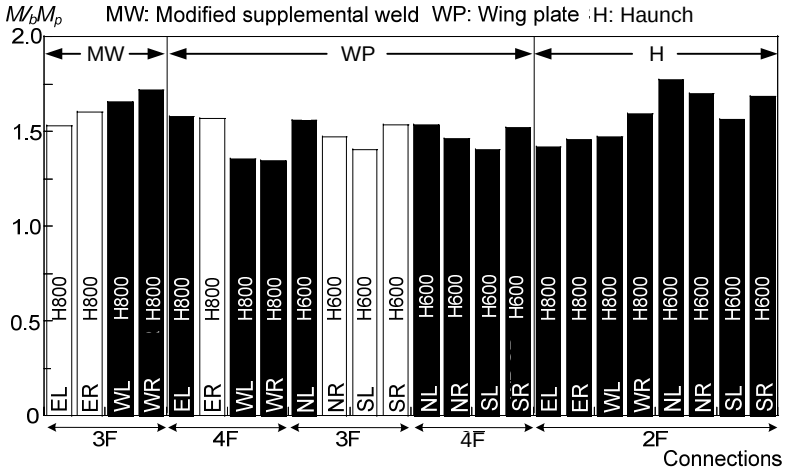

Figure 6.20 Maximum strength of connections

6.5.2 Strain concentration

Figure 6.21 shows the strain values at a few locations along the beam length under various drift angle loadings. The values at the bottom flange and top flange are plotted when the connection sustained positive and negative bending for the same amplitude. The two member connections whose details are described in Chapter 5: connection with supplemental welds and wing plate connection are also included. Locations of the strain gauges and the measured connections are illustrated in Figure 6.11.

For both the connection with supplemental welds and the connection with modified supplemental welds, the maximum strain was concentrated at the bottom and top flange weld access holes in the positive and negative bending. The CJP weld at the beam web to the column face and the supplemental plate of the modified supplemental welds significantly reduced the bottom flange

strain to 1.1% from over 10.0% of the counterpart connection and the top flange's maximum strain was also reduced to 0.5% form 3.0%. The effects of welding the web and the column face make the concentration of the strain gentle. In reference to the strain of the plate attached on the bottom flange access hole, the plate transferred the stress close to the yield strength and provided the effects to the size of the hole smaller (Figure 6.11, the maximum strain was 0.2%).

For the wing plate connection of the member test, the strain was concentrated at the bottom flange weld access holes at a value of 1.7% under the 2% drift angle loading while the strain at the top flange weld access hole reached 3.5% under negative bending (Figure 6.21(b)). The high strain concentration caused the fracture of the top flange. In the retrofitted E-Defense test, strains at the bottom flange weld access hole of the two wing plate connections were also reduced notably to about 0.7% and 0.5% and the strain at the top flange remained elastic. The difference between member tests and E-Defense test is the effective width of floor concrete slab. In reference to the ratio of the negative bending moment to positive bending moment, the values of E-Defense test are much closer to 1.0 than the values of member tests. That is, the contribution of the floor slab to the negative bending moment made the strain concentration gentle in the real steel frame. In addition, because the bottom flange was enlarged to the width of the column (300 mm in the member test and 400 mm in this test) by attaching wing plates. The section of the bottom flange (40 mm far from the column face) became larger in this test and lead the strain at this section be reduced. As a result, the strain concentration area was moved to the tip of wing plates where was 200 mm far from the column face. The strain of the two E-Defense connections reached 1.0% under 1.8% and 1.5% drift angle loadings and made the fracture occur at beam instead of the top flange of connection.

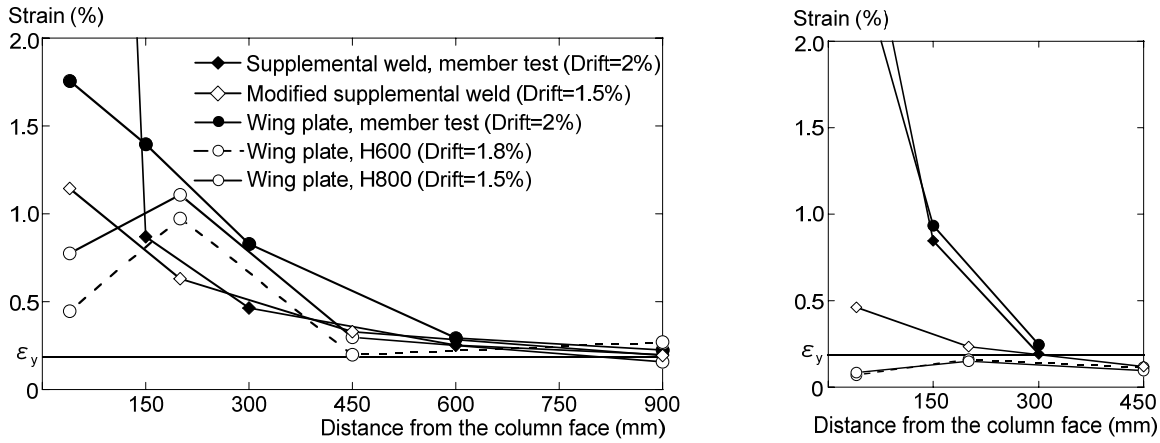

Figure 6.21 Strain values at flange weld access holes: (a) Strain at bottom flange; (b) Strain at top flange

6.5.3 Cumulative plastic rotation

Relationship between member test and full-scale test

Figure 6.22 summarizes the cumulative plastic rotation of the connections in the member test and the retrofitted E-Defense tests. The rotation was the summed value of those given in the level 2 El

Centro wave, the Hog wave, and the San waves up to the fracture.

The connections in the member test have notably different from those of the retrofitted E-Defense test. Connection with supplemental welds fractured at the bottom flange at the cumulative plastic rotation of 0.12 rad. In the past test (Ricles et al., 2000), the WUF-W connection which adopted fillet welds at the shear tab to the web and the CJP weld at the beam web to column face was able to sustain maximum drift angle of 4% and cumulative plastic rotation of 0.37rad while the RC slab was attached on the top of beam. In the retrofitted E-Defense test, the connection with fillet welds, CJP weld at the beam web to column face and the supplemental plate at the web connection enhanced the connection to be able to sustain cumulative plastic rotation of 1.58 rad. The higher restraint at the web connection lead to higher cumulative plastic rotation capacity of these three connections. In addition, the strain at the bottom flange weld access hole of the connection with supplemental welds was reduced to 0.19% from 2.5% when the CJP welds and supplemental plate were applied. The cumulative plastic rotation capacity increased about thirteen times. Besides, the capacity (1.58 rad) was also larger than the average value of the fractured wing plate connections (with the capacity of 1.36 rad), which fractured at the beam section, although the connection with modified supplemental welds fractured at the bottom flange welding boundary. The higher restraint at the web connection can effectively reduce the strain concentration at the bottom flange and lead to higher cumulative plastic rotation capacity.

In the member test, the wing plate connection sustained 10 cycles of the 2% drift angle loading. The connection fractured at the top flange at a cumulative plastic rotation of 0.35 rad while the strain at the top flange reached 2.0%. In the retrofitted E-Defense test, because the maximum strain was shifted from the beam end to the tip of wing plates at a value of 1.0% (Figure 6.21(a)), fracture occurred at beam section and lead the capacity improve to 1.36 rad which was four times larger than that of the counterpart member connection.

Haunch connections in the retrofitted E-Defense sustained a cumulative plastic rotation of 1.24 rad without serious damages like fractures or cracks. The cumulative plastic ration capacities of the three types of retrofitted connections were confirmed by the serious of full-scale shaking table tests.

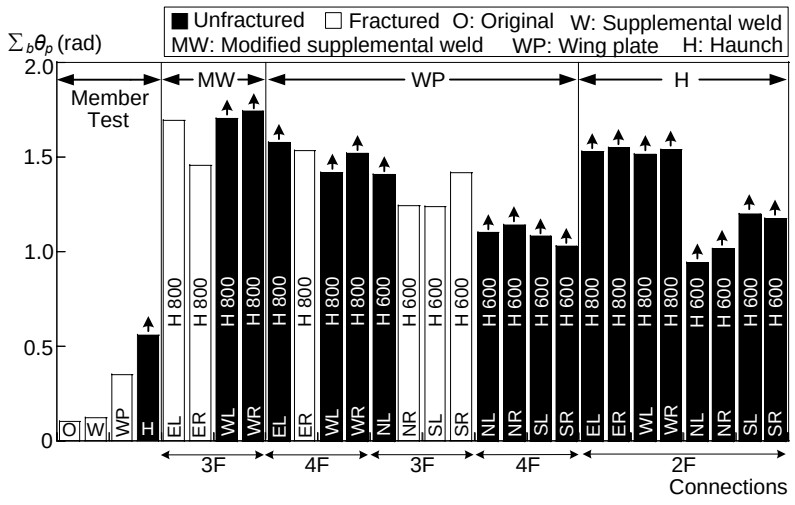

Figure 6.22 Cumulative plastic rotation

Relationship between minimum capacity and maximum demand

Figure 6.23 summarizes the averaged cumulative plastic rotation capacity of the fractured field weld connections, shop weld connections and two retrofitted field weld connections: connection with modified supplemental welds and wing plate connections of the E-Defense tests. Here the values are defined as the minimum capacities of the connections, respectively. That means 33% of connections in the damaged frame part will fracture.

Hog is predicted in Kawasaki, metropolitan area assuming a rupture of the Tokai trough, and San waves is predicted in Nagoya by assuming the simultaneous ruptures of the Tokai and Tounankai troughs. Those long-period ground motions have the peak input energy, which is almost proportional to the rotation demands, at a certain natural period. Here, the maximum demands are defined in reference to the possible maximum input energy. First, the cumulative plastic rotation is individually, calculated as an average value of the third floor connections in the longitudinal direction, which showed larger drift than in traverse direction. The average demands of El Centro, Hog and San waves are 0.03 rad, 0.09 rad and 0.23 rad, respectively. E-Defense test specimen which was synthesized by assuming the simultaneous ruptures of the Tokai and Tounankai troughs. The first mode period of the unretrofitted test specimen was about 2.4 sec. From the pseudo velocity response spectra of the waves, the predominant period of both waves is about 3 sec. The input energy of Hog and San wave at the predominant period were about 1.6 and 1.8 times of that when the first mode period of test specimen located at 2.4 sec. Thus, the maximum demand at Hog wave and Nagoya San wave were estimated as 0.14 rad and 0.43 rad.

For the unretrofitted E-Defense test, which represents the performance of existing connections in high-rise buildings, the average cumulative plastic rotation capacities of the fractured field weld connections and shop weld connections were 0.16 rad and 0.93 rad. Field weld connection had 15% capacity of the shop weld connection. That connection is able to sustain the demands of the level 2 design wave El Centro with the margin of 80%. However, the long-period ground motion predicted in metropolitan area, Hog waves, shows very close demand value to the capacity with difference of 11%. The level 3, San wave demanded two times larger cumulative plastic rotation than the capacity of field weld connections. Connections were unlikely to sustain the demand but shop weld connections remained safety with difference of 50%. Meanwhile, the test result of retrofitted field weld connections shows a significantly improvement of the capacity. The cumulative plastic rotation capacities were improved to 1.58 rad and 1.36 rad. The values were nine and eight times of that of field weld connections when the modified supplemental welds and wing plates were applied. The retrofitted capacity was at least three times even the maximum demand induced by the San wave.

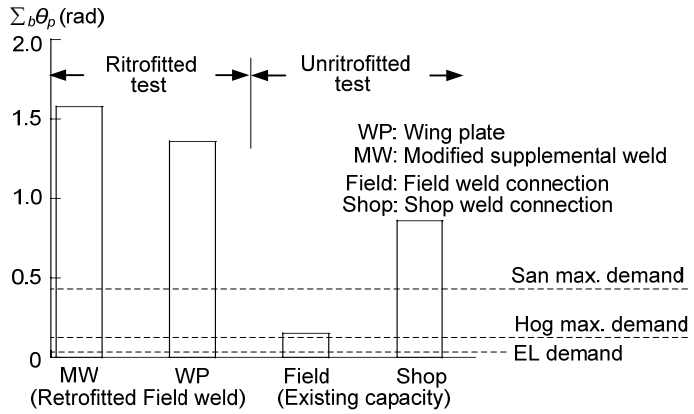

Figure 6.23. Comparison of minimum capacity and maximum demand

6.6 Conclusions

A series of E-Defense shaking table tests were conducted to evaluate the upgrade of seismic resistance capacity of high-rise buildings when subjected to long-period ground motions. The test specimen was designed to be identical with the last E-Defense test specimen which that represented an 80 m height high-rise building excepted for one difference: all connections were retrofitted by the prequalified retrofit methods examined by in the member test. The retrofitted test specimen was tested by input design waves and long-period ground motions waves sequentially until fractures to evaluate their retrofit performance. The main observations are concluded as below:

1. In the test, two fractures of the four connections with modified supplemental welds occurred during the fifth San wave loading. The connection fractured at the bottom flange welding boundary. Comparing with the connection with supplemental welds in the member test, the strain at the bottom flange weld access hole was reduced to 1.2% from 10% when the CJP weld at web to column face and supplemental plate were applied at the web connection. Higher restraint at the web connections significantly reduced strain concentration at the bottom flange and enhanced the cumulative plastic rotation capacity of connection from 0.12 rad to 1.58 rad. The capacity was improved thirteen times and even larger than that of the wing plate connections that fractured at beam section.
2. Four fractures occurred among the twelve wing plate connections under the third San wave loading. The connection in the large-scale E-Defense test shows a different fractured mode from that observed in member test. The strain at the top flange was significantly reduced. The strain concentration area was moved to the tip of the wing plates from beam end, have lead to fracture at the beam section. The cumulative plastic rotation capacity was improved to 1.36 rad from 0.35 rad of the member connection in which the top flange was fractured.
3. In the unretrofitted E-Defense test, the field weld connection and shop weld connections fractured at an the average cumulative plastic rotation capacity of 0.16 rad and 0.86 rad, respectively. Here the values are defined as the minimum capacities of the connections, respectively. Field weld connection performed only about 15% of the capacity of shop weld connection, That connection is able to sustain the demands of level 2 design wave with the margin

of 80%, but long-period ground motion predicted in Kawasaki, which is close to metropolitan area of Japan, shows very close value to the capacity with the difference of 11%. Apparently, connection is unable to satisfy the demand of level 3 long-period ground motion of San wave which was two times larger than the capacity. Meanwhile, the capacity of the field weld connection was able to be improved to nine and eight times larger when the modified supplemental welds and wing plates were applied. The retrofitted capacity was two times larger than the maximum demand of San wave.

REFERENCES

[6.1] Architectural Institute of Japan. (2006). Recommendation for Design of Connections in Steel Structures. (in Japanese)

[6.2] Federal Emergency Management Agency（FEMA-350）Recommended Seismic Design Criteria for New Steel Moment-Frame buildings，2000.7.

[6.3] Uang, C. M., Yu, Q. S., Noel, S., Gross, J., (2000) Cyclic testing of steel moment connections rehabilitated with RBS or welded haunch, *J. Struct. Engrg.*, Volume 126, Issue 1, pp.57-68.

[6.4] Lee, C. H., Jung, J. H., Oh, M. H., Koo, E. S., (2003) Cyclic testing of steel moment connections reinforced with welded straight haunch，*Engrg. Struct.*, 25, 1743-1753.

[6.5] Matsumiya, T., Suita, K., Nakashima, M., Liu, D., Zhou, F., Mizobuchi, Y. (2005) Effect of RC Floor Slab on Hysteretic Characteristics of Steel Beams Subjected to Large Cyclic Loading. *Journal of structural and construction engineering, Architectural Institute of Japan.* 598, 141-147. (in Japanese with English abstract).

[6.6] Architectural Institute of Japan. (2002). Recommendation for Limit State Design of Steel Structures. (in Japanese)

CHAPTER 7

Summary and Conclusions

Japan has been predicted to experience long-period ground motions, which are generated by large subduction zone earthquakes, by the middle of this century. Long-period ground motions tend to resonate high-rise buildings and accordingly the energy input to the high-rise buildings is expected to reach more than several times what has been expected in Japanese seismic design. Cumulative deformations would increase significantly in those buildings, and severe structural damage may occur. Damage to nonstructural components due to large velocities may also lead to great functional losses. The 1994 Northridge earthquake and the 1995 Hyogoken-Nanbu earthquake tested the seismic performance of steel moment frames, and severe damage was observed in their welded unreinforced flanges and bolted web connections (WUF-B). A number of Japanese high-rise buildings built in the 1970s had also adopted the field weld connection which is a type of WUF-B, although connection details differed rather significantly. Long-period ground motions are likely to demand much larger energy dissipation in such connections than that expected in the seismic design. Considering these observations, the seismic performance of existing high-rise buildings should be evaluated with urgency, and if the performance is found insufficient, necessary measure, i.e., retrofit, is to be exerticed.

Many tests had been conducted after the 1994 Northrigde and 1995 Hyogoken-Nanbu earthquakes for the evaluation and enhancement of ductility capacity of field weld connections. However, most of the connection retrofit tests did not consider the effects of RC slabs. In addition, a very few data have been available for retrofit of large size connections used commonly in the high-rise buildings. The actual data about the seismic performance of retrofitted connections are deemed still very limited. In this study, existing performance and effects of retrofitted of steel high-rise buildings are examined by a serious of large scale shaking table tests applied to a full-scale steel structure, together with supplemental quai-static tests applied to beam-to-column subassemblages.

In the shaking table test to explore into the existing performance of a high-rise building, a substructural test specimen that represents an 80m height high-rise building is designed and tested using the E-Defense shaking table facilities. The test specimen consists of a four-story frame structure that features full-scale steel members and reinforced concrete slabs, and substitute layers that are placed on top of the frame and represents the upper stories. The field weld connection and the shop weld connection, both popularly used for Japanese high-rise buildings constructed in late

1960s to 1970s, are adopted in the frame. Multiple ground motions, including one motion used in Japanese seismic design, one near fault motion and two long-period ground motions are applied sequentially with increasing magnitudes until the fractures of multiple connections so that their ductility capacity can be quantified. The maximum deformation, story shear force distributions, damage progress and deterioration of the test specimen are recorded. The cumulative plastic rotation and ductility capacity of existing beam-to-column connections are also examined.

To characterize the deformation capacity of retrofitted connections of early time high-rise buildings, a series of quasi-static member tests are conducted. Three types of retrofit methods are adopted, considering the construction feasibility and the effect of RC slab. To acquire the real data on the retrofit performance in terms of the comparison with the test results obtained from the unretrofitted E-Defense test, a full-scale shaking table test is conducted. The test specimen is designed exactly identical with the E-Defense test applied to the original structure except for one difference. All the connections are modified in accordance with the retrofit methods qualified by the member test. The specimen is tested up to the fractures of multiple connections by the repeated applications of the specified input motion. The maximum strength and cumulative plastic rotation of all connections are examined, and the quantified retrofitted performance is examinaed.

This dissertation consists of seven chapters. Chapter 1 is the introduction, including the background and objectives of the dissertation. Chapter 2 to Chapter 4 deal with the development of the shaking table test method to assess the seismic resistance capacity of steel high-rise building, and the test results including the global behavior and damage distribution in the steel frame and seismic capacity of their beam-to-column connections. As a prelude of Chapter 6, Chapter 5 presents the preliminary member tests on the performance of retrofitted field weld connection. Chapter 6 presents a full-scale experimental investigation on the seismic capacity of retrofitted frame in existing steel high-rise building. A summary and major findings obtained from each component of this dissertation is presented below.

Development of Shaking Table Test Method to Assess Seismic Resistance Capacity of Steel Frame in High-Rise Building

To evaluate the existing performance of high-rise buildings subjected to long-period ground motions, a series of large scale shaking table tests were conducted using the E-Defense shaking table. The main observations are summarized below:

(1) To represent the realistic response of an 80 m height high-rise building, a substructure test method was proposed. The test specimen was developed that consisted of a four-story test frame in the lower part and the substitute layers on top of the frame. The substitute layers made of concrete slabs and rubber bearings were used to represent the vibration characteristics of the prototype.

(2) From preliminary vibration tests, the equivalence between the test specimen and the prototype was verified to match reasonably for the first three mode natural periods and corresponding mode shapes.

Global Behavior and Damage Distribution in Steel Frame

In the serious of shaking table tests, global behaviors, damage progress and deterioration of the test specimen are examined when it subjected to various levels of seismic loadings. The main observations are summarized below:

(1) The maximum drift angles of the test specimen were smaller than 0.5% and 1.0% under the level 1 and level 2 design earthquake loadings. The test specimen remained elastic under the level 1 test, and no serious damage was observed in the level 2 loading. The story shear force distribution along the height was similar to the distribution specified in the Japanese building standard. The story shear force and inter-story drift relationships obtained from the test also showed notable correspondence with the design values. These indicated that the test specimen shaking in this study satisfied the requirements stipulated in the Japanese seismic design code and reasonably represented the actual high-rise buildings.

(2) A few beam-to-column connections fractured under the level 3 long-period ground motion loadings, i.e., San-1 to San-3. Connections in the transverse direction of the test specimen fractured in four locations under the first San wave loading (San-1). Connections in the longitudinal direction fractured in four locations when subjected to the third San wave loading (San-3). Fractures made the maximum story drift angle grew to 1.7 and 2.2% in the transverse and longitudinal directions, respectively. Comparing with the initial stiffness (before the tests), stiffness of the two directions of the test specimen decreased 18 and 9%, respectively, in the San-1 and San-3 wave loadings.

(3) When subjected to long-period ground motion (Hog wave), the test specimen diclosed cumulative ductility ratios more than four times that considered in the design (level 2 El Centro), while the maximum story drifts remained nearly the same as the design value. The story cumulative ductility ratio of the level 3 San wave reached fifteen times that given in the Level 2 El Centro wave. This is the most notable behavior that characterizes the responses in the long period ground motions. The long-period ground motion (San wave) generated similar magnitudes of acceleration with the design wave at a value of about 6 m/s^2, but significant larger floor velocity and displacement of about 2 m/s and 1m while those of the design wave were 1.2 m/s and 0.4 m. The large velocity and displacement lasted for over two minutes and generated significantly large cumulative ductility ratio.

(4) For the level 1 El Centro wave loading, no damage was observed in the nonstructural components except for small cracks and deformation of the panels in the ALC panel partition and drywall partitions. For the level 2 loading, cracks and deformation of the panel grew, but there were no drops or deformation of the doors that could affect the functionality of the interior space. When subjected to the level 3 San wave loading (with the maximum drift angle of 1.7%), no further damage was observed in the ALC panel partition. Plaster panels of the drywall partition dropped in multiple locations especially at the corner of the wall. Doors which were installed in the drywall partition were seriously deformed and made the doors unable to close again.

Seismic Capacity of Beam-to-Column Connection of Existing High-rise Building

The field weld connection and shop weld connection with early time connection details are adopted in the test frame and tested by input the long-period ground motions sequentially until the test specimen sustained serious damage, i.e., fractures of multiple beam-to-column connections. Major findings obtained from this investigation are summarized below.

(1) Between the two types of beam-to-column connection adopted in the test, i.e., the field weld connection and shop weld connection, the field weld connection tended to have lower ductility, particularly in terms of the cumulative plastic rotation and cumulative ductility. According the test results of twenty four connections recorded in detail, the field weld connection had the cumulative plastic rotation and ductility ratio of 0.16 rad and 9 in the 67% probability, while the shop weld connection had the plastic rotation and ratio of 0.86 rad and 71 in the 85% probability.

(2) The significant difference in ductility capacity was attributed to the combination of difficulty in quality control and greater concentration of strains. The presence of RC floor slab promoted the strain concentration at the toe of weld access hole in the bottom flange by over 100% on the average as compared to the case for bare steel beams, which resulted in a reduction of cumulative plastic rotation by about 50%.

Preliminary Member Tests on Retrofitted Field Weld Connection

A quasi-static test on beam-to-column subassemblages that mimicked the E-Defense connections was conducted. Retrofit was considered, and the original connection was modified by three types of retrofit particularly in consideration of constructability. The loading history included cyclic plastic deformations determined in reference to the seismic response of the E-Defense test when subjected to the long-period ground motion. The connections were tested until fracture or the development of very large plastic deformations. The main observations are summarized below:

(1) The strain at the bottom flange weld access hole of the original connection reached 1.5% under the 1% drift angle and exceeded 10% under the 2% drift angle loading. The high strain concentration made a crack occur at the toe of weld access hole and fractured along the base metal of beam. The cumulative ductility ratio was 13, which was located between that of the fractured and unfracutred field weld connections in the E-Defense test. Comparing with the shop weld connections in the E-Defense test, the field welded original connection generated a strain value four times as large at the bottom flange, while those two connections had an identical beam depth and slab thickness. The filed weld connection with early time connection details tended to generate larger strain concentration at the bottom flange.

(2) The supplemental welds at the web changed the strain distribution at the connection. The strain concentration at the bottom flange was not reduced, but it increased at the top flange instead. The connection cracked at the bottom flange weld access hole and fractured eventually at the same instant with the original connection.

(3) The cumulative plastic rotation of the wing plate and haunch connections were at least four times the value obtained for the original connection. The connections were not fractured at the

bottom flange at the end of loading, because the strain concentration at the bottom flange was effectively reduced by the retrofit in the bottom flange. Retrofit on the bottom flange increased the strain concentration on the top flange and lead to fracture of the wing plate connection after experiencing ten cycles of the 2% drift angle loading. The cumulative strain at the top flange measured up to fracture was 1.7 times of that at the bottom flange of the original connection. The plastic hinge occurred at the tip of the haunch under the 2% drift angle. The connection was able to sustain a 3% drift angle without fracture.

(4) The accuracy of the proposed strength estimation equations developed for the retrofitted composite beams was verified. Comparing with the test results, the estimation were smaller at a difference of about 10%. The equations were able to estimate the strength of the retrofitted connections reasonably.

(5) Comparing with the original connection, the supplemental weld at web changed the strain concentration at the top flange and lead the cumulative ductility ratio increased. However, the cumulative plastic rotation remained unchanged. The haunch showed the best performance in this test. However, the maximum strength was increased to two times the full plastic moment of the bare beam, which may make the connection stronger than the column and lead the column failure in the end. The maximum strength of the wing plate connection increased to about 1.6 times of the full plastic moment of the bare beam, and the cumulative plastic rotation was improved to 3.6 times that of the original connection. Considering the performance and constructability, the wing plate haunch connection appears the most efficient retrofit.

Seismic Capacity of Retrofitted Frame in Existing Steel High-Rise Building

A series of E-Defense shaking table tests were conducted to evaluate the upgrade of seismic resistance capacity of high-rise buildings when subjected to long-period ground motions. The test specimen was designed to be identical with the last E-Defense test specimen excepted for one difference: all connections were retrofitted by the retrofit methods examined by the member test. The main observations are concluded as below:

(1) In the test, two fractures of the four connections with modified supplemental welds occurred during the fifth San wave loading. The connection fractured at the bottom flange welding boundary. Comparing with the connection with supplemental welds in the member test, the strain at the bottom flange weld access hole was reduced to 1.2% from 10% when the CJP weld at web to column face and supplemental plate were applied at the web connection. Higher restraint at the web connections significantly reduced strain concentration at the bottom flange and enhanced the cumulative plastic rotation capacity of connection from 0.12 rad to 1.58 rad. The capacity was improved thirteen times and even larger than that of the wing plate connections that fractured at beam section.

(2) Four fractures occurred among the twelve wing plate connections under the third San wave loading. The connection in the large-scale E-Defense test shows a different fractured mode from that observed in member test. The strain at the top flange was significantly reduced. The strain concentration area was moved to the tip of the wing plates from beam end, have lead to fracture at

the beam section. The cumulative plastic rotation capacity was improved to 1.36 rad from 0.35 rad of the member connection in which the top flange was fractured.

(3) In the unretrofitted E-Defense test, the field weld connection and shop weld connections fractured at an the average cumulative plastic rotation capacity of 0.16 rad and 0.86 rad, respectively. Here the values are defined as the minimum capacities of the connections, respectively. Field weld connection performed only about 15% of the capacity of shop weld connection, That connection is able to sustain the demands of level 2 design wave with the margin of 80%, but long-period ground motion predicted in Kawasaki, which is close to metropolitan area of Japan, shows very close value to the capacity with the difference of 11%. Apparently, connection is unable to satisfy the demand of level 3 long-period ground motion of San wave which was two times larger than the capacity. Meanwhile, the capacity of the field weld connection was able to be improved to nine and eight times larger when the modified supplemental welds and wing plates were applied. The retrofitted capacity was two times larger than the maximum demand of San wave.

ACKNOWLEDGEMENT

First, I would like to express my gratitude to my thesis advisor, Professor Masayoshi Nakashima. Throughout the past three years of my study, his profound knowledge, encouragement and patience always provide me clear objectives, and more importantly, confidence, especially when I met with difficulties. His rigorous scholarship to his work and his kindness to his students are always worthwhile for me to keep in mind and take as my guideline. I have been fortunate to have such a kind, generous, and also intelligent person as my advisor.

Great thanks are due to Professor Yasuhiro Hayashi and Professor Keiichiro Suita for their kindness to be the members of the dissertation committee, and for their thorough reviews and inspiring comments for this dissertation.

Special thanks are due to Dr. Takuya Nagae for providing many suggestions and supports while I had difficulties. Without his encouragement and advices, it would not possible for me to finish these big tests presented in the dissertation. He also set a good example for me by his research attitude and his kindness to help others.

I also deeply appreciate Professor Toko Hitaka for giving many supports during the tests. Her kindness and cheerful disposition enrich my life in Japan and would be the valuable memory for me.

I am grateful to Mr. Kunio Fukyama, Dr. Kouichi Kajiwara and the E-Defense research fellows for providing professional comments on the tests and shearing their knowledge to me.

I wish to thank Dr. Tao Wang and Prof. Xiaodong Ji for their great help to my study in Japan.

I wish to thank my friends Dr. Jason McCormick, Dr. Yao Chi and Mr. Andres Jacobsen for their sharing my happiness and support.

I am grateful to Mrs. Chisato Gamou, Mrs. Kimura Mieko and Mrs. Tomomi Shinagawa for their kind assistance regarding office matters.

I would also like to show my thankfulness to my group members, Mr. Ryotai Yamamoto, Mr. Tadamasa Daibou for their great assistance on preparing and conducting physical experiments.

I am also grateful to my other colleagues, Dr. Masahiro Ikenaga, Dr. Hisatoshi Kashiwa and Mr. Yosuke Murada, Mr. Hiroya Hanafusa, Mr. Toru Tai, Mr. Shuhai Song, and Miss. Saji Hurugawa for their kindness to help me with the difficulties I have met in Japan.

Finally, I would like to show my sincere gratitude to my families, especially to my parents and my lovely wife, for their continuous understanding and selfless support for these three years, and for their in-time consolation when I met with frustrations. Therefore, I would like to share my happiness with them.